ISSN 2355-5058
e-ISSN 2622-4852

JURNAL ECOTIPE

Electronic, Control, Telecommunication, Information, and Power Engineering

https://ecotipe.ubb.ac.id/

Volume 12, Issue 1, April 2025

Accreditation by Kemdikbudristek
Decree. No.158/E/KPT/2021 (rank. SINTA 3)

Electrical Engineering Department
Bangka Belitung University

JURNAL ECOTIPE
Electronic, Control, Telecommunication, Information, and Power Engineering

Volume 12, Issue 1, April 2025
DOI : 10.33019/jurnalecotipe.v12i1

Accredited by Kemdikbudristek RI
Decree No.158/E/KPT/2021 **(rank. SINTA 3)**

ISSN 2355-5068 e-ISSN 2622-4852

Editorial Board

Publisher Address:
Electrical Engineering Department
Faculty of Science and Engineering - Bangka Belitung University
Balunijuk, Bangka Regency, Bangka Belitung Islands Province, Indonesia
Phone (0717) 4260033 ext. 2125, 2128
Website : https://journal.ubb.ac.id/index.php/ecotipe
E-mail : jurnal.ecotipe@yahoo.com / jurnalecotipe@ubb.ac.id

Preface

Jurnal Ecotipe (Electronic, Control, Telecommunication, Information, and Power Engineering) published by the Electrical Engineering Department, Bangka Belitung University currently starting volume 7 issue 2, October 2020 to volume 12 issue 1, April 2025 has been accredited by the Ministry of Education, Culture, Research, and Technology of the Republic of Indonesia based on Decree No. 158/E/KPT/2021 with 3rd rank (SINTA 3).

Currently, Jurnal Ecotipe volume 12 issue 1, April 2025 has been published. In this edition of the journal, the journal articles are in full English. Starting from volume 9 issue 2 October 2022, for the next editions of the articles in Jurnal Ecotipe, articles will be published using English in their writing and presentation. The articles in this edition of the journal come from academics both from within and from outside the institution.

Our highest appreciation goes to the Reviewers, Editorial Board, Authors, and all parties involved in the preparation and publication of the Jurnal Ecotipe volume 12 issue 1 April 2025. Hopefully, this journal can provide benefits and add scientific insight into the field of Electrical Engineering in particular and engineering in general. Therefore, we still hope for suggestions and constructive criticism for improvements and improvements for the progress of this journal.

Editor-in-Chief

Indexed journal on:

Volume 12, Issue 1, April 2024
DOI : 10.33019/jurnalecotipe.v12i1

JURNAL ECOTIPE
Electronic, Control, Telecommunication, Information, and Power Engineering

Accredited by Kemdikbudristek RI
Decree No.158/E/KPT/2021 **(rank. SINTA 3)**

Table of Content

JURNAL ECTIPE
Electronic, Control, Telecommunication, Information, and Power Engineering
Volume 12, Issue 1, April 2025, pp. 1-10
ISSN 2355-5068 ; e-ISSN 2622-4852
DOI: 10.33019/jurnalecotipe.v12i1.4529

Implementation of Fuzzy Logic for Early Warning System for Flood Disaster in Cilacap District

Erna Alimudin[1], Arif Sumardiono[2], Zaenurrohman[3]
[1,2,3] Electronics Engineering, Cilacap State of Polytechnic, Jl. Dr. Soetomo No. 1, Cilacap 53212, Indonesia

ARTICLE INFO

Article historys:

Received : 28/10/2024
Revised : 15/01/2025
Accepted : 12/02/2025

Keywords:

EWS; Flooding; Fuzzy Logic; Mamdani; Membership Function

ABSTRACT

Indonesia's tropical climate and high rainfall frequently lead to unnoticed river overflows, causing significant health and economic losses. A Flood Early Warning System (EWS) using LoRa communication and an Arduino Mega2560 microcontroller was developed, incorporating ultrasonic, DHT11, rain gauge, and anemometer sensors to measure water level, temperature, humidity, rainfall, and wind speed. Unlike previous systems, it applies fuzzy logic for improved accuracy by considering rainfall and wind speed. Sensor errors ranged from 2.14% to 3.19%, with data transmission to ThingSpeak taking 11 seconds (99.94% accuracy) and to a website averaging 15.03 seconds. Fuzzy logic enhanced the system's warning accuracy.

Corresponding Author:

Erna Alimudin
Electronics Engineering, Cilacap State of Polytechnic, Jl. Dr. Soetomo No. 1, Cilacap 53212, Indonesia
Email: ernaalimudin@pnc.ac.id

1. INTRODUCTION

Indonesia, as a tropical country, experiences two main seasons: rainy and summer. [1] Prolonged rainy seasons accompanied by extreme weather have often caused extreme weather changes in recent years [2]. Unexpected high rainfall can cause flooding, as happened in Cilacap Regency in 2021 in Jeruklegi District and Kawunganten District in 2021 [3]. BMKG Climatology Station Semarang recorded rainfall with moderate to extreme intensity in the central and southern parts of the district. Concentrations of rainfall with extreme intensity exceeding 150 mm/min in 24 hours occurred [4]. The district had extreme rainfall causing the overflowing of existing rivers, so that many houses were submerged in water [5], [6].

The flood resulted in many houses being submerged and agricultural land damaged, causing huge losses to the community [7, 8]. In addition to physical damage, the flood also had an impact on economic and social aspects [7, 9]. Many farmers experienced crop failure, and small business owners suffered financial losses due to damaged or lost products [10]. Flooding also made access to health facilities difficult, disrupting community activities and increasing the risk of diseases such as diarrhea and dengue fever [11]

Looking at the above cases to overcome this problem, the development of a more sophisticated Early Warning System (EWS) is needed [12]. An EWS that combines rainfall, water level and wind speed sensors, and using the Fuzzy Logic method, will provide more accurate early warnings. With this system, the community can be better prepared for flooding and reduce the impact caused.

JURNAL ECTIPE
Electronic, Control, Telecommunication, Information, and Power Engineering
Volume 12, Issue 1, April 2025, pp. 1-10
ISSN 2355-5068 ; e-ISSN 2622-4852
DOI: 10.33019/jurnalecotipe.v12i1.4529

2. RESEARCH METHOD

2.1. Block Diagram

The block diagram shown in Figure 1 is an overview of the Early Warning System (EWS) system for flood disasters using the Arduino Mega 2560 microcontroller. The system is designed to detect extreme weather conditions, such as high rainfall, temperature and humidity, wind speed, and water level, through connected sensors. The data collected is then sent through the LoRa communication module to be monitored and processed to provide early warning to the community.

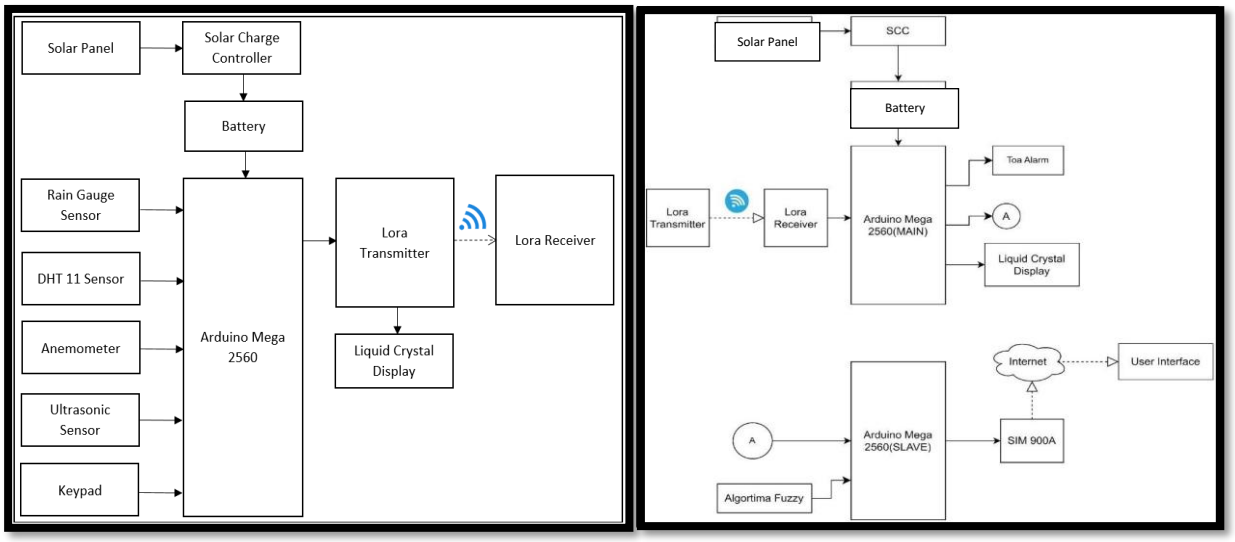

(a) (b)

Figure 1. Block diagram of (a) transmitter and (b) receiver

Figure 1 (a) explains that the system consists of several main components that work together. The solar panel is connected to the Solar Charge Controller (SCC) to charge the battery, which serves as the system's power source. The Arduino Mega 2560 acts as the main controller that collects data from the Rain Gauge sensor (rainfall), DHT11 (temperature and humidity), Anemometer (wind speed), and Ultrasonic sensor (water level). The data is then displayed on the LCD screen and sent through the LoRa Transmitter to the LoRa Receiver for further processing in Figure 1 (b). The keypad is used as a manual input tool if needed.. The sensor data is processed by Fuzzy Logic algorithms to obtain more accurate results and transmitted to the database for further analysis. The whole system is well integrated between hardware and software, and has redundancy in data transmission, ensuring high system reliability for web-based monitoring.

The process starts with the initialization of the I/O pins, serial UART, and LCD in the system. The sensor then reads the environmental data, which is displayed on the LCD of the transmitter node before being sent to the receiver node. If the data is successfully sent, it is further processed by the Arduino Mega 2560 at the receiver node, and the data is sent to the Fuzzy Logic algorithm to get more accurate results. The processed data is displayed on the LCD and sent to the SIM900A module to be uploaded to the internet. If the internet is available, the sensor data is sent to the ThingSpeak database to be displayed on the web interface. If the data is received properly, the system will display the sensor data and output from Fuzzy Logic on the website for further monitoring.

2.2. Block Diagram of Receiver Node

The Receiver Node block diagram describes an Early Warning System (EWS) system for flood disasters that uses LoRa technology and an Arduino Mega 2560 microcontroller. This system is designed to detect and provide early warnings related to potential flooding through connected sensors and utilizes

JURNAL ECTIPE
Electronic, Control, Telecommunication, Information, and Power Engineering
Volume 12, Issue 1, April 2025, pp. 1-10
ISSN 2355-5068 ; e-ISSN 2622-4852
DOI: 10.33019/jurnalecotipe.v12i1.4529

the Fuzzy Logic method for data analysis. Data transmission is done wirelessly through the LoRa network and SIM 900A and displayed on the screen and user interface to increase community preparedness in the face of flood disasters.

Figure 1 (b) explains that this system consists of two main parts, namely the transmitter and receiver units. The solar panel charges the battery through the Solar Charge Controller (SCC), which then supplies power to the Arduino Mega 2560 (MAIN) as the main controller. Data received from the LoRa Receiver is sent to the alarm (Toa) and displayed on the Liquid Crystal Display. The signal is forwarded to the Arduino Mega 2560 (SLAVE) which processes the data using the Fuzzy Logic algorithm, then sends the results via the SIM 900A module to the internet to be displayed on the user interface.

2.3. Block Diagram of Fuzzy Logic On EWS

The following block diagram illustrates the application of the Fuzzy Logic method to an Early Warning System (EWS) system for flood detection. Utilizing various sensors that measure rainfall, water level, and wind speed, the resulting data is analyzed using fuzzy logic to produce more accurate decisions in detecting potential flooding. The system is designed to provide early warnings to the community in order to take appropriate precautions.

Data from ultrasonic sensors, anemometer, and rain gauge enter the fuzzification stage, where the data is converted into fuzzy values. Next, the predefined fuzzy rules are used in the fuzzy inference process to analyze the data. The results of this inference then go through the defuzzification stage to convert the fuzzy values into concrete values, which then produce outputs in the form of early warnings or other decisions related to flood potential.

2.4. Tool Design

1. The Overall Design

Figure 2. Overall Design

Figure 2 shows the overall design of the device used in the IoT-based monitoring and early warning system. The device is equipped with a solar panel at the top as a power source, which allows the device to operate autonomously in remote locations without relying on external power sources. There is a control box at the bottom of the panel that serves to control and display data from the sensors. It is designed with a sturdy iron frame structure to support the equipment and ensure its stability when installed in the field.

JURNAL ECTIPE
Electronic, Control, Telecommunication, Information, and Power Engineering
Volume 12, Issue 1, April 2025, pp. 1-10
ISSN 2355-5068 ; e-ISSN 2622-4852
DOI: 10.33019/jurnalecotipe.v12i1.4529

2.5. Electrical System Design

1. Electrical Design of Transmitter Node

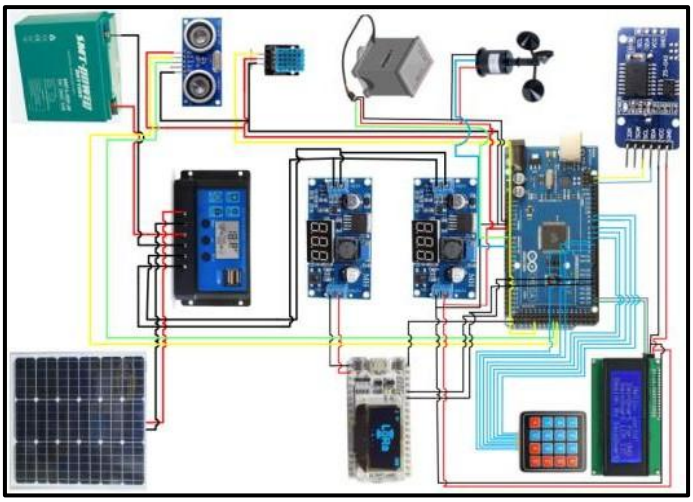

Figure 3. Transmitter Node Electrical Design

Figure 3 shows the electrical system design of the transmitter node in the Early Warning System (EWS) development project. This transmitter node includes several main components, such as a solar panel used to charge the battery as a power source, an ultrasonic sensor, a rain sensor (rain gauge), a temperature and humidity sensor (DHT11), and an anemometer to measure wind speed. All of these sensors are connected to the Arduino Mega 2560, which serves as the data processing center. The Arduino is also connected to a LoRa communication module to transmit data to the receiving node, as well as an LCD screen and keypad as the user interface. This design enables the collection and transmission of environmental data to detect potential flood disasters.

3. RESULTS AND DISCUSSION

This research aims to design and develop an Early Warning System (EWS) system for flood detection using the Fuzzy Logic method. The system integrates various sensors, such as rain gauge, ultrasonic water level sensors, and anemometer, to monitor environmental conditions that could potentially cause flooding. The data obtained from these sensors is then processed using a Fuzzy Logic algorithm to provide more accurate predictions of potential flooding.

3.1 Equation Result of Fuzzy Logic EWS Implementation with MATLAB

The Mamdani method in the Early Warning System (EWS) for flood detection is used to improve accuracy in disaster detection, by utilizing ultrasonic sensors, wind speed sensors, and rainfall at the sending node (transmitter). Data from these sensors is sent to the receiver node and processed using the Mamdani fuzzy logic algorithm. The defuzzification process is carried out using the centroid (center of area) method, which aims to find the center point of the area under the fuzzy output curve. This technique calculates the ratio between the integral of the membership value multiplied by the output variable, and the integral of the membership value itself. The centroid method was chosen because it provides accurate and representative results. The stages start from fuzzification, which is the process of converting crisp input data into fuzzy input, with several variables used in this study.

1. Fuzzification

Fuzzification is a process where the input data of definite values (crips input) is entered into fuzzy input. In this study, several variables were used.

JURNAL ECTIPE
Electronic, Control, Telecommunication, Information, and Power Engineering
Volume 12, Issue 1, April 2025, pp. 1-10
ISSN 2355-5068 ; e-ISSN 2622-4852
DOI: 10.33019/jurnalecotipe.v12i1.4529

Table 1. Fuzzification

Variables	Sets	Domains	Membership Function
Water Level	Low	[0 0 60 108]	Trapezoid
	Medium	[80 150 220]	Triangle
	High	[180 240 300 300]	Trapezoid
Wind Speed	Low	[0 0 6 12]	Trapezoid
	Medium	[10 12 14]	Triangle
	Fast	[12 22 50 50]	Trapezoid
Rainfall	Low	[0 0 12 25]	Trapezoid
	Medium	[15 35 55]	Triangle
	Heavy	[45 102 160]	Triangle
	Extreme	[150 175 180 180]	Trapezoid

Table 1 shows the fuzzification stage in the fuzzy system for flood detection, which includes three input variables: water level, wind speed, and rainfall. Each variable has several fuzzy sets, such as "low," "medium," and "high" for water level, "low" and "fast" for wind speed, and "low," "medium," "heavy," and "extreme" for rainfall. Each set has a different domain with a trapezium or triangle-shaped membership function, which is used to convert the exact input data into fuzzy values. This process is essential for interpreting sensor data in a fuzzy logic-based flood detection system.

2. Implication Function Application

Tests that have been carried out, the Mamdani fuzzy logic system in the flood disaster EWS is able to integrate water level, wind speed, and rainfall data well, resulting in accurate predictions of safe, alert, or dangerous conditions. Using the centroid defuzzification method, this system can provide a more representative early warning according to the input from the sensor.

Table 2. Rule Fuzzy

No	Water Level	Wind Speed	Rainfall	Output
1	Low	Toned	Heavy	Safe
2	Low	Toned	Extreme	Safe
3	Medium	Low	Low	Safe
4	Medium	Low	Medium	Alert
5	Medium	Low	Heavy	Alert
6	Medium	Toned	Medium	Safe
7	Medium	Toned	Heavy	Alert
8	Medium	Toned	Extreme	Alert
9	High	Medium	Medium	Alert
10	High	Medium	Heavy	Danger
11	High	Medium	Extreme	Danger
12	High	Toned	Low	Alert

Based on the data in Table 2, the Mamdani fuzzy logic system successfully classifies flood conditions into three main categories: safe, alert, and danger, taking into account the variables of water level, wind speed, and rainfall. In conditions of low to moderate water levels with wind speed and rainfall that are also low or moderate, the system outputs "safe". However, when the different variables show higher values, such as moderate or high water levels and heavy to extreme rainfall, the output changes to "alert" or "danger". The system shows good capability in providing early warning based on the environmental conditions measured by the sensors.

3. Deffuzzification

Defuzzification is converting the output fuzzy set to the form of firm numbers (crips). In the Mamdani method using the Centroid (Center of area) calculation method in Equation 1, 2, and 3.

JURNAL ECOTIPE
Electronic, Control, Telecommunication, Information, and Power Engineering
Volume 12, Issue 1, April 2025, pp. 1-10
ISSN 2355-5068 ; e-ISSN 2622-4852
DOI: 10.33019/jurnalecotipe.v12i1.4529

$$Output = \frac{Momentum}{Area} \quad (1)$$

$$Momentum = \int_a^b x.\mu\,(z).dx \quad (2)$$

$$Area = \int_a^b \mu\,.dx \quad (3)$$

Before performing defuzzification, the fuzzification process must be carried out first. This is because fuzzification changes clear (crisp) input data into fuzzy values that can be processed with fuzzy logic rules. After the fuzzy rules are applied and produce fuzzy values, then defuzzification is carried out to change the results back to crisp values that can be understood or applied in practical decisions. Thus, fuzzification is the initial step to prepare data in a form that can be processed using fuzzy logic, and defuzzification is the final step to change the results back into a useful form. Fuzzification of water level, wind speed, dan rainfall shown at Figure 7-9.

Case example: The implementation case in this case takes an example, When the water level is (150) cm, wind speed is (25) m/s, and rainfall is (60) ml/min what is the output result? The water level can calculated by equation 4,5, or 6. The wind speed can calculated by equation 7, 8, or 9. And the rainfall level can calculated by equation 10, 11, 12, or 13.

a. Fuzzification

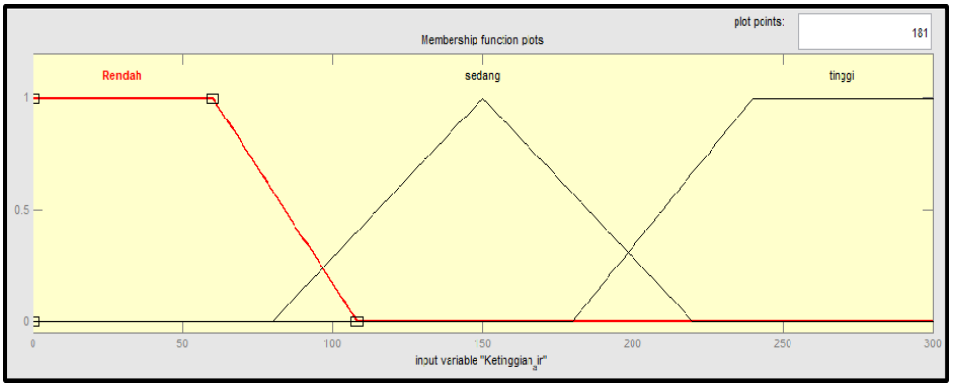

Figure 7. Water Level Fuzzification

Water Level

Low = 0 (4)

$$Medium = \frac{x-a}{b-a} = \frac{150-80}{150-80} \quad (5)$$

High = 0 (6)

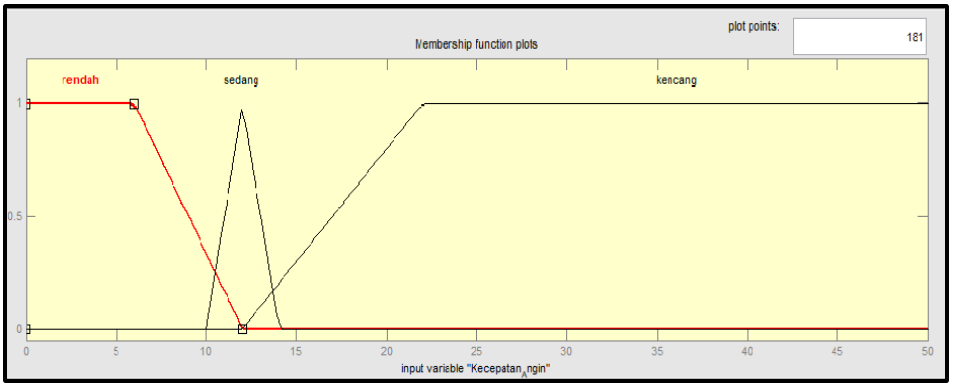

Figure 8. Wind Speed Fuzzification

JURNAL ECOTIPE
Electronic, Control, Telecommunication, Information, and Power Engineering
Volume 12, Issue 1, April 2025, pp. 1-10
ISSN 2355-5068 ; e-ISSN 2622-4852
DOI: 10.33019/jurnalecotipe.v12i1.4529

Wind Speed

Low = 0 (7)

Medium = 0 (8)

Fast = 1 (9)

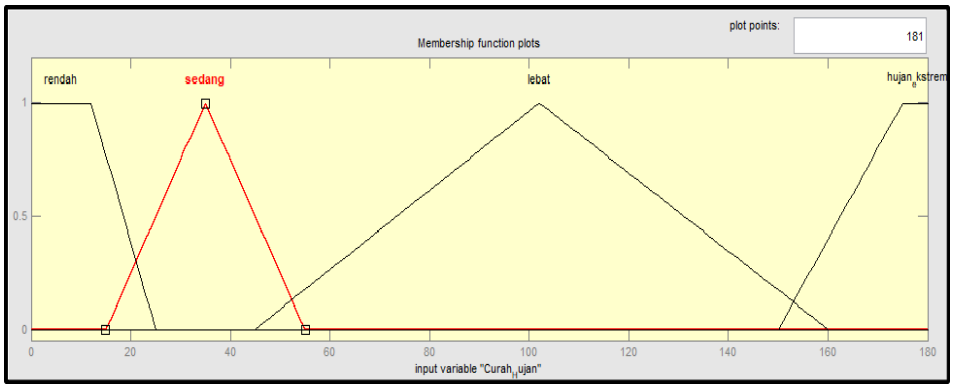

Figure 9. Rainfall Fuzzification

Rainfall

Low = 0 (10)

Medium = 0 (11)

Heavy $= \frac{x-a}{b-a} = \frac{60-45}{102-45} = 0.263$ (12)

Extreme = 0 (13)

b. Inference

After knowing the membership degree of each membership function, the next step is inference, which is taking the MIN output value of each membership function:

[R23] = water(medium)&&wind(fast)&&rainfall(heavy)Then Caution.
= MIN water(1) && wind(1) && rainfall(0.263)
= MIN(1, 1, 0.263) = 0.263

c. Deffuzification

In the Mamdani method, affirmation uses the centroid (center of area) method. Calculated by Equation 14-18. Supervised output range = 4 – 6.

$Centroid = \frac{Momentum}{Area}$ (14)

$Momentum = \int_a^b x.0.263\ dx$ (15)

$= 0.263(\frac{1}{2})_4^6 = 0.263\ \left(\frac{1}{2}6^2 - \frac{1}{2}4^2\right) = 0.263\left(\frac{36}{2} - \frac{16}{2}\right) = 2.63$

$Area = \int_4^6 0.263\ dx = 0.263\ [4]\ ^6 = 0.263\ (6-4) = 0.526$ (16)

$Output = \frac{Momentum}{Area}$ (17)

$= \frac{2.63}{0.526}$ (18)

= 5 (Manual calculation result)
= 5 (Arduino program result)
= 5 (Matlab result)

JURNAL ECTIPE
Electronic, Control, Telecommunication, Information, and Power Engineering
Volume 12, Issue 1, April 2025, pp. 1-10
ISSN 2355-5068 ; e-ISSN 2622-4852
DOI: 10.33019/jurnalecotipe.v12i1.4529

From this comparison, it can be concluded that manual calculations cannot be used as a reference because the difference between rule 1 and the others has almost the same difference. In the Arduino program results, a program is made that references calculations based on matlab. Thus, the Arduino generated program can be classified to distinguish the output shown in Figure 10-12.

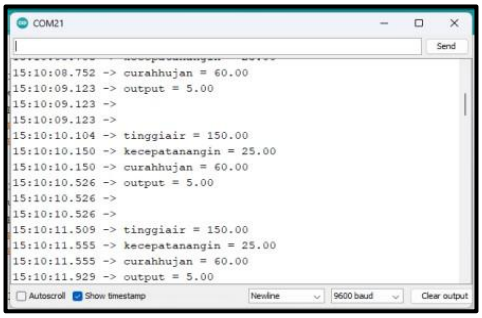

Figure 10. Results on Arduino IDE serial monitor

Figure 11. Results in MATLAB

From Table 2, there are 36 rows indicating there are 36 rules and there are 4 columns consisting of 3 fuzzy inputs and 1 fuzzy output from each rule made. In the input column there is a red line indicating the value of the input rule, and there is the oldest color among the outputs that is the appropriate rule from the input that has been determined in the lower input column, the mark on each output rule indicates the membership of the resulting output.

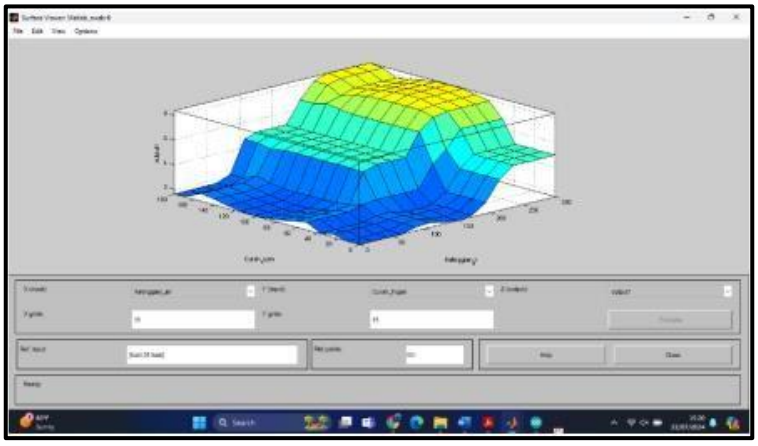

Figure 12. Surface graph in MATLAB

JURNAL ECTIPE
Electronic, Control, Telecommunication, Information, and Power Engineering
Volume 12, Issue 1, April 2025, pp. 1-10
ISSN 2355-5068 ; e-ISSN 2622-4852
DOI: 10.33019/jurnalecotipe.v12i1.4529

From Figure 12, the surface graph in MATLAB shows that rainfall and water level are very influential in flood disasters, because the graph shows that when the water level increases and rainfall increases, the fuzzy logic output is also higher, while wind speed is not very influential in the occurrence of flood disasters.

3.2 Fuzzy Logic Algorithm Testing with MATLAB

The EWS that has been designed and has been completed is then tested and compared to the results of the Fuzzy Logic Algorithm with simulations in MATLAB. The results of the Fuzzy Algortima Test can be seen in the test images between EWS and MATLAB in attachments 2 and 3. From these 11 tests it can be concluded that there is a difference of 0%, so the Fuzzy Logic Algorithm on EWS is very good.

4. CONCLUSION

Rainfall and water level greatly affect the results of flood detection, while wind speed is less important while wind speed is not very influential in flood detection influence in flood disaster detection. This can be known from the rules and results of the Fuzzy Algorithm. The Fuzzy Logic algorithm that has been carried out and the results are very accurate with 11 data that has been tested with MATLAB software, while on the website when the water level is 157, the wind speed is 0, and the rainfall is 54.40 has the same fuzzification value as the MATLAB software with a difference of 0 by 0.

REFERENCES

[1] I. Suhardjo, "Operasi Pintu Air Bendung Gerak Serayu Dalam Usaha Pengendalian Banjir Dan Irigasi," *Teodolita (Media Komun. Ilm. di Bid. ...*, pp. 1–11, 2011, [Online]. Available: http://e-journal.unwiku.ac.id/teknik/index.php/JT/article/download/73/59

[2] I. N. W. Satiawan, I. B. F. Citarsa, and others, "Desain Buck Converter Untuk Charging Batere Pada Beban Bervariasi: Buck Converter Design For Battery Charging On Various Loads," *DIELEKTRIKA*, vol. 5, no. 1, pp. 30–35, 2018.

[3] ASEAN Coordinating Centre for Humanitarian Assistance, "Indonesia, Flooding in Cilacap Regency, Central Java (21 Jul 2021)," 2021. https://reliefweb.int/report/indonesia/indonesia-flooding-cilacap-regency-central-java-21-jul-2021

[4] I. W. Harmoko and B. Ruslana, Zauyik Nana (Stasiun Klimatologi Klas I Semarang, "Analisis Singkat Kejadian Banjir Di Kabupaten Cilacap (Tanggal 21 Juli 2021)," 2021.

[5] Asian Disaster Infomration Network, "Indonesia, Flooding in Cilacap Regency, Central Java." [Online]. Available: https://adinet.ahacentre.org/report/indonesia-flooding-in-cilacap-regency-central-java-20210721

[6] I. Nozomi, "Penerapan Data Mining Untuk Peringatan Dini Banjir Menggunakan Metode Klastering K-Means (Studi Kasus Kota Padang)," *J. Sains Inform. Terap.*, vol. 2, no. 2, pp. 39–44, 2023, doi: 10.62357/jsit.v2i2.165.

[7] H. P. Adi, I. Wahyudi, and F. (Universitas I. S. A. Ni'am, "Model Mitigasi Dan Penanganan Banjir Air Pasang Laut Untuk Ketahanan Pangan Dan Permukiman (Studi Kasus Di Kecamatan Kawunganten, Kabupaten Cilacap)," 2019.

[8] E. Alimudin, A. Sumardiono, and Zaenurrohman, "Sistem Peringatan Dini Bencana Banjir Menggunakan Multi Sensor," S00202212254, 2022

[9] F. R. Usman, W. Ridwan, and I. Z. Nasibu, "Sistem Peringatan Dini Bencana Banjir Berbasis Mikrokontroler Arduino," *Jambura J. Electr. Electron. Eng.*, vol. 1, no. 1, pp. 1–6, 2019, doi: 10.37905/jjeee.v1i1.2721.

[10] R. A. Priatim, M. Asri, and S. Abdussamad, "Rancang Bangun Prototipe Peringatan Dini Banjir Menggunakan Raspberry Pi Berbasis IoT," *Jambura J. Electr. Electron. Eng.*, vol. 5, no. 2, pp.

Volume 12, Issue 1, April 2025, pp. 1-10
ISSN 2355-5068 ; e-ISSN 2622-4852
DOI: 10.33019/jurnalecotipe.v12i1.4529

216–221, 2023, doi: 10.37905/jjeee.v5i2.19696.

[11] L. Soulibouth, H. S. Hwang, and D. H. Shin, "The Impact of Flood Damage on Farmers, Agricultural Sector and Food Security in Laos: A Regional Case Study of Champhone District, Savannaket Province," *J. Int. Dev. Coop.*, vol. 16, no. 2, pp. 151–170, 2021, doi: 10.34225/jidc.2021.16.2.151.

[12] A. Nurdianto, D. Notosudjono, and H. Soebagia, "Rancang bangun sistem peringatan dini banjir (early warning system) terintegrasi internet of things," *J. Online Mhs. Bid. Tek. Elektro*, vol. 01, pp. 1–10, 2018.

JURNAL ECOTIPE
Electronic, Control, Telecommunication, Information, and Power Engineering

Volume 12, Issue 1, April 2025, pp. 11-19
ISSN 2355-5068 ; e-ISSN 2622-4852
DOI: 10.33019/jurnalecotipe.v12i1.4536

Design of PID Controller using LQR-Based Parameter Selection for DC Motor Position Control

Hartono[1], Eka Budiarto[2], Henry Nasution[3]
[1]Mechatronics Engineering Department, Swiss German University, Jalur Sutera Barat No. 15, Tangerang 15143, Indonesia
[2]Information Technology Department, Swiss German University, Jalur Sutera Barat No. 15, Tangerang 15143, Indonesia
[3]Renewable Energy Engineering Technology, Bung Hatta University, Jl. Sumatera Ulak Karang Utara, Padang 25133, Indonesia

ARTICLE INFO

Article historys:

Received : 22/01/2025
Revised : 09/02/2025
Accepted : 18/02/2025

Keywords:

DC Motor; Linear Quadratic Regulator (LQR); Position Control; Proportional Integral Derivative (PID); Ziegler–Nichols

ABSTRACT

DC motors are widely applied in various fields due to their simple design, ease of control, and capability to generate high torque at low speeds. Position control of DC motors is crucial to ensure the performance and accuracy of the motorized electro-mechanical systems. The most common conventional control utilized in DC motors is the Proportional Integral Derivative (PID) controller. In this paper, the Linear Quadratic Regulator (LQR) approach is used to determine PID controller parameters for DC motors. The LQR approach, based on optimal control theory, offers a systematic alternative to traditional methods for tuning PID controllers. The results show that the designed controllers outperform the Ziegler–Nichols tuned PID, with the recommended controller Ctrl 1, achieves a settling time of 1.2953 s, an overshoot of 0.5%, and a steady-state error of 0.0043.

Corresponding Author:

Hartono
Mechatronics Engineering Department, Swiss German University, Jalur Sutera Barat No. 15, Tangerang 15143, Indonesia
Email: har.tono@sgu.ac.id

1. INTRODUCTION

DC motors are electric motors that provide high starting torque and precise speed control by converting direct current electrical energy to mechanical energy [1−3]. Due to their simple design, ease of control, and capability to produce high torque at low speeds, DC motors are widely utilized in a variety of applications, including industrial automation, robotics, automotive, agriculture, and home appliances [4−7]. Since these motors are the main actuator component of the system, the appropriate controller should be designed to these motors to achieve good performance, precise speed and position, and efficient energy usage.

There are numerous studies related to speed and position control for DC motors. The most popular control technique is the PID controller, with its simplicity, intuitive design, good performance in linear systems, and capability for real-time adjustment [8]. PID parameters can be decided by several techniques, such as classical methods like manual tuning [9], Ziegler–Nichols, and Cohen-Coon that use reaction curves or ultimate gain [10] and optimization methods by minimizing error for better performance [11]. Additionally, frequency domain approaches ensure robustness, while modern techniques, including trial-and-error, genetic algorithms, and fuzzy logic, adapt to complex systems [12]. The other techniques are machine learning methods [13], Model Predictive Control (MPC) [14], and software tools like auto-tuners to provide convenient automated tuning solutions [15].

JURNAL ECTIPE
Electronic, Control, Telecommunication, Information, and Power Engineering
Volume 12, Issue 1, April 2025, pp. 11-19
ISSN 2355-5068 ; e-ISSN 2622-4852
DOI: 10.33019/jurnalecotipe.v12i1.4536

In this study, PID parameters will be selected using Linear Quadratic Regulator (LQR) approach, that offers a systematic framework for optimizing control gains. The LQR method is based on optimal control theory and offers a reliable alternative to the trial-and-error tuning methods often used in PID control design. By formulating the PID controller as a three-term structure compatible with the quadratic cost function of the LQR. This theory was first introduced in 1971 by Williamson and Moore [16].

2. RESEARCH METHOD

This research began with a literature study on DC motors and their control methods. It proceeded with mathematical modeling, followed by the design of the controllers. Simulations were then conducted using software to evaluate the performance of the designed controllers compared to Ziegler–Nichols method and analyze which controller is suitable for the system requirement.

2.1. Mathematical Model

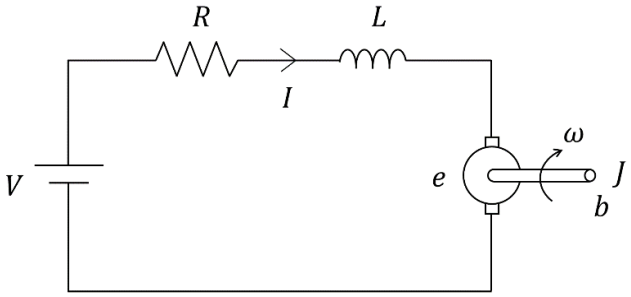

Figure 1. Equivalent circuit of a DC motor

DC motor is an actuator that uses the magnetic field force between the induced magnet from the winding, which is powered by an electric current flowing through the rotor, and the permanent magnet on the stator to transform electrical energy into mechanical energy [17]. Figure 1 illustrates a DC motor's equivalent circuit. The armature circuit's voltage equation can be expressed as the following equation using Kirchhoff's voltage law.

$$V = IR + L\frac{dI}{dt} + e \tag{1}$$

Where V is the voltage supply of DC motor, I is electric current, L is the inductance of the winding, R is resistance, and e is back electromotive force voltage, which is the product of the angular velocity ω and a constant k_e. Then, the electric circuit equation can be rewritten as equation (2).

$$\frac{dI}{dt} = -\frac{k_e}{L}\dot{\theta} - \frac{R}{L}I + \frac{1}{L}V \tag{2}$$

Meanwhile, the mechanical equation of the DC motor can be written as follows.

$$\tau = J\alpha + b\omega \tag{3}$$

With τ as the induced torque, J as the moment of inertia, α as the angular acceleration, b as the friction coefficient, and ω as the angular velocity. The induced torque is the product of the torque constant k_τ and the electric current I flowing through the rotor windings. Therefore, the mechanical equation can be expressed as:

$$k_\tau I = J\ddot{\theta} + b\dot{\theta}$$

$$\frac{d\dot{\theta}}{dt} = -\frac{b}{J}\dot{\theta} + \frac{k_\tau}{J}I \tag{4}$$

Based on equation (2) and (4), by defining the state variables $x_1 = \theta$, $x_2 = \dot{\theta}$, $x_3 = I$, and $u = V$, the system's state space can be written as:

JURNAL ECTIPE
Electronic, Control, Telecommunication, Information, and Power Engineering
Volume 12, Issue 1, April 2025, pp. 11-19
ISSN 2355-5068 ; e-ISSN 2622-4852
DOI: 10.33019/jurnalecotipe.v12i1.4536

$$\begin{bmatrix}\dot{x}_1\\ \dot{x}_2\\ \dot{x}_3\end{bmatrix} = \begin{bmatrix}0 & 1 & 0\\ 0 & -\frac{b}{J} & \frac{k_\tau}{J}\\ 0 & -\frac{k_e}{L} & -\frac{R}{L}\end{bmatrix}\begin{bmatrix}x_1\\ x_2\\ x_3\end{bmatrix} + \begin{bmatrix}0\\ 0\\ \frac{1}{L}\end{bmatrix}u \tag{5}$$

$$y = \begin{bmatrix}1 & 0 & 0\end{bmatrix}\begin{bmatrix}x_1\\ x_2\\ x_3\end{bmatrix} \tag{6}$$

Table 1. Physical parameters of DC motor used in this study

Parameter	Value
Friction coefficient, b	0.00105 Nms
Moment of inertia, J	0.0054 $kg\ m^2$
Torque constant, k_τ	0.507 Nm/A
Back emf constant, k_e	0.507 $V/rad/s$
Inductance, L	0.0125 H
Resistance, R	7.102 Ω

The physical parameters of the DC motor used in this study are shown in Table 1. Then, by substituting those physical parameters, the state space matrixes are obtained.

$$A = \begin{bmatrix}0 & 1 & 0\\ 0 & -0.19 & 93.89\\ 0 & -40.56 & -568.16\end{bmatrix} \qquad B = \begin{bmatrix}0\\ 0\\ 80\end{bmatrix} \qquad C = \begin{bmatrix}1 & 0 & 0\end{bmatrix} \qquad D = 0$$

2.2. Controller Design

Before designing the controller, the controllability of the system is analyzed to determine whether the system is controllable. If the system is able to change from one state to another in a limited amount of time, it is said to be controllable [18]. The controllability matrix M can be expressed as follows.

$$M = \begin{bmatrix}B & \vdots & AB & \vdots & A^2B\end{bmatrix}$$

$$M = \begin{bmatrix}0 & 1 & 7511.11\\ 0 & 7511.11 & -4.27\times10^6\\ 80 & -40.56 & 2.55\times10^7\end{bmatrix}$$

The rank of the matrix was calculated as 3, matching with the system's dimension ($n = 3$). This indicates that the controllability matrix is full rank, and the system is fully controllable. Furthermore, in this article the controller to be designed is an LQR−tuned PID, which is a PID control with LQR as the parameter's selector for PID gain values K_p, K_i, and K_d.

JURNAL ECTIPE
Electronic, Control, Telecommunication, Information, and Power Engineering
Volume 12, Issue 1, April 2025, pp. 11-19
ISSN 2355-5068 ; e-ISSN 2622-4852
DOI: 10.33019/jurnalecotipe.v12i1.4536

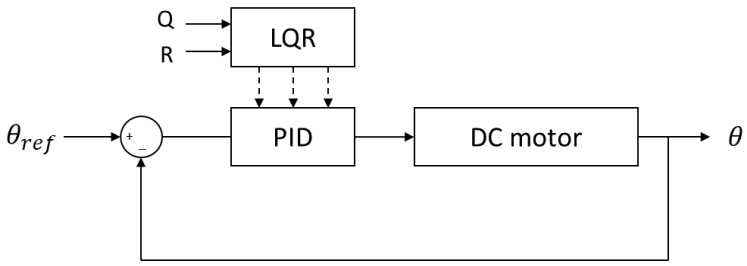

Figure 2. Block diagram of designed DC motor position control

The block diagram of the designed system to control the position of a DC motor is shown in Figure 2. Mathematical model of DC motor from equation (5) and (6) can be rewritten as follows:

$$\dot{x} = Ax + Bu \qquad x(t_o) = 0$$
$$y = Cx \tag{7}$$

x is the solution of equation (7), u is assumed as the output from the PID controller with input y, so that the output can be expressed as the equation (8).

$$u = K_1 \int_0^t y\, dt + K_2 y + K_3 \dot{y} \tag{8}$$

with K_1, K_2, and K_3 are PID gains.

$$K_1 = \frac{K_p}{T_i}; \quad K_2 = K_p; \quad K_3 = K_p T_d$$

Where K_p is proportional gain, T_i represents time integral, and T_d denotes time derivative from PID controller. Then, control law (8) is stated as state feedback control by using equation (7). From those equations, it can be obtained:

$$y = Cx$$
$$\dot{y} = CAx + CBu \tag{9}$$
$$\ddot{y} = CA^2x + CABu + CB\dot{u}$$

by applying the equation (9) to equation (8), result in:

$$\dot{u} = K_1 y + K_2 \dot{y} + K_3 \ddot{y}$$
$$(1 - K_3 CB)\dot{u} = (K_3 CA^2 + K_2 CA + K_1 C)x + (K_3 CAB + K_2 CB)u \tag{10}$$

The notation $\hat{K}$ is used to denote the normalized value of K.

$$\hat{K}^T = \begin{bmatrix} \hat{K}_1 \\ \hat{K}_2 \\ \hat{K}_3 \end{bmatrix} = (1 - K_3 CB)^{-1} \begin{bmatrix} K_1 \\ K_2 \\ K_3 \end{bmatrix} \tag{11}$$

$$\dot{u} = \hat{K}^T \begin{bmatrix} C^T \\ A^T C^T \\ (A^2)^T C^T \end{bmatrix} x + \hat{K}^T \begin{bmatrix} 0 \\ B^T C^T \\ B^T A^T C^T \end{bmatrix} u \tag{12}$$

The equation (12) can be simplified as:

$$u_a = K_a x_a \tag{13}$$

with

$$u_a = \dot{u}, \; x_a = [x \quad u]^T$$

Volume 12, Issue 1, April 2025, pp. 11-19
ISSN 2355-5068 ; e-ISSN 2622-4852
DOI: 10.33019/jurnalecotipe.v12i1.4536

$$K_a = \begin{bmatrix} C^T & A^T C^T & (A^2)^T C^T \\ 0 & B^T C^T & B^T A^T C^T \end{bmatrix} \widehat{K} = \Gamma \widehat{K} \tag{14}$$

the augmented system equation based on equations (7) and (14) is as follows.

$$\dot{x}_a = A_a x_a + B_a u_a \tag{15}$$

$$A_a = \begin{bmatrix} A & B \\ 0 & 0 \end{bmatrix}; \qquad B_a = \begin{bmatrix} 0 \\ 1 \end{bmatrix} \tag{16}$$

By solving the Riccati equation (17), $\widehat{K}$ can be determined, and the values of K_1, K_2, and K_3 can be calculated. In other words, the gains for PID control can be obtained.

$$A_a^T P + P A_a - P B_a R^{-1} B_a^T P + Q = 0 \tag{17}$$

$$\widehat{K}^T = -R^{-1} B_a^T P \tag{18}$$

3. RESULTS AND DISCUSSION

To verify the feasibility of the designed controller, simulations were conducted by using the software. In these simulations, the matrices Q and R are chosen for the LQR parameters. Where Q represents the weighting matrix for the state variables, influencing how deviations from desired states affect the control effort. Matrix R, on the other hand, specifies the weighting on control inputs, influencing how much control effort is penalized relative to the state deviations.

$$Q = \begin{bmatrix} q_1 & 0 & 0 & 0 \\ 0 & q_2 & 0 & 0 \\ 0 & 0 & q_3 & 0 \\ 0 & 0 & 0 & q_4 \end{bmatrix} \qquad R = 1$$

The fixed value for parameter R is chosen, while parameter Q is varied by changing the values of elements q_1, q_2, q_3, and q_4. The elements of matrix Q are selected through the empirical approach of trial and observation. Initially, random values were set to test how they affected the system. The values are then improved in steps where each step response is compared, and the aim is to reach a reasonable trade-of between system stability, response speed, and the amount of control effort needed. While this approach does not rely on a systematic optimization method, it does provide a means of practical tuning according to how the system performs. With these variations in the LQR parameters, different PID gains and step responses of the system are obtained, as shown in the following Table 2 and Table 3 respectively.

Table 2. LQR parameters and PID gains

Controller	LQR parameter					PID Gain		
	q_1	q_2	q_3	q_4	R	K_p	K_i	K_d
Ctrl 1	0.0001	15	1	5	1	1.0514	0.0100	0.0019
Ctrl 2	0.001	10	2	4	1	0.7640	0.0316	0.0014
Ctrl 3	0.01	5	3	3	1	0.4405	0.1000	0.0008
Ctrl 4	0.1	20	2	2	1	1.3686	0.3162	0.0024
Ctrl 5	1	25	2	6	1	1.6644	1.0000	0.0030

The relationship between the corresponding PID gains and the LQR parameters (Q and R) is shown in Table 2. The diagonal elements of state cost matrix Q (q_1, q_2, q_3, q_4) affect the weight given to state variables in the optimization process, while the control input cost matrix R, is kept constant at R=1 to maintain consistent penalty on control effort. These LQR parameters are used to tune the PID gains (K_p,

JURNAL ECTIPE
Electronic, Control, Telecommunication, Information, and Power Engineering
Volume 12, Issue 1, April 2025, pp. 11-19
ISSN 2355-5068 ; e-ISSN 2622-4852
DOI: 10.33019/jurnalecotipe.v12i1.4536

K_i, K_d), where K_p adjusts the system's response to current errors, K_i addresses accumulated errors to eliminate steady-state error, and K_d mitigates future errors to reduce overshoot.

As q_1 and other elements of Q increase, the PID gains show a corresponding adjustment to achieve the desired control performance. Lower q_1 values (e.g., Ctrl 1) result in more conservative gains, while higher q_1 values (e.g., Ctrl 5) lead to higher gains, figuring responsiveness and control effort. This trend reflects a systematic method to tune the balance between system responsiveness, stability, and control effort, offering flexibility in designing controllers for various applications, from conservative to aggressive control strategies. Furthermore, the effect of other elements of Q must also be considered. The value of q_2 primarily influences the integral gain K_i, which affects steady-state performance. A higher q_2 tends to result in a higher K_i, improving steady-state accuracy but also increasing the risk of oscillations. The elements q_3 and q_4 impact the derivative gain K_d, which affects the damping characteristics of the system. Lower values of q_3 and q_4 may lead to a lower K_d, potentially reducing overshoot but also slowing down the response. On the other hand, higher values of q_3 and q_4 contribute to increased K_d, improving damping but possibly require higher control effort. The step responses of the designed controllers, compared with Ziegler–Nichols (ZN) tuned PID with gain $K_p = 175.8$, $K_i = 3516$, and $K_d = 2.1975$ are displayed in Figure 3.

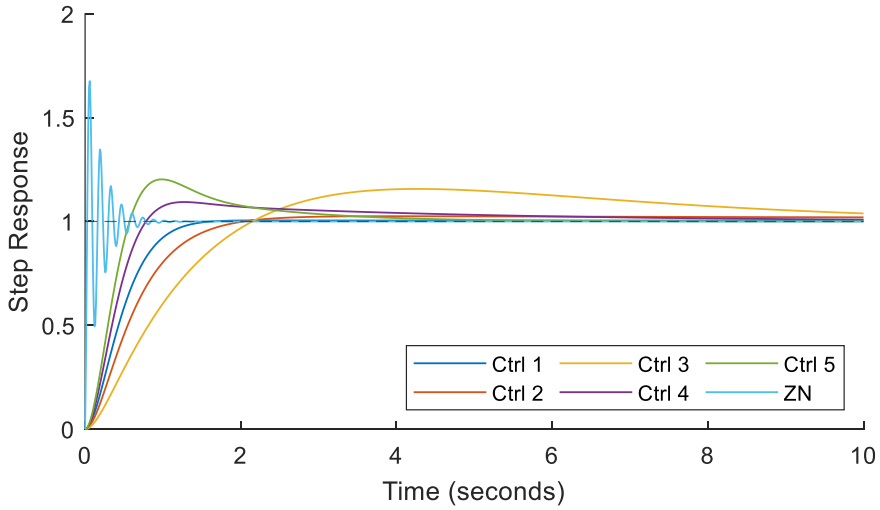

Figure 3. Step responses of designed controllers and ZN-tuned PID

Table 3. Comparison of step responses for different controllers

Controller	Step response performance			
	Rise Time (s)	Settling Time (s)	Overshoot (%)	Steady-State Error
Ctrl 1	0.7947	1.2953	0.50	0.0043
Ctrl 2	1.1133	9.9806	2.53	0.0200
Ctrl 3	1.5050	11.8510	15.66	0.0388
Ctrl 4	0.5219	6.8382	9.36	0.0089
Ctrl 5	0.3930	3.7631	20.27	0.0002
ZN	0.0197	0.6898	68.21	3.33×10^{-16}

For DC motor position control, choosing the proper controller is crucial, depending on the specific performance requirements of the application, including response speed, stability, and precision. Based on the step response data shown in Table 3, it can be seen that Ctrl 1 stands out with a balanced performance, featuring a moderate rise time of 0.7947 seconds and a settling time of 1.2953 seconds, with minimal overshoot at 0.50% and a very small steady-state error of 0.0043. This makes it a good option for applications where precision and stability are important. In other side, Ctrl 5 achieves the

JURNAL ECTIPE
Electronic, Control, Telecommunication, Information, and Power Engineering
Volume 12, Issue 1, April 2025, pp. 11-19
ISSN 2355-5068 ; e-ISSN 2622-4852
DOI: 10.33019/jurnalecotipe.v12i1.4536

fastest rise time of 0.3930 seconds and a settling time of 3.7631 seconds, with an impressive steady-state error of 0.0002, however it comes with a significant overshoot of 20.27%. This indicates that Ctrl 5 is more suitable for the system where a quick response is necessary, and the overshoot can be accepted. Meanwhile, Ctrl 4 strikes a balance with a relatively quick rise time of 0.5219 seconds, moderate overshoot of 9.36%, and a low steady-state error of 0.0089, making it suitable for applications that need a compromise between speed and precision.

The other controllers, Ctrl 2 and Ctrl 3, show longer settling times, greater overshot, and higher steady-state errors, making them less suitable for precise position control tasks. In the other hand, ZN-tuned PID controller provides the best response time with a very small steady-state error of 3.33×10^{-6} which is almost zero, but with very high overshoot of 68.21%. This excessive overshoot makes the ZN-tuned PID unsuitable for motor position control in this case. In summary, Ctrl 1 is recommended for applications that prioritize stability and accuracy, while is preferable for those emphasizing speed.

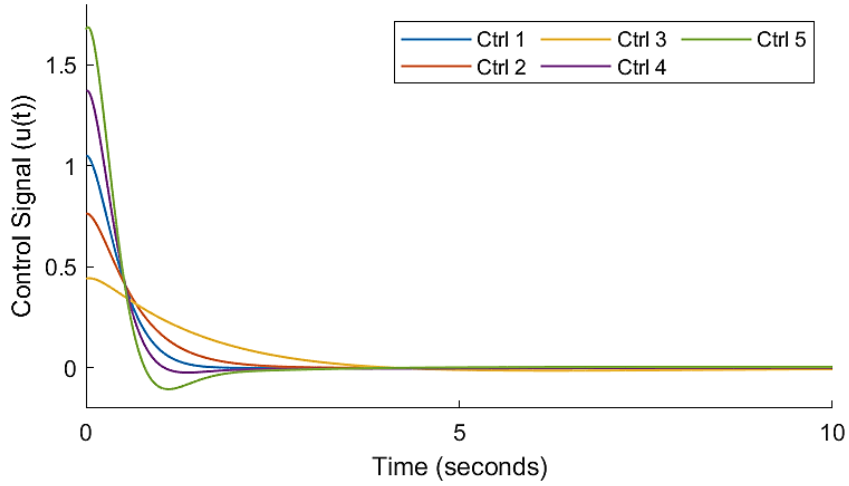

Figure 4. Control signal of designed controllers

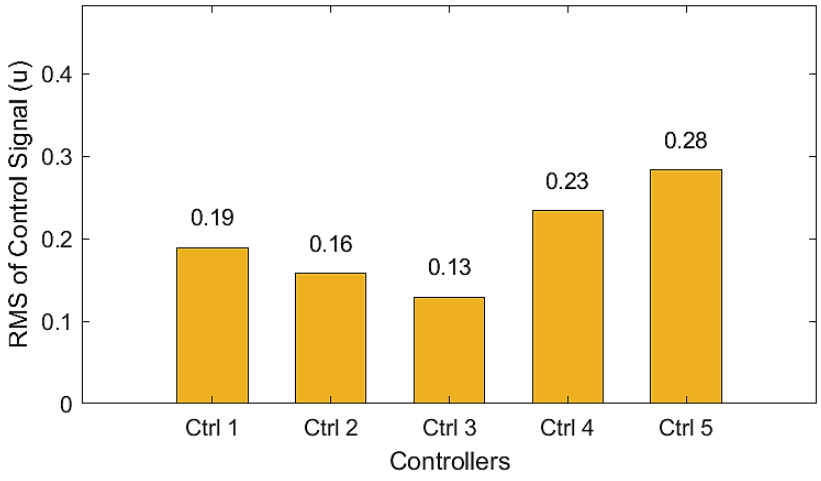

Figure 5. RMS of control signal

Additionally, the root mean square (RMS) values of control signal are shown in Figure 5, illustrating the value that is proportional with the energy required by each controller. Lower RMS values indicate less energy consumption, with Ctrl 3 being the most energy-efficient while Ctrl 5 consuming the highest energy. This highlights the trade-off between energy efficiency and performance, as more responsive controllers like Ctrl 5 tend to require greater control effort. For applications emphasizing energy savings, controllers like Ctrl 3 are more suitable, while high-performance tasks may justify higher energy consumption. Based on the step responses and control signal graphs, Ctr 1 is chosen for DC motor position control due to its good response and moderate energy consumption compared to

Volume 12, Issue 1, April 2025, pp. 11-19
ISSN 2355-5068 ; e-ISSN 2622-4852
DOI: 10.33019/jurnalecotipe.v12i1.4536

another designed controllers. Furthermore, the ZN-tuned PID controller is not chosen for this system due to its high control signal magnitude, with the RMS value of 22.49, indicating excessive energy consumption. The control signal of the ZN-tuned PID controller is shown in Figure 6.

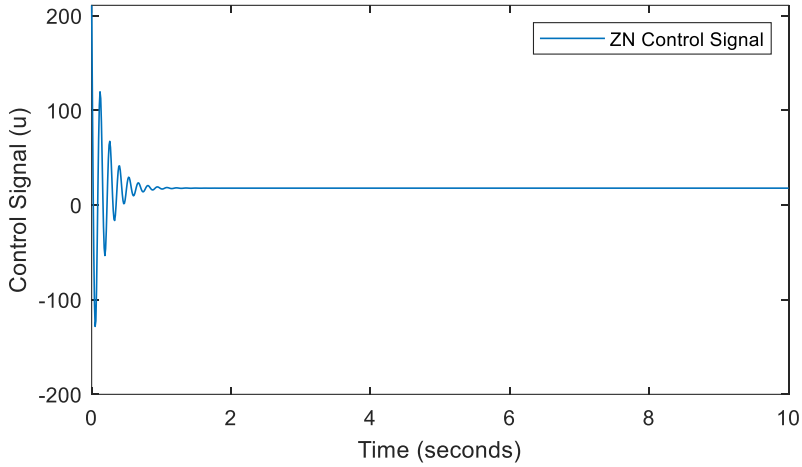

Figure 6. Control signal of ZN-tuned PID controller

4. CONCLUSION

This study demonstrates the effective tuning of PID controller gains using LQR parameters by varying the state weighting matrix Q while keeping R constant. The diagonal elements of Q significantly influence PID gains, shaping the system's response. Step response analysis highlights the controller's suitability for various applications. Ctrl 1 delivers balanced performance with minimal overshoot, short settling time, and negligible steady-state errors, ideal for precision tasks. Ctrl 5 provides the fastest response with very low steady-state error but high overshoot, suitable for speed-prioritized tasks. Ctrl 4 strikes a balance between quick response and moderate overshoot, suiting systems needing both speed and precision. In contrast, Ctrl 2 and Ctrl 3 exhibit longer settling times and higher errors, making them less effective for precise tasks. These results emphasize the effectiveness of LQR-based PID parameters selection to meet specific control objectives compared to the ZN tuning method. For future work, experimental validation on a physical DC motor system is recommended to validate the simulation results. Additionally, investigating these controllers under disturbances and model uncertainties could enhance their robustness for real-world practical applications.

Acknowledgments

The authors acknowledge the financial support of Swiss German University through internal research funds program.

REFERENCES

[1] D. Mohanraj, J. Gopalakrishnan, B. Chokkalingam, and L. Mihet-Popa, "Critical Aspects of Electric Motor Drive Controllers and Mitigation of Torque Ripple—Review," *IEEE Access*, vol. 10, pp. 73635–73674, 2022, doi: 10.1109/ACCESS.2022.3187515.

[2] K. S. Mohammad and A. S. Jaber, "Comparison of electric motors used in electric vehicle propulsion system," *Indonesian Journal of Electrical Engineering and Computer Science*, vol. 27, no. 1, pp. 11–19, July 2022, doi: 10.11591/ijeecs.v27.i1.pp11-19.n

[3] A. Hughes and B. Drury, *Electric Motors and Drives: Fundamentals, Types and Applications*. Newnes, 2019.

Volume 12, Issue 1, April 2025, pp. 11-19
ISSN 2355-5068 ; e-ISSN 2622-4852
DOI: 10.33019/jurnalecotipe.v12i1.4536

[4] E. Akpama, E. Effiong, and R. Ezenwosu, "Simulink design of a DC motor control for water pump using fuzzy logic," *International Conference on Electrical Power Engineering (ICEPENG 2021)*, 2021, pp. 16–19.

[5] S. Krishnamoorthy and P. P. K. Panikkar, "A comprehensive review of different electric motors for electric vehicles application," *International Journal of Power Electronics and Drive Systems (IJPEDS)*, vol. 15, no. 1, pp. 74–90, Mar. 2024, doi: 10.11591/ijpeds.v15.i1.pp74-90.

[6] Y. B. Koca, Y. Aslan and B. Gökçe, "Speed Control Based PID Configuration of a DC Motor for An Unmanned Agricultural Vehicle," *2021 8th International Conference on Electrical and Electronics Engineering (ICEEE)*, Antalya, Turkey, 2021, pp. 117-120, doi: 10.1109/ICEEE52452.2021.9415908.

[7] Hartono, E. Leksono and E. Joelianto, "Type-2 Fuzzy Sliding Mode Control Design for Self-Balancing Mobile Robot," *2023 6th International Conference on Information and Communications Technology (ICOIACT)*, Yogyakarta, Indonesia, 2023, pp. 494-498, doi: 10.1109/ICOIACT59844.2023.10455780.

[8] R. P. Borase, D. K. Maghade, S. Y. Sondkar, and A. G. Keskar, "A review of PID control, tuning methods and applications," *International Journal of Dynamics and Control*, vol. 9, no. 3, pp. 818–827, 2021. doi: 10.1007/s40435-020-00665-4.

[9] A. Mulyadi, M. Amin, and M. Anam, "Control Mass-Spring-Damper Based on Tuning Trade-off PID Controller", *Jurnal Ecotipe*, vol. 10, no. 1, pp. 52-60, Apr. 2023.

[10] S. Das, A. Chakraborty, J. K. Ray, S. Bhattacharjee, and B. Neogi, "Study on Different Tuning Approach with Incorporation of Simulation Aspect for Z-N (Ziegler-Nichols) Rules," *International Journal of Scientific and Research Publications*, vol. 2, no. 8, pp. 1-5, 2018.

[11] M. P. Dev, S. Jain, H. Kumar, B. N. Tripathi, and S. A. Khan, "Various Tuning and Optimization Techniques Employed in PID Controller: A Review," *Proceedings of International Conference in Mechanical and Energy Technology*, vol. 174, pp. 797–805, 2020.

[12] F. Cao, "PID controller optimized by genetic algorithm for direct-drive servo system," *Neural Computing and Applications*, vol. 32, pp. 23–30, 2020.

[13] A. Ahmadi and R. M. Esfanjani, "Automatic tuning of PID controllers using deep recurrent neural networks with pruning based on tracking error," *Journal of Instrumentation*, vol. 19, no. 02, p. P02028, Feb. 2024.

[14] A. A. Abdelrauf, M. Abdel-Geliel and E. Zakzouk, "Adaptive PID controller based on model predictive control," *2016 European Control Conference (ECC)*, Aalborg, Denmark, 2016, pp. 746-751, doi: 10.1109/ECC.2016.7810378.

[15] L. Wang, *PID Control System Design and Automatic Tuning Using MATLAB/Simulink*. Hoboken, NJ, USA: John Wiley & Sons, 2020.

[16] D. Williamson and J. B. Moore, "Three-Term Controller Parameter Selection Using Suboptimal Regulator Theory," *IEEE Transactions on Automatic Control*, vol. 16, no. 1, pp. 82–83, 1971.

[17] B. Bilgin, J. Liang, M. V. Terzic, J. Dong, R. Rodriguez, E. Trickett, and A. Emadi, "Modeling and Analysis of Electric Motors: State-of-the-Art Review," *IEEE Transactions on Transportation Electrification*, vol. 5, no. 3, pp. 602-617, Sept. 2019, doi: 10.1109/TTE.2019.2931123.

[18] K. Ogata, *Modern Control Engineering*, 5th ed. Upper Saddle River, NJ, USA: Pearson, 2010.

JURNAL ECOTIPE
Electronic, Control, Telecommunication, Information, and Power Engineering

Volume 12, Issue 1, April 2025, pp. 20-30
ISSN 2355-5068 ; e-ISSN 2622-4852
DOI: 10.33019/jurnalecotipe.v12i1.4541

PI Control Application for Low Speed Stepper Motor in Medical Infusion Pump for Flow Rate Stability

Muhammad Achsanul In'am[1], Nana Sutarna[2], Astri Era Hamijaya[3]
[1] Universitas Muhammadiyah Yogyakarta, Jl. Brawijaya, Kasihan, Bantul, Yogyakarta 55183, Indonesia
[2] Politeknik Negeri Jakarta, Jl. Prof. Dr. G.A. Siwabessy, Kampus UI, Depok, 16425, Indonesia
[3] Universitas PGRI Yogyakarta, Jl. PGRI I Sonosewu No. 117 Daerah Istimewa Yogyakarta 55182 Indonesia

ARTICLE INFO

Article historys:

Received : 02/02/2025
Revised : 14/02/2025
Accepted : 02/04/2025

Keywords:

Flow Rate; Infusion Pump; PI Control System; Stepper Motor

ABSTRACT

The infusion pump is an intravenous injection machine for administering high-alert drugs. Failure to administer this type of drug can result in patient death. One cause of failure is interference with the flow rate of infusion fluid, which is influenced by the performance of the stepper motor. This study proposes a PI control design for controlling the stability of the flow rate in an infusion pump machine. The tuning method used is the Ziegler Nicholes type 1 tuning method, and the creation of a first-order transfer function using the Cian Cone method. The system is also applied directly to the hardware and tested using an Infusion device analyzer. The simulation results show that PI control can reach the set point and remain stable with a rise time of 19.49 seconds and a settling time of 32.39 seconds. In actual testing of the infusion pump machine with PI control, the average flow rate accuracy level reached 98%, and its stability reached below 0.3 ml/hour. This proves that the infusion pump that was successfully created can be used to administer high-alert drugs appropriately according to the dose and can be used for a long time with constant delivery quality.

Corresponding Author:

Muhammad Achsanul In'am
Universitas Muhammadiyah Yogyakarta, Jl. Brawijaya, Kasihan, Bantul, Yogyakarta 55183, Indonesia
muhammad.achsanul@umy.ac.id

1. INTRODUCTION

Hospital service quality assurance standards are implemented through inpatient safety regulations. This includes fully procuring medical equipment to support more optimal patient treatment. The act of administering medication, especially high-alert medication, must be considered an aspect of patient safety [1]. Nurses still make errors when handling patients, especially when administering drug injections. The number of cases of errors in administering drug doses is relatively high, which results in patient death. In the United States, these cases reach as many as 48,000–100,000 per year. Meanwhile, in Indonesia, the percentage of cases reached 24.8 percent of reported cases [2]. Therefore, when administering medication, you must follow the ten principles of correct medication administration [3]. The ten principles are drug, dose, patient, route, time, information, expiration, assessment, evaluation and documentation.

One technique for administering high-alert-type drugs is through an intravenous infusion device. The action of administering high-alert drugs must be done carefully and precisely. On the other hand, until now, manual/conventional infusion models are still found and used in hospitals. This conventional infusion method has many disadvantages. These disadvantages include still using gravity, an arterial

JURNAL ECTIPE
Electronic, Control, Telecommunication, Information, and Power Engineering
Volume 12, Issue 1, April 2025, pp. 20-30
ISSN 2355-5068 ; e-ISSN 2622-4852
DOI: 10.33019/jurnalecotipe.v12i1.4541

drop rate of ≥ 20%, and a flow rate that is difficult to regulate accurately [4]. Based on this study, the manual infusion model is not appropriate when used for high-alert drug injection.

Bright infusion is an infusion model that works automatically. This method uses an infusion pump. The tool works on the principle of a peristaltic pump to distribute infusion fluids [5]. The infusion pump must be WHO standard with a flow rate accuracy of at least ±5% [6]. Using non-standard infusion pumps results in system failure and the pump working uncontrollably [7]. The following are several failures in the infusion pump working system that were found. Using an infusion pump that is too long can cause heat and slow the rotation speed. Likewise, the condition of the infusion pump is old, which impacts inaccurate dosing. Apart from that, tools that do not comply with the specified test specifications are often found to have non-linearities. Based on the description of the failure of the infusion pump model. several researchers have innovated automatic infusion machines to improve the quality of administering high-alert drugs so that the dosage is correct. [8]. Previous research has been done on the innovation of automatic infusion machines to improve the quality of high-alert drug delivery so that the dose is correct. The working system uses a cuff pressure control system. The cuff is used to press the infusion bottle. The cuff pressure is adjusted based on the drip rate as a control reference. The control used is fuzzy logic control. The results are pretty good, with a precision of 96.75%. However, this design does not comply with the design required by WHO because this design has the potential to cause bubbles in the infusion line so that air enters the intravenous, which can cause death; this incident is called embolism [9]. The application of fuzzy logic for stepper motor speed control shows good results, but it was used for high speeds above 300rpm in this study [10]. The PI control method was chosen because, in several studies, motor controllers showed that PI control was better than PID controllers for control stepper motor [11]. Apart from that, this type of control is also easy to implement and develop for low-speed control of stepper motors because it has been proven to eliminate resonance at low speeds and reduce vibrations at high speeds [12].

Referring to the problems and literature review, this research designs a PI control system for controlling low-speed stepper motors in the range of 0 - 100 RMP to determine the flow rate in infusion machines. This research implements a simulated and actual PI control system on hardware and is verified with a medical-grade standard calibration tool. This research aims to improve the stability and accuracy of the infusion fluid flow rate by looking at the performance results of the PI control system design applied to the infusion pump machine.

2. RESEARCH METHOD

This research aims to create an infusion pump machine based on Arduino nano control in a close loop using PI Control. The tuning method used is the Ziegler Nicholes type 1 method and the Cian Cone method to produce the system transfer function. The results of the PI constant tuning are applied to the Arduino microcontroller so that the microcontroller can work to control the infusion pump machine hardware. System testing takes data in real-time using the IDA analyzer measuring instrument and system simulation using Simulink Matlab. The speed control application on a stepper motor is done by adjusting the frequency of the square wave signal that enters the stepper motor driver; the higher the frequency, the faster the rotation speed will be [13]. In addition, motor speed control is also applied to molding; the control used is PID control. PID control works by regulating the PWM signal input that enters the motor driver to achieve a constant stepper motor speed during the printing process [14].

2.1. Block Diagram and Wiring Diagram of infusion pump

The overall design of the system block diagram is shown in Figure 1. The infusion pump consists of several parts: a keypad to enter the desired set point value, an AS5600 speed sensor, a microcontroller, a TMC2088 motor driver, a Nema 17 stepper motor, and an LCD. The AS5600 sensor is used because it works based on changes in angle, making it possible to read small changes in the stepper motor's rotation. The advantage of this sensor is that it is suitable for important parts in low-speed control of a stepper motor.

JURNAL ECOTIPE
Electronic, Control, Telecommunication, Information, and Power Engineering
Volume 12, Issue 1, April 2025, pp. 20-30
ISSN 2355-5068 ; e-ISSN 2622-4852
DOI: 10.33019/jurnalecotipe.v12i1.4541

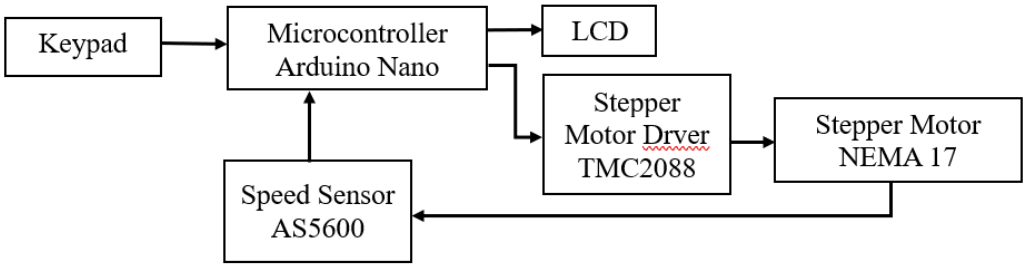

Figure 1. Infusion pump block diagram

A 12V-3A DC power supply provides power to the infusion pump machine. The control center uses an Arduino nano-type microcontroller. Command instructions to determine the desired flow rate and volume of infusion fluid are used using a keypad. Meanwhile, to regulate the flow rate of infusion fluid using a Nema 17 stepper motor and TMC2088 as a motor driver. This infusion pump machine is built in a closed loop system with an AS5600 speed sensor as feedback. The display for monitoring the results of the process uses an LCD screen in digital form. Figure 2 shows a schematic form of an electronic circuit. To read low speeds below 50 rpm, a data smoothing method or average calculation is needed. The data for stable reading requires 200 samplings, and the average data sampling delay is 10ms.

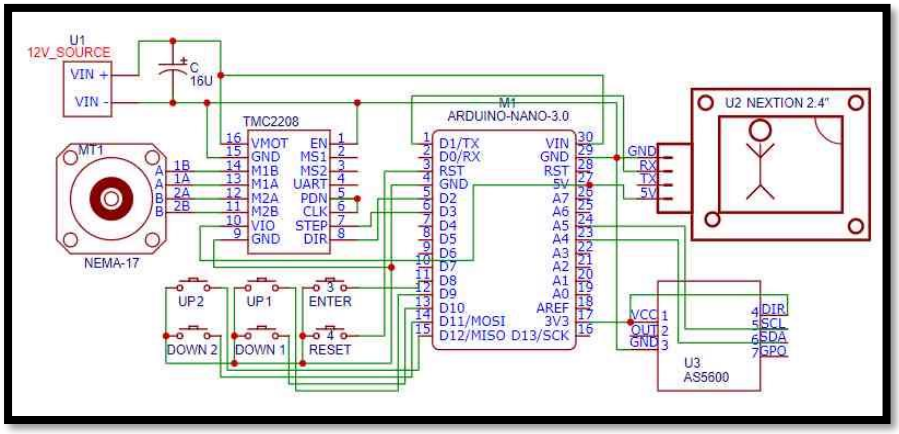

Figure 2. Infusion pump schematic circuit

2.2. Infusion Pump System Mechanical Diagram

The linear peristaltic pump mechanism is used in the proposed design. The main driver is a Nema 17 bipolar stepper motor with a gear ratio of 16:40. The mechanical diagram and physical form of the Pump motor are shown in Figure 3 and Figure 4.

Figure 3. Linear peristaltic pump

JURNAL ECOTIPE
Electronic, Control, Telecommunication, Information, and Power Engineering
Volume 12, Issue 1, April 2025, pp. 20-30
ISSN 2355-5068 ; e-ISSN 2622-4852
DOI: 10.33019/jurnalecotipe.v12i1.4541

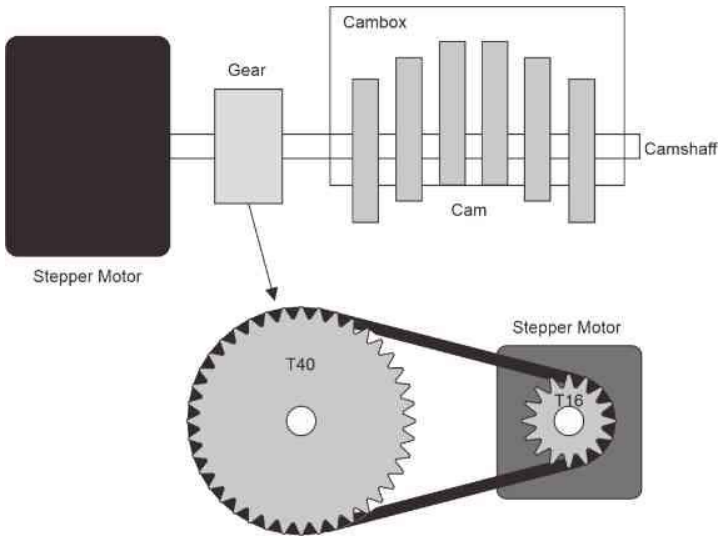

Figure 4. Linear peristaltic pump mechanics

2.3. Convert RPM to ml/h

The method for changing the RPM value to ml/h is done by conducting a trial set point RPM at several points, looking at the flow rate value read on the IDA, and then recording it. The following is a graph of the flow rate against RPM, shown in the Figure 5.

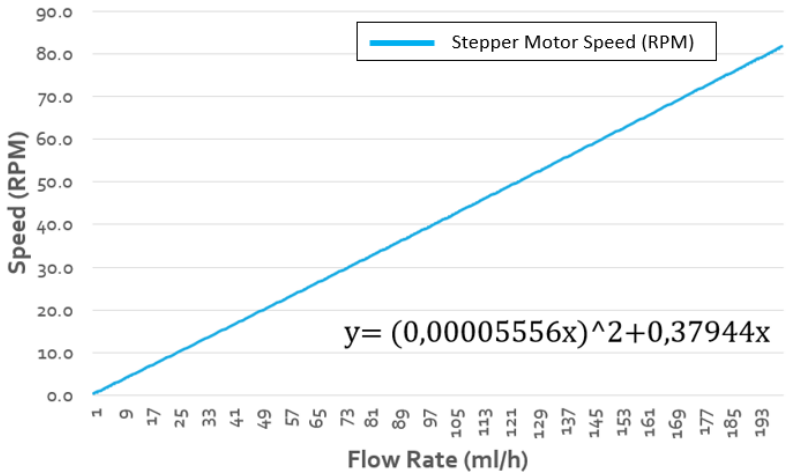

Figure 5. RPM to ml/h conversion graph

2.4. Transfer Function Design

The transfer function of the infusion pump is obtained through experiment. The plant is given an input signal in the form of a step unit in an open loop position, and then the output signal is recorded. The transfer function is obtained using the the Cian cone method [15], using the first-orderthe approach. Transfer function equation (1) is obtained from the result of response graph identification in Figure 6.

JURNAL ECOTIPE
Electronic, Control, Telecommunication, Information, and Power Engineering
Volume 12, Issue 1, April 2025, pp. 20-30
ISSN 2355-5068 ; e-ISSN 2622-4852
DOI: 10.33019/jurnalecotipe.v12i1.4541

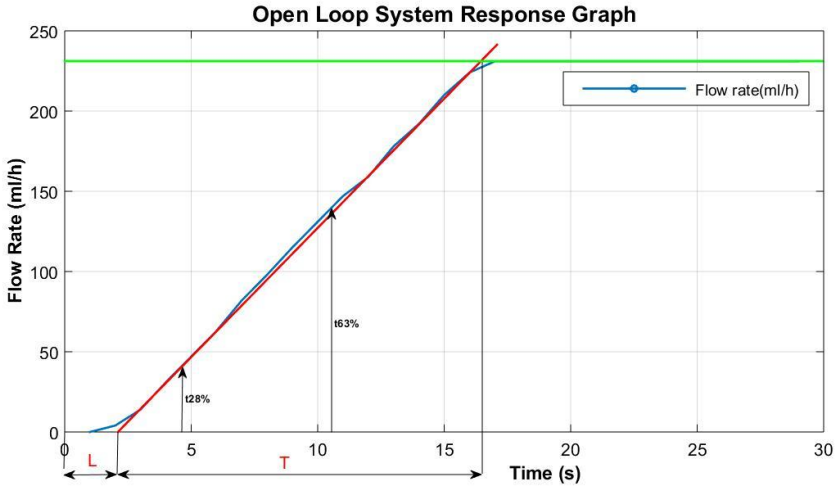

Figure 6. Open loop system response graph

From the image above, it can be seen that the smoothing effect of data causes changes in flow velocity to experience a delay. *L* is the time delay when the flow velocity value begins to increase. *T* is the time delay from the first change in the flow velocity value until the flow velocity begins to experience a stable point. The red line is an aid line to draw the S graph. The green line is the maximum flow rate point that can be achieved.

t28% : 4,76s
t63% : 10,71s
Δ : 231
δ : 231

$Kp = \frac{\Delta}{\delta} = \frac{231}{231} = 1$

τ = 1,5 (t63% - t28%)
= 1,5 (10,71 - 4,76)
= 16,065 – 7,14
= 8,925

Θ = t63% - τ
= 10,71 – 8,925
= 1,785

$\frac{Y(s)}{X(s)} = \frac{Kpe^{-\theta s}}{\tau s + 1}$
$= \frac{1e^{-1,785s}}{8,925s + 1}$

Transfer function :

$$G(s) = \frac{1}{8,925s + 1} \quad (1)$$

The open loop response graph is also used to find the constant values of Kp and Ki using the Ziegler Nichols type 1 method. The following is a calculation to find Kp and Ki:

$Kp = 0.9 \frac{T}{L}$
$= 0.9 \times \frac{14}{2}$
= 6.3

$Ti = \frac{L}{0.3}$
$= \frac{2}{0.3}$
= 6.66

$Ki = \frac{Kp}{Ti}$
$= \frac{6.3}{6.66}$
= 0.945 (2)

JURNAL ECTIPE
Electronic, Control, Telecommunication, Information, and Power Engineering
Volume 12, Issue 1, April 2025, pp. 20-30
ISSN 2355-5068 ; e-ISSN 2622-4852
DOI: 10.33019/jurnalecotipe.v12i1.4541

3. RESULTS AND DISCUSSION

3.1. PI Control Simulation Result

The system transfer function obtained using the Ciancone method is applied to PI control which is simulated in Simulink, the following is the Simulink block diagram shown in Figure 7 and the response graph is shown in Figure 8.

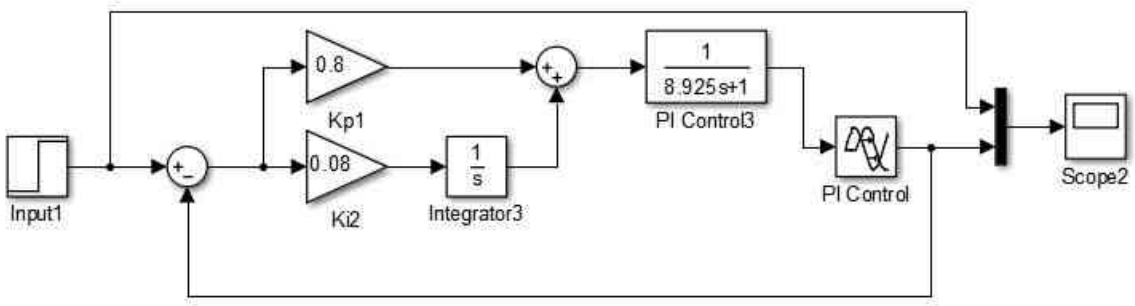

Figure 7. Diagram block simulink simulation

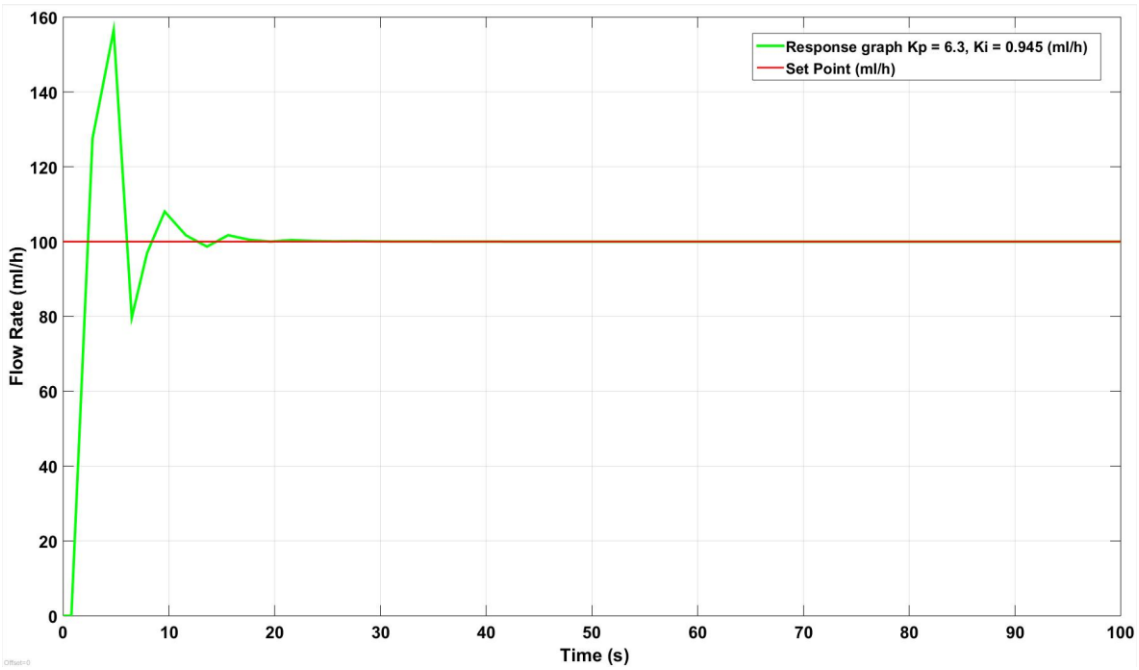

Figure 8. System response graph

A response graph is obtained in the simulation, as shown in Figure 13. The response graph shows that the PI control system with Ziegler Nicholes type 1 tuning constants, namely with Kp = 6.3 and Ki = 0.945, can reach the stability point but still experiences a very high overshot. This is not allowed in the infusion pump working system because overshot occurs, resulting in an excess dose of medication entering the patient. Therefore, adjusting the PI constant with initial adjustments to Kp and Ki from the Ziegler Nicholes tuning results is necessary. Adjustments are made by trial and error, referring to the rules of the PID control system. The following trial error results are shown by the response graph in Figure 9.

JURNAL ECTIPE
Electronic, Control, Telecommunication, Information, and Power Engineering
Volume 12, Issue 1, April 2025, pp. 20-30
ISSN 2355-5068 ; e-ISSN 2622-4852
DOI: 10.33019/jurnalecotipe.v12i1.4541

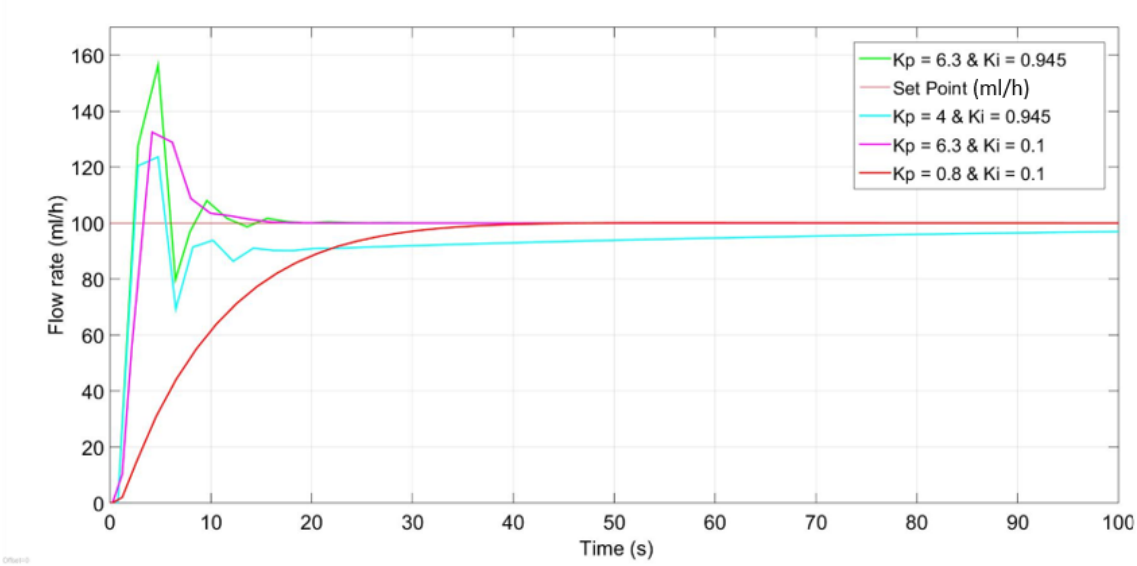

Figure 9. Response graph from adjusting the PI constant

In the trial-error process, a simulation is carried out by increasing and decreasing the Kp and Ki values. So, we get several response graphs. The first experiment was carried out by reducing the Kp value; the resulting impact was that the system experienced an overshoot and did not reach stability. The second experiment reduced the Ki value; the resulting impact was that the overshot decreased but did not wholly eliminate the overshot, and the system achieved stability. The third experiment reduced both values to Kp = 0.8 and Ki = 0.1. It produces pretty good results; for example, the response graph does not experience overshot and can achieve stability. This system cannot be maximized to the fastest rise time speed except with control modification. Because this system delays sensor reading when focusing on the rise time speed, the simulation and accurate measurement using IDA will not be synchronized. It would be better if the display and real-time IDA measurements were always synchronized with each change. The Kp = 0.8 and Ki = 0.1 is the fastest rise time point and is synchronous between the control system and accurate monitoring of IDA measurements. The following is a detailed response time shown in Table 1.

Table 1. Response time

Kp	Ki	Rise Time (s)	Settling Time (s)	Overshot	Error Steady State (%)
6.3	0.945	1.25	11.50	56.53	0
4	0.945	1.86	12.86	32.50	0
6.3	0.1	1.32	-	-	Not Achieved
0.8	0.1	19.49	32.39	0	0

3.2. Machine Design Results

The following is a manifestation of the results of the tool that was successfully built. The tool is a prototype that has been neatly packaged and quickly set up by the nurse. The overall shape of the tool is shown in Figure 10. Moreover, the electronic part is also shown in Figure 11.

JURNAL ECTIPE
Electronic, Control, Telecommunication, Information, and Power Engineering
Volume 12, Issue 1, April 2025, pp. 20-30
ISSN 2355-5068 ; e-ISSN 2622-4852
DOI: 10.33019/jurnalecotipe.v12i1.4541

Figure 10. Infusion pump Prototype results

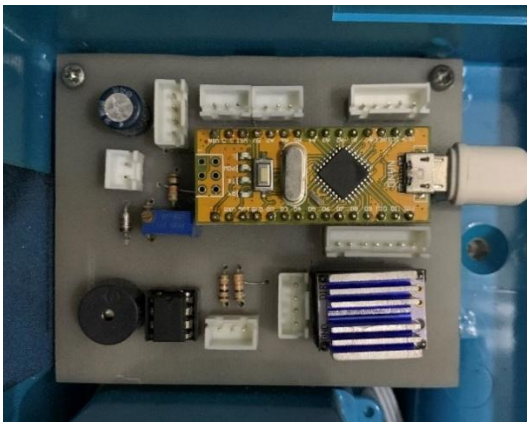

Figure 11. Electronics Board

3.3. Performance Testing

Furthermore, the results of implementing the fuzzy-PI control design on the infusion pump machine were standardized measurements using the Infusion Device Analyzer (IDA) calibration measuring tool. Measurements were performed 5 times with a 10-minute break between each data collection. Figure 18 shows the measurement technique; the results are recorded in Tables 2 and 3.

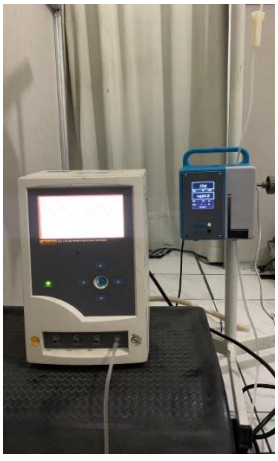

Figure 12. Documentation of Flow rate data collection process using IDA

JURNAL ECTIPE
Electronic, Control, Telecommunication, Information, and Power Engineering
Volume 12, Issue 1, April 2025, pp. 20-30
ISSN 2355-5068 ; e-ISSN 2622-4852
DOI: 10.33019/jurnalecotipe.v12i1.4541

Table 2. Flow rate measurement results

Set point (ml/h)	Flow rate Tertampil (ml/h)	Flow rate terukur (ml/h)				
		1	2	3	4	5
25	25	25,40	25,46	25,47	25,42	25,43
50	50	50,44	50,48	50,31	50,25	50,31
75	75	75,11	75,07	75,23	75,10	75,23
100	100	100,11	100,01	100,05	100,04	100,04
125	125	125,40	125,37	125,34	125,34	125,33
150	150	150,98	151,09	151,21	151,24	151,27

In Table 6a, the data is obtained by recording the flow rate on the infusion pump display and compared with the actual flow rate measurement using the IDA analyzer in real-time. Actual flow rate data was taken 5 times with a data collection range of 10 minutes. If we observe the tool's performance at each set point, the infusion pump can reach the set point and maintain the flow rate at the set point. This indicates that the PI control system on the infusion pump is working correctly.

Table 3. Results calculation

Mean (ml/h)	correction value (ml/h)	Relative Correction (%)	Max (ml/h)	Min (ml/h)	Accuracy (%)	Stability
25,44	0,44	1,73	25,47	25,40	98,27	0,07
50,36	0,36	0,72	50,48	50,25	99,28	0,23
75,15	0,15	0,20	75,23	75,07	99,80	0,16
100,05	0,05	0,05	100,1	100	99,95	0,1
125,36	0,36	0,28	125,4	125,3	99,72	0,07
151,16	1,16	0,77	151,3	151	99,23	0,29

In table 3, data table 2 is processed to produce numbers used to analyze the system's success, namely accuracy, relative correction, and stability from 5 tests at the target value to be achieved. Relative correction is the correction value to the average value multiplied by 100%. The accuracy of the presentation calculation is obtained from 100 minus the relative correction value. Meanwhile, the stability value is the difference between the maximum data and the minimum data.

From the data obtained, such as accuracy, relative correction, and stability, the Correlative correction obtained with the highest correction percentage permitted by ECRI is 10%. From the data above, the relative correction of measurements at each set of points is only 2%, far below the maximum limit. Accuracy is the ability of a tool to reach a target. If it is closer to the target, it is more accurate. The data above shows that the minimum accuracy is 98.26%, and the maximum accuracy is 99.95%. WHO recommends a maximum specification of ±5% of the set point. Compared with WHO provisions, the tool results show good accuracy—the more excellent the accuracy, the better the tool's performance. In terms of stability level, with a stability value of 0.29 at set point 150 and 0.07 at set point 25, the maximum flow stability allowed is 2 ml/h. This shows good stability.

Volume 12, Issue 1, April 2025, pp. 20-30
ISSN 2355-5068 ; e-ISSN 2622-4852
DOI: 10.33019/jurnalecotipe.v12i1.4541

4. CONCLUSION

From the results obtained, it can be concluded that the PI control system applied to the infusion pump can work well, as proven by simulation results and direct application, and the machine can reach and maintain the flow rate at the set point. It has been proven that the relative correction value obtained is still far from the limit allowed by ECRI, namely 10%. In terms of accuracy, the infusion pump that can be made can reach an accuracy of above 98%, meaning that the greater the accuracy, the infusion pump can enter the drug dose accurately according to the patient's needs and, of course, avoid over-dose and under-dose. In terms of stability, it also shows good results, namely less than 0.3 ml/h, which means it is safe if used for a long time. Modifying the control or combining control methods allows for the optimization of rise time while still paying attention to overshot and real-time flow rate synchronization.

Acknowledgments

Thank you to Mr. Nana, who is my thesis mentor at PNJ. I can establish myself as someone who can pursue the field of control systems.

REFERENCES

[1] Menteri Kesehatan Republik Indonesia, "Standar Pelayanan Kefarmasian Republik Indonesia di Rumah Sakit," Indonesia, 2016.

[2] A. Hasan Basri and A. Taufiq, "Hubungan Tingkat Stress Kerja Perawat IGS Dengan Ketepatan Waktu Pemberian Obat High Alert," *J. Ners Community*, vol. 12, no. 02, pp. 258–267, 2021.

[3] P. Studi and T. Elektromedik, "Efektivitas Penggunaan Infuse Pump Terhadap Pasien," *BALI Heal.*, vol. 2, no. November, p. 69, 2018.

[4] E. Greau *et al.*, "Automatic versus manual changeovers of norepinephrine infusion pumps in critically ill adults: a prospective controlled study," *Ann. Intensive Care*, vol. 5, no. 1, pp. 1–9, Dec. 2015, doi: 10.1186/s13613-015-0083-7.

[5] E. A. Smith and G. Gray, "Developing a Smart Infusion Pump Dedicated to Infusion Safety," *Ergon. Des.*, vol. 30, no. 2, pp. 4–12, 2022, doi: 10.1177/1064804620944760.

[6] World Health Organization, "Technical specifications for infusion devices," in *Technical specifications for infusion devices*, World Health Organization, 2020. [Online]. Available: https://ismp.org

[7] M. Baeckert *et al.*, "Performance of modern syringe infusion pump assemblies at low infusion rates in the perioperative setting," *Br. J. Anaesth.*, vol. 124, no. 2, pp. 173–182, Feb. 2020, doi: 10.1016/j.bja.2019.10.007.

[8] R. T. Yunardi, D. Setiawan, F. Maulina, and T. A. Prijo, "Pengembangan Sistem Kontrol dan Pemantauan Tetesan Cairan Infus Otomatis Berbasis Labview dengan Logika Fuzzy," *J. Teknol. Inf. dan Ilmu Komput.*, vol. 5, no. 4, p. 403, Oct. 2018, doi: 10.25126/jtiik.201854766.

[9] W. Syahputra, "Aspek Klinis dan Tatalaksana Emboli Paru pada Anak," *Ked. N. Med* |, vol. 4, no. 1, pp. 22–29, 2021.

[10] C. Wang and D. Cao, "New sensorless speed control of a hybrid stepper motor based on fuzzy sliding mode observer," *Energies*, vol. 13, no. 18, Sep. 2020, doi: 10.3390/en13184939.

[11] M. S. Zaky, "A self-tuning PI controller for the speed control of electrical motor drives," *Electr. Power Syst. Res.*, vol. 119, pp. 293–303, 2015, doi: 10.1016/j.epsr.2014.10.004.

[12] K. M. Le, H. Van Hoang, and J. W. Jeon, "An Advanced Closed-Loop Control to Improve the Performance of Hybrid Stepper Motors," *IEEE Trans. Power Electron.*, vol. 32, no. 9, pp. 7244–7255, 2017, doi: 10.1109/TPEL.2016.2623341.

[13] B. C. Wibowo and F. Nugraha, "Kendali Kecepatan Motor Stepper Menggunakan Metode Start

Volume 12, Issue 1, April 2025, pp. 20-30
ISSN 2355-5068 ; e-ISSN 2622-4852
DOI: 10.33019/jurnalecotipe.v12i1.4541

– Stop Berbasis PLC," *J. Tek. Elektro dan Komput.*, vol. 10, no. 3, p. 213, 2021, doi: 10.35793/jtek.10.3.2021.35623.

[14] A. A. P. Anggiana, M. Rifa'i, and H. K. Safitri, "Implementasi sistem kontrol penggerak motor stepper pada proses molding microplastic berbasis PID menggunakan PLC," *J. Eltek*, vol. 21, no. 2, pp. 58–67, 2023, doi: 10.33795/eltek.v21i2.2024.

[15] I. Kholis, "Pemodelan Sistem Pengendali PID Dengan Metode Ciancone Berbasis MATLAB Simulink pada Sistem Pressure Process RIG 38-714," *J. Tek. dan Ilmu Komput.*, vol. 06, no. 23, pp. 257–268, 2017.

JURNAL ECOTIPE
Electronic, Control, Telecommunication, Information, and Power Engineering

Volume 12, Issue 1, April 2025, pp. 31-42
ISSN 2355-5068 ; e-ISSN 2622-4852
DOI: 10.33019/jurnalecotipe.v12i1.4542

Development and Design A Queue Service System Banyumudal Health Center Using the Waterfall Method

Wifqi Wifakul Azmi[1], Yohani Setiya Rafika Nur[2]
[1,2]Informatic Engineering, Telkom University, Purwokerto, Jawa Tengah 53147, Indonesia

ARTICLE INFO

Article historys:

Received : 10/02/2025
Revised : 25/02/2025
Accepted : 14/04/2025

Keywords:

Black Box; Community Health Center Services; Design and Build; Waterfall

ABSTRACT

Puskesmas Banyumudal is a health care facility in Pemalang Regency, located at KM 1, Banyumudal, Jalan Raya Moga-Karangsari, Moga District, Central Java. This health center aims to improve the standard and equity of health services for all levels of society. one of the main obstacles that is often faced is the lack of management of patient queues that still use manual systems, causing long and irregular queues resulting in inefficient and ineffective patient waiting times. this research was conducted to build a more efficient and effective Banyumudal Health Center queue service system. by using the waterfall method, through this system, it is hoped that service efficiency will increase by reducing the duration of patient queues and improving better service quality. This method involves clear stages, starting from analyzing needs, designing designs, and testing. The results of the study show that the application of the waterfall method in the development of the Banyumudal health center queuing service system is able to improve queue management efficiently and effectively and provide information to patients regarding queue status, as well as facilitate health center officers and doctors in monitoring the queuing process. blackbox testing results show that all systems function properly according to predetermined specifications. thus, the queuing system designed is expected to have a positive impact on improving the quality of queuing services at the Banyumudal Health Center.

Corresponding Author:

Yohani Setiya Rafika Nur
Informatic Engineering, Telkom University, Purwokerto, Indonesia
Email: yohanin@telkomuniversity.ac.id

1. INTRODUCTION

Banyumudal Community Health Center is a health care facility in Pemalang Regency, Central Java. The motto of the Banyumudal Health Center is “Healthy people, Happy people” with the intention of improving the quality and equitable distribution of health services so that it can be felt by all levels of society. in order to improve public services, all state institutions are required to build websites in accordance with Presidential Instruction Number 07 of 2003 establishing national policies and plans for building E-Government. therefore the quality of health services is needed to be better for an effective and efficient service system [1]. one of the main challenges faced by Puskesmas is patient queue management, which can affect the efficiency and quality of services provided.

Queues are conditions in which several people or objects are in a certain order to wait for their turn and people often experience queues in public places such as banks and hospitals, as well as other places where they can get public services [2]. queues occur because the capacity of facilities and services exceeds the demand for services, so there will be queues. queuing situations are conditions that occur as part of random operational activities within a service facility. In addition, many health centers still use

JURNAL ECOTIPE
Electronic, Control, Telecommunication, Information, and Power Engineering
Volume 12, Issue 1, April 2025, pp. 31-42
ISSN 2355-5068 ; e-ISSN 2622-4852
DOI: 10.33019/jurnalecotipe.v12i1.4542

manual methods in recording patient visits that come on that day, which has an impact on the performance and efficiency of the health center and reduces services to patients [4]. manual queues can cause inconvenience to patients seeking treatment. therefore, it is necessary to design and require a queuing system that can be organized and managed to be organized and comfortable [5].

At the Banyumudal Health Center, there is a problem in managing patient queues that still use a manual system, causing long and irregular queues that can result in inefficient and ineffective patient waiting times. the manual system also results in a lack of queue information so that patients do not know the order number that has been called, so patients have to stay around the registration area to make sure they don't miss their turn in the queue. thus, based on these conditions, there is a need for a solution that is more efficient and effective in managing the patient queue [6]. The website-based queuing system is expected to be an alternative solution to overcome the queuing problem at the Banyumudal Health Center, so as to improve service efficiency by reducing patient waiting time and providing a better experience for patients as a whole [7]. with this system, patients can register practically through the website, avoid long physical queues and allow them to get queue numbers digitally.

Based on the above background, the purpose of this study is to design and build a system to improve the queuing service of Banyumudal Health Center which is more efficient and effective. the Waterfall method was chosen because it provides a structured and systematic framework. this method involves clear stages, starting from initial needs analysis, system planning, implementation, testing and maintenance. each step must be completed before going to the next step, to ensure every aspect of development gets enough attention. thus it is hoped that through this research, it can reduce patient waiting time, improve patient experience, and help Puskesmas officers manage queues better.

2. RESEARCH METHOD

This research involves several stages that must be passed. The following is a research flow chart that describes the research process for compiling this report. can be seen in Figure 1

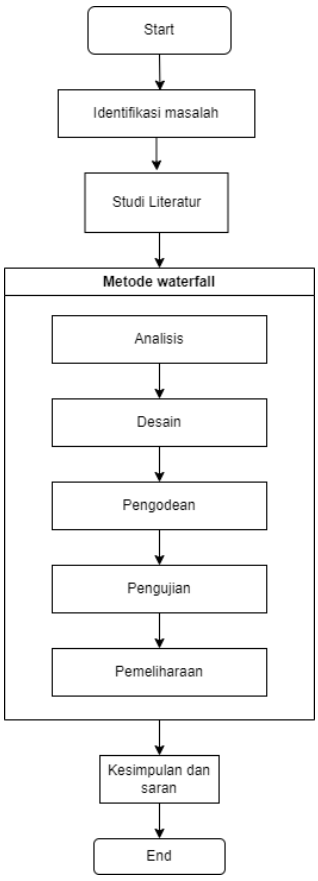

Figure 1. Research Flow Diagram

JURNAL ECOTIPE
Electronic, Control, Telecommunication, Information, and Power Engineering
Volume 12, Issue 1, April 2025, pp. 31-42
ISSN 2355-5068 ; e-ISSN 2622-4852
DOI: 10.33019/jurnalecotipe.v12i1.4542

2.1. Problem Identification

This stage is a step to identify problems that aim to identify obstacles in the queuing service used at the Banyumudal Health Center. This activity is carried out to analyze existing problems in depth, so that the designed solution can provide an improvement in the quality of queuing services at the Banyumudal Health Center.

2.2. Literature Review

At this stage, it is necessary to conduct a theoretical basis and references related to the design of information systems obtained from various sources, including previous books and journals. This literature study aims to add to the understanding of the concepts and theories needed for this research.

2.3. Analysis

In the analysis stage, data collection and evaluation are carried out to identify user needs and the required system. in this analysis stage includes identifying the process of collecting data to obtain information from user needs. the data collection method used in this analysis stage is through observation, and direct interviews with the Banyumudal Health Center.

2.4. Design

After analyzing the necessary requirements, the next step is the design stage which is the design stage in which the software structure is designed based on the previously identified requirements specifications. at this design stage, some important elements that will be explained include *Use case diagrams*, *Activity diagrams*, and basic user interface (UI) designs. these elements are designed to ensure each element of user requirements and functionality is met.

2.5. Coding

After the design step, the next stage is coding, at this stage, PHP will be used as a programming language and MySQL as a database management system. the coding stage will be implemented into a web-based system program that will be used by patients, doctors and Puskesmas admins.

2.6. Testing

In this step to ensure that the solution that has been created can operate effectively and provide the best results, testing is needed. at this stage, the method used is *Black Box* Testing. *Black Box* Testing is a test used to describe a system or element designed to perform testing, without the need to examine the details of the program implementation in it. As for testing the actors involved in this system, namely admin, doctor, and patient.

Table 1. User Testing

No	User	Description
1.	Admin	Admin is a user who has full access to the queue service system. his duties include data management and system settings,
2.	Doctor	Doctors are users who have access to view the patient queue list as a whole. In addition, doctors can see the status of the queue being handled.
3.	Patient	Patients are users who can register queues independently through the system. In addition, patients can also see the available service schedule and see the history of previous queues.

2.7. Maintenance

At the maintenance stage is a system that has been developed. The main focus is to ensure the system continues to function properly, perform regular updates, and fix errors.

JURNAL ECOTIPE
Electronic, Control, Telecommunication, Information, and Power Engineering
Volume 12, Issue 1, April 2025, pp. 31-42
ISSN 2355-5068 ; e-ISSN 2622-4852
DOI: 10.33019/jurnalecotipe.v12i1.4542

3. RESULTS AND DISCUSSION

3.1 Analysis

The analysis stage was carried out after conducting direct observations and interviews with Banyumudal Health Center officers. This process aims to understand real user needs and identify the main problems that occur in the current queuing system. Based on the results of data collection in the field, it was found that patient queue management was still done manually. Patients must come directly to the health center and register by showing an identity card, which often causes long lines and inefficient waiting times. These findings are the main basis for the need to develop a website-based queuing system. the proposed system offers a more effective and efficient solution, allowing patients to register and collect queue numbers online without having to come directly to the service location.

This research applies a systematic approach in exploring user needs through direct interaction in the field, as well as designing digital technology solutions specifically aimed at solving problems at the Banyumudal Health Center. therefore, the development of this system is an innovative step that is expected to improve the quality of public health services at Puskesmas Banyumudal. With the implementation of this system, patients are expected to no longer experience long physical queues, so that the service process becomes efficient and organized. Based on these conclusions, the analysis of the needs required in the development of the queuing system for the banyumudal puskesmas is as follows:

Table 2. Functional requirements

Actor	System Requirements
Patient	- Patients can create a new queue through the system - Patients can view information about queue numbers, queue status, and estimated waiting time. - Patients can view the service schedule - Patients can view queue history
Doctor	- Doctors can view a list of patients who are queuing. - Doctors can access detailed information on the queue of patients being treated.
Admin	- Admin have access to the dashboard to manage the system. - Admin can see the list of patients who are queuing. - Admin can provide information to patients regarding their queue status. - Admin can add new entries for admin, and doctor data into the system. - Admin can edit existing information for admin, patient, and doctor data. - Admin have the ability to delete entries that are no longer required from admin, patient, and doctor data. - Admin can access reports or history of completed patient queues.

3.2 System Design

System design is an important stage in the software development process, which aims to design the structure, workflow, and main components of the system so that it can run as needed. In this study, system design was carried out with a focus on developing a website-based queuing system that was tailored to the conditions and needs at the Banyumudal Health Center.

This design process includes three main aspects, namely the design of Use Case Diagrams, Activity Diagrams, and Interface Design (Wireframe). These three elements are used to illustrate how the system will interact with users, as well as how the flow of the queue registration process takes place online.

1. Use Case Diagram

Use Case Diagram explains the intertwined relationship between users and the Banyumudal Health Center queuing service system. This diagram is a system analysis and design process, because it helps visualize the main functions and interactions that occur in system development. The following is a Use Case Diagram that is applied to the Banyumudal Health Center Queuing Service System.

JURNAL ECOTIPE
Electronic, Control, Telecommunication, Information, and Power Engineering
Volume 12, Issue 1, April 2025, pp. 31-42
ISSN 2355-5068 ; e-ISSN 2622-4852
DOI: 10.33019/jurnalecotipe.v12i1.4542

Figure 2. *Use Case* Diagram *User* Pasien, Doctor and Admin

2. Activity Diagram

Activity Diagram, also known as Activity Diagram, is a visual representation used to show and explain the stages in a process that takes place in a system. The following is an activity diagram applied to the Banyumudal Health Center Queuing Service System.

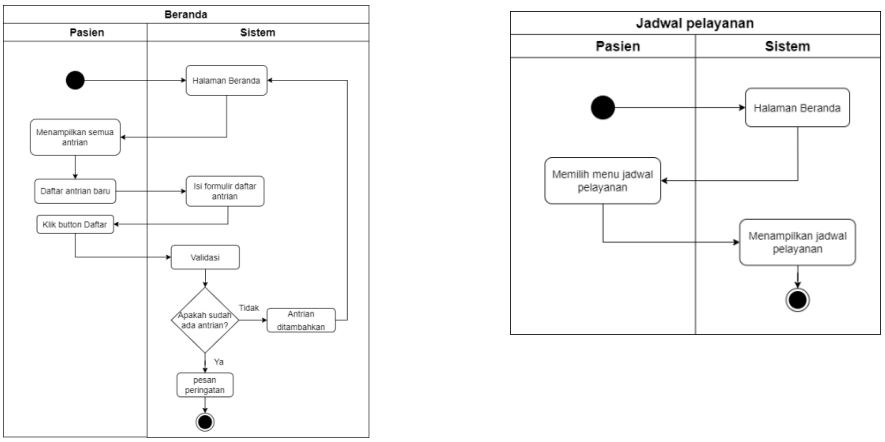

Figure 3. *Activity* Diagram *User* Pasien

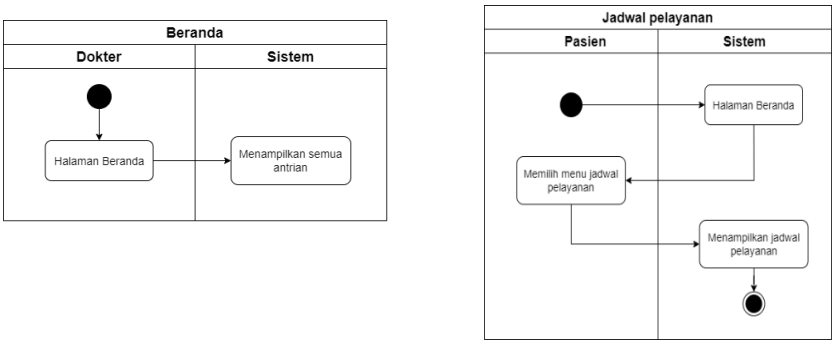

Figure 4. *Activity* Diagram *User* Doctor

JURNAL ECOTIPE
Electronic, Control, Telecommunication, Information, and Power Engineering
Volume 12, Issue 1, April 2025, pp. 31-42
ISSN 2355-5068 ; e-ISSN 2622-4852
DOI: 10.33019/jurnalecotipe.v12i1.4542

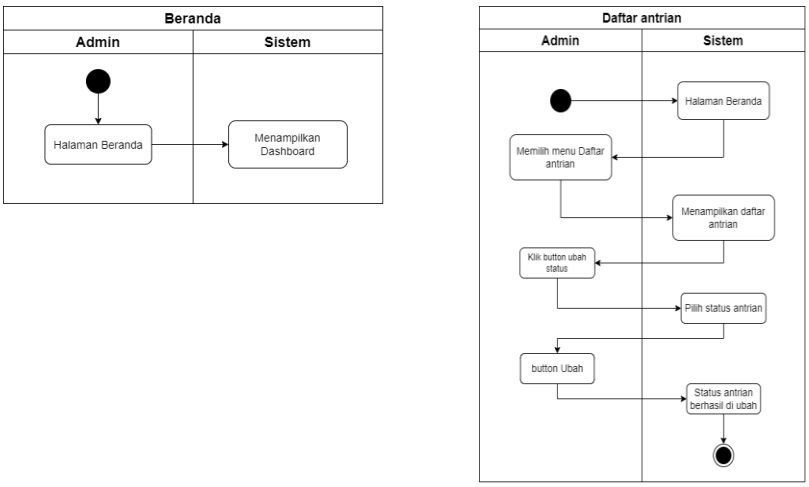

Figure 5. *Activity* Diagram *User* Admin

3. Design Interface (*Wireframe*)

The following are some pages in the basic design interface for the Banyumudal Health Center queuing system:

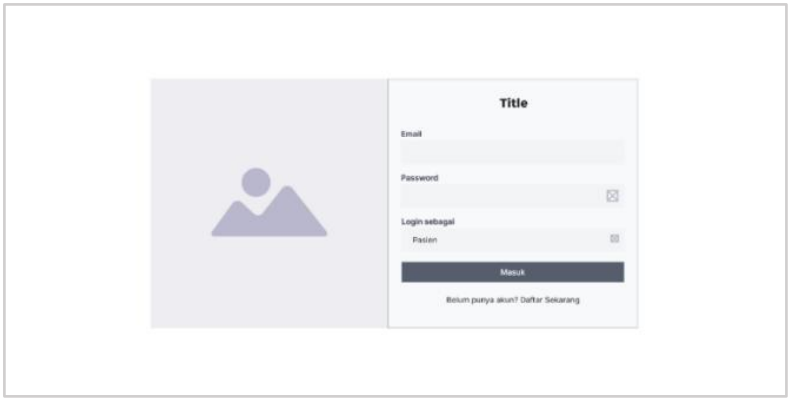

Figure 6. *Design Interface* Patient, Doctor and Admin Login

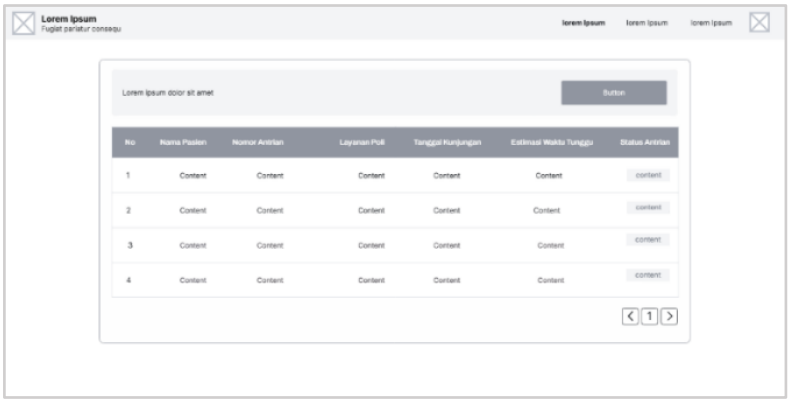

Figure 7. *Design Interface* Patient User Home Page

JURNAL ECTIPE
Electronic, Control, Telecommunication, Information, and Power Engineering
Volume 12, Issue 1, April 2025, pp. 31-42
ISSN 2355-5068 ; e-ISSN 2622-4852
DOI: 10.33019/jurnalecotipe.v12i1.4542

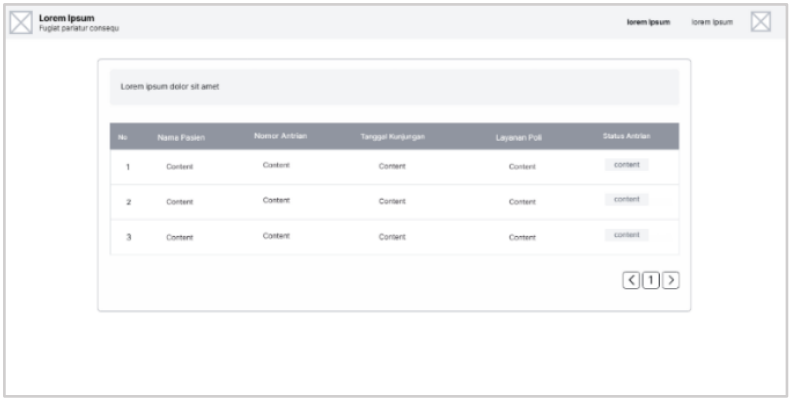

Figure 8. *Design Interface* Doctor User Home Page

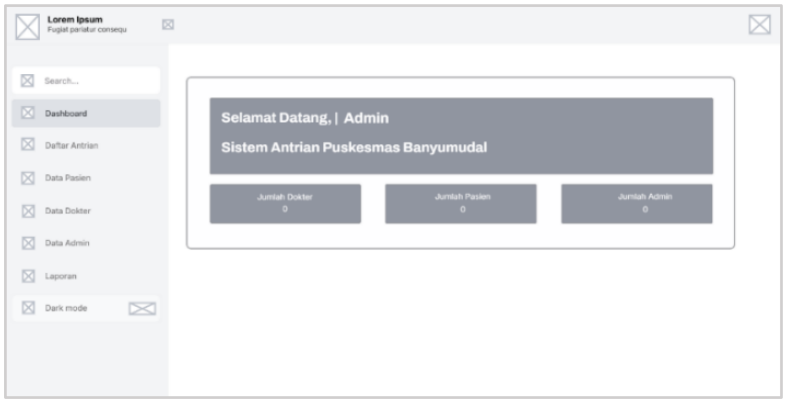

Figure 9. *Design Interface* Halaman dashboard Admin

3.3 Results of the Health Center Queuing Service System Website

The following is a view of the website of the queuing service system for puskesmas banyumudal.

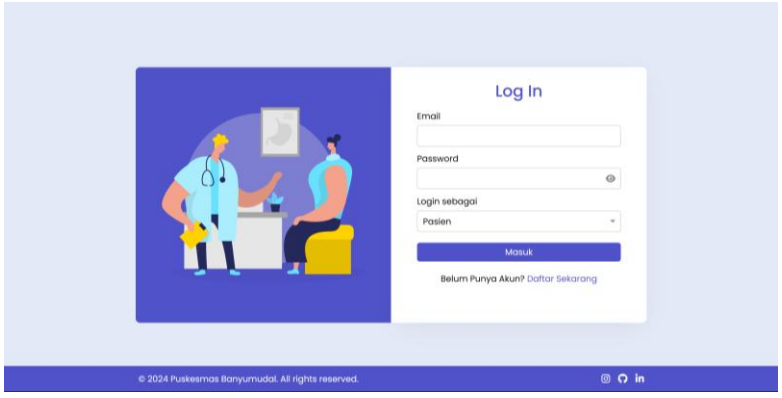

Figure 10. Page Login Patient, Doctor and Admin

In Figure 5 is the login page for patients, doctors and admins to enter the puskesmas queuing system. on this page, User patients, doctors and admins are asked to enter email, password, and select a role. If the data entered is valid, the system will direct the patient to the home page.

JURNAL ECTIPE
Electronic, Control, Telecommunication, Information, and Power Engineering
Volume 12, Issue 1, April 2025, pp. 31-42
ISSN 2355-5068 ; e-ISSN 2622-4852
DOI: 10.33019/jurnalecotipe.v12i1.4542

Figure 11. Home Page User Patient

In Figure 11 is a patient home page that displays a list of all existing queues. on this page, there is a button to register a new queue.

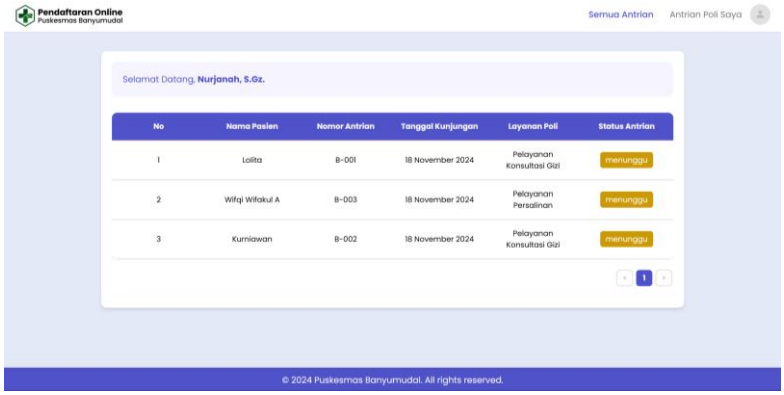

Figure 12. Home Page User Doctor

In Figure 12 is a doctor's home page that displays a list of all existing queues. on this page, doctors can see information about patients who are queuing.

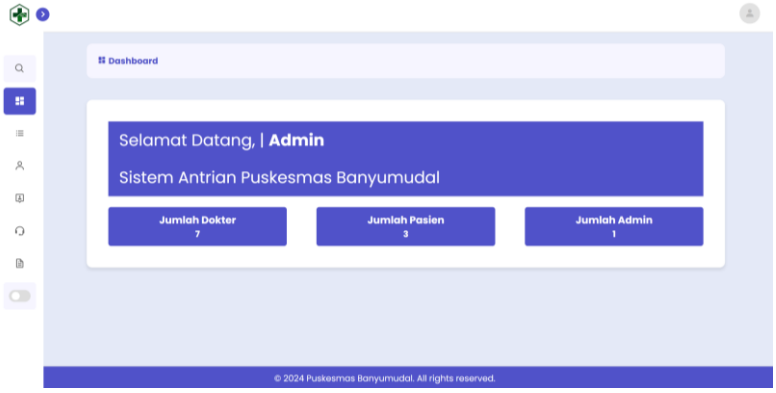

Figure 13. Admin User Dashboard Page

In Figure 13 is the admin dashboard home page that displays information on the number of doctors, patients, and admins. on this page provides a summary of data that is easily accessible by the admin to see the total number of registered doctors, the number of registered patients, and the number of admins in the system.

JURNAL ECOTIPE
Electronic, Control, Telecommunication, Information, and Power Engineering
Volume 12, Issue 1, April 2025, pp. 31-42
ISSN 2355-5068 ; e-ISSN 2622-4852
DOI: 10.33019/jurnalecotipe.v12i1.4542

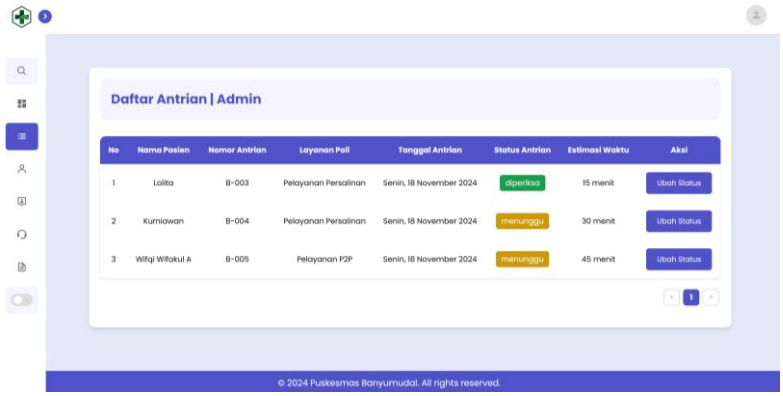

Figure 14. Admin User Queue List Management Page

In Figure 4.113 is the User admin queue list page that displays all patient queue lists. on this page displays all active patient queues, with related information such as queue number and patient status. admins can view the list to monitor ongoing patient queues.

3.4 Blackbox System Testing

After the system development stage is complete, a testing process is carried out to ensure that all system functions run as they should. Testing is carried out using the Blackbox Testing method, which is a test focused on observing system outputs based on certain inputs, without examining internal code.

This method is used to identify logic errors, input-output flow errors, and ensure that key features such as registration, queue number retrieval, and login access run correctly. at this stage, structured and thorough test documentation is carried out on the puskesmas banyumudal queuing system, This process also ensures that the system is ready to be used directly by users.

Table 3. Patient User Testing Table

No	Scenario Testing	Test Case	Expected results	Results	Conclusion
1.	Patient home page	Patient home page displayed after successful login	The system will display the patient's name, the “New Queue List” button, and display the list of active patient queues.	Passed	Valid
2.	New queue list	Click the Register New Queue button	The system will display a pop up modal form for queue registration	Passed	Valid
3.	Service Schedule Menu	Click on the service schedule menu	The system will display the service schedule page	Passed	Valid
4.	Menu Riwayat Antrian	Click on the queue history menu	The system will display the queue history page	Passed	Valid
5.	View queue history details	Click or select the details button	The system will display the queue history detail page	Passed	Valid

JURNAL ECOTIPE
Electronic, Control, Telecommunication, Information, and Power Engineering
Volume 12, Issue 1, April 2025, pp. 31-42
ISSN 2355-5068 ; e-ISSN 2622-4852
DOI: 10.33019/jurnalecotipe.v12i1.4542

Table 4. Doctor User Testing Table

No	Scenario Testing	Test Case	Expected results	Results	Conclusion
1.	Doctor Home Page	The doctor's home page is displayed after a successful login	The system will display all active patient queue lists.	Passed	Valid
2.	My poly queue menu	Click on My poly queue menu	The system will display my poly queue page	Passed	Valid
3.	Menu View patient queue data details	Click or select the details button	The system will display a pop up of patient queue data details	Passed	Valid

Table 5. Admin User Testing Table

No	Scenario Testing	Test Case	Expected results	Results	Conclusion
1.	Admin Dashboard Page	Admin Dashboard page displayed after successful login	The system will display data on the number of doctors, number of patients, and number of admins	Passed	Valid
2.	Queue list menu to see the queue list page display	Click the queue list menu	The system will display the queue list page	Passed	Valid
3.	Patient data menu to display the patient data management page	Click the patient data menu	The system will display the patient data management page	Passed	Valid
4.	Doctor data menu to display the doctor data management page	Click the doctor data menu	The system will display the doctor data management page	Passed	Valid
5.	Admin data menu to display the admin data management page	Click the admin data menu	The system will display the admin data management page	Passed	Valid
6.	Report menu to display the Report page	Click the report menu	The system will display the completed queue report page	Passed	Valid

Based on the results of tests that have been carried out on each user, accurate data and conclusions are obtained. This indicates that the system functions properly and in accordance with predetermined needs.

3.5 Maintenance of the System

At this stage, system maintenance is carried out to ensure that the system continues to run optimally and can adapt to changes or obstacles that may arise during use. The following are the maintenance steps that will be carried out regularly, including solutions to problems that may arise, such as errors on the login page, popups that do not appear, or home pages that cannot be clicked.

Conduct periodic system evaluations to ensure that the Banyumudal Health Center queuing service system still meets user needs and meets the desired performance standards. This evaluation includes:

a) Daily Evaluation:

JURNAL ECOTIPE
Electronic, Control, Telecommunication, Information, and Power Engineering
Volume 12, Issue 1, April 2025, pp. 31-42
ISSN 2355-5068 ; e-ISSN 2622-4852
DOI: 10.33019/jurnalecotipe.v12i1.4542

Checking whether there are problems such as login errors or problems not being able to access the main page.

b) Weekly Evaluation:
Evaluate the performance of the queuing system so that it runs optimally and meets user needs.

c) Monthly Evaluation:
Evaluating user feedback and analyzing the overall performance of the system.

Perform regular data backups by copying and storing data to a secure location. The goal is to prevent data loss or data corruption that can occur due to system failure The following is a backup schedule:

a) Daily Backup:
Stores constantly changing data, such as patient information and queue schedules, to avoid data loss due to technical difficulties.

b) Weekly Backup:
Performs a more complete backup that covers the entire system, including login settings and user data.

c) Monthly Backup:

d) Perform a full backup of the entire system and database to protect data from damage or loss.

4. CONCLUSION

Based on the results of the discussion related to the development of the banyumudal puskesmas queuing service system, the researchers concluded as follows:

1. The queuing service system was successfully developed using the Waterfall method which is applied by going through the stages of needs analysis, design, and testing. Each stage is carried out sequentially to ensure that the system developed is in accordance with user needs. The queuing service system that has been designed is able to improve queue management, provide information to patients regarding queue status, and make it easier for Puskesmas officers and doctors to monitor the queuing process.
2. Testing the system with a Black Box Testing approach shows that all functions in the system operate in accordance with predetermined specifications. This test involves the role of patients, doctors, and Puskesmas officers, where the results prove that each component of the system provides outputs that match expectations and function properly.

REFERENCES

[1] Al Faruq, U. (2023). Rancang bangun aplikasi rekam medis poliklinik universitas trilogi. J. Inform, 9(1), 1017-1027.

[2] Murodi, A. (2023). Sistem Informasi Nomor Antrian Pasien Berbasis Web. ProTekInfo (Pengembangan Riset dan Observasi Teknik Informatika), 10(1), 6-10.

[3] R. Kurniati dan J. Jaroji, "Sistem Antrian Multi Channel Rumah Sakit Berbasis Web," INOVTEK Polbeng - Seri Informatika, vol. 3, no. 2, hlm. 140, Nov 2018, doi: 10.35314/isi.v3i2.827.

[4] Syah, V. A., & Farell, G. (2024). Rancang Bangun Sistem Informasi Antrian Pengambilan Obat Berbasis Web. Scientica: Jurnal Ilmiah Sains dan Teknologi, 2(4), 109-115.

[5] R. A. Zulfikar dan A. A. Supianto, "Rancang Bangun Aplikasi Antrian Poliklinik Berbasis Mobile," Jurnal Teknologi Informasi dan Ilmu Komputer, vol. 5, no. 3, hlm. 361, Agu 2018, doi: 10.25126/jtiik.201853891.

[6] Dewi, L. F., Zaidiah, A., & Matondang, N. (2021, July). Perancangan Website Sistem Informasi Pelayanan Rawat Jalan Pada Puskesmas Benda Baru Pamulang. In Prosiding Seminar Nasional Mahasiswa Bidang Ilmu Komputer dan Aplikasinya (Vol. 2, No. 1, pp. 137-147).

JURNAL ECOTIPE
Electronic, Control, Telecommunication, Information, and Power Engineering
Volume 12, Issue 1, April 2025, pp. 31-42
ISSN 2355-5068 ; e-ISSN 2622-4852
DOI: 10.33019/jurnalecotipe.v12i1.4542

[7] U. Tsani Abdurrahman, D. Nursanto, M. Anas Sobarnas, K. Kunci, dan P. kesehatan, "Rancang bangun aplikasi sistem booking pendaftaran berobat pasien poliklinik (simbolik) berbasis android menggunakan metode agile scrum", doi: 10.37373/infotech.v5i1.963.

[8] Alex, K. D. J., Feoh, G., & Gunawan, P. W. (2023). Rancang Bangun Sistem Informasi Rekam Medis Pasien Rawat Jalan Berbasis Web (Studi Kasus: Puskesmas Kanatang). Jurnal Kesehatan, Sains, Dan Teknologi (Jakasakti), 2(1).

[9] M. Fadhli, Dini Nurmalasari, dan Memen Akbar, "Penggunaan Metode FIFO pada Real-Time Monitoring Antrian Pendaftaran Pasien Puskesmas Berbasis Web," Jurnal Komputer Terapan, vol. 9, no. 1, hlm. 39–49, Jun 2023, doi: 10.35143/jkt.v9i1.5915.

[10] Mahdiah, S., & Irwanto, D. (2023). Rancang Bangun Sistem Informasi Manajemen Posyandu Berbasis Web pada Puskesmas Kalanganyar. Oktal: Jurnal Ilmu Komputer dan Sains, 2(04), 1082-1089.

[11] Sahal, A., Zaidir, Z., & Aini, F. N. (2023). Rancang Bangun Sistem Informasi Pelayanan pada Pusat Kesehatan Masyarakat. Progresif: Jurnal Ilmiah Komputer, 19(1), 81-92.

[12] Ardimansyah, A., Rahman, B., & Syam, A. (2023). Perancangan Sistem Informasi Antrian Pasien Puskesmas Berbasis Website Menggunakan Metode Queue (Studi Kasus: Puskesmas Antang). In SISITI: Seminar Ilmiah Sistem Informasi dan Teknologi Informasi (Vol. 12, No. 1, pp. 533-539).

[13] E. Haryanto, "Queuing System Dengan Voice Untuk Rumah Sakit Atau Klinik Menggunakan Php Mysql Dengan Konsep First In First Out", doi: 10.13140/RG.2.2.14972.10886.

[14] Usada, E., Yuniarsyah, Y., & Rifani, N. (2022). Rancang bangun sistem informasi jadwal perkuliahan berbasis jquery mobile dengan menggunakan php dan mysql. Jurnal Infotel, 4(2), 40-51.

JURNAL ECOTIPE
Electronic, Control, Telecommunication, Information, and Power Engineering

Volume 12, Issue 1, April 2025, pp. 43-53
ISSN 2355-5068 ; e-ISSN 2622-4852
DOI: 10.33019/jurnalecotipe.v12i1.4551

Optimization of Small-Scale Coffee Roasting Machine with Servo Temperature and Angle Control for Consistent Roasting Results

Hendi Purnata[1], Supriyono[2], Raafi Absor[3] , Marshal Kurniabayu[4]
[1] Mechatronics Engineering, Cilacap State of Polytechnic, Jl. Dr. Soetomo No. 1, Cilacap 53212, Indonesia
[2,3,4] Electronics Engineering, Cilacap State of Polytechnic, Jl. Dr. Soetomo No. 1, Cilacap 53212, Indonesia

ARTICLE INFO

Article historys:

Received : 28/02/2025
Revised : 07/03/2025
Accepted : 02/04/2025

Keywords:

Coffee Roasting Machine; IoT Blynk; Monitoring System; Servo Angle; Remote Monitoring; Temperature Control; Thermocouple

ABSTRACT

The coffee roasting process is essential for creating distinctive aromas and Flavors. Manual roasting often results in uncontrolled temperatures, resulting in uneven and burnt coffee beans. Therefore, an automatic roasting machine was developed to control stable temperatures at setpoints of 180°C (light roast), 220°C (medium roast), and 250°C (dark roast), with a monitoring system to ensure optimal results. Servo angle settings are used to optimize temperature stabilization, while a DC fan serves to remove excess heat from the machine. The system uses an Arduino Uno and ESP32, with a Thermocouple Type K temperature sensor and an I2C LCD display for real-time monitoring. Integration with IoT Blynk allows remote monitoring and control through a mobile application. Research shows that a servo angle of 140° provides the optimal temperature increase, while an angle of 100° is effective for lowering the temperature when it exceeds the setpoint. These angles are used in the system to keep the temperature controlled according to the specified target.

Corresponding Author:

Hendi Purnata
Electronics Engineering, Cilacap State of Polytechnic, Jl. Dr. Soetomo No. 1, Cilacap 53212, Indonesia
Email: hendipurnata@pnc.ac.id

1. INTRODUCTION

Coffee is a grain that comes from highland plantations and is the main ingredient in making a very famous drink, not only in Indonesia, but also in various parts of the world[1]. Coffee originated in Yemen, which developed coffee into powder and then brewed it to produce a distinctive aroma that no other beverage has. Coffee quickly spread throughout the world and evolved in various processing methods, leading to unique and delicious flavors [2].

The coffee roasting process is an important stage that aims to produce the distinctive aroma and flavor of the coffee beans[3, 4]. The duration of roasting can be measured through changes in the color of the coffee beans, where a darker color indicates a longer roasting process[5]. The longer the roasting time, the darker the color of the coffee beans, this process involves heating green coffee beans to develop certain organoleptic properties through chemical reactions [4, 5].

As coffee evolves, so does the roasting process. Initially, roasting was done manually using a pan and hand stirrer[6, 7]. However, this method resulted in heat wastage due to uncovered pans, and required more time and labor[8, 9]. Research by [1] shows that the manual process causes uncontrolled temperatures, resulting in uneven roasting and burnt coffee beans. In addition, the manual process is less efficient when done on a large scale, which impacts the quality of the coffee.

Volume 12, Issue 1, April 2025, pp. 43-53
ISSN 2355-5068 ; e-ISSN 2622-4852
DOI: 10.33019/jurnalecotipe.v12i1.4551

Different degrees of roasting (light, medium, dark) are achieved by varying the temperature and time, which can be monitored by changes in the colour of the beans [10]. Optimal roasting temperatures range from 200°C to 300°C, with different profiles affecting the chemical composition and sensory qualities of the final product [11, 12]Roasting duration, including development time after the first crack, affects the flavour profile and chemical markers in coffee [4].

The impact of roasting on coffee quality in Roasting affects the bulk density, hardness, moisture content, ash content, pH level, and caffeine content of coffee beans [13]. Sensory properties, such as aroma, bitterness, acidity, and sweetness, are also affected by the roasting method and degree [14].

To overcome these problems, various studies have developed automatic roasting machines [8], [15]. Some studies such as [16, 17] the importance of temperature control in coffee roasting with flavour quality where the roasting process significantly affects the flavour profile of the coffee. Proper temperature control is essential to achieve the desired degree of roasting (light, medium, dark) and to develop specific Flavors. In addition, in order to achieve high consistency, traditional roasting methods often result in inconsistent roasting due to manual temperature management. An automatic temperature control system can ensure uniform roasting, improving the consistency and quality of the final product [16, 18, 19].

This technological solution by maintaining the temperature but ensuring that the actuator is a servo mechanism for the stirring mechanism ensures even heat distribution and uniform roasting. This reduces the need for manual intervention and minimizes the risk of uneven baking [20]. Therefore, for the development of making machines utilizing small-scale roasting machines which have accessibility are designed to be easy to use and do not require extensive training to operate, making them accessible to small business owners and home roasters [14].

Developing a small-scale coffee roasting machine with precise temperature control and servo mechanism fulfils the need for consistency, quality, and economic viability in coffee roasting for small businesses. The machine is designed to automatically regulate temperature and time using a heating element, but the results are still limited as the temperature achieved is only around 130°C, whereas to achieve optimal light roast results, the required temperature ranges from 160°C to 180°C. Coffee roasting types, such as light roast, medium roast, and dark roast, produce different characteristics and Flavors. Therefore, the developed roasting machine must be able to control the temperature accurately in order to produce roasting quality that complies with the standard.

2. RESEARCH METHOD

This research aims to develop an automatic coffee roasting machine that can control temperature stably and allow remote monitoring. The method used includes designing the system with block diagrams and flowcharts to describe the workflow and relationships between components, such as thermocouple temperature sensors, servo motors, and DC fans. After the system is designed, experiments are conducted to collect temperature data and test the effectiveness of the system in maintaining the temperature at the desired setpoint, using the Blynk application to monitor the temperature in real-time and control the machine remotely. With this approach, it is expected that the developed coffee roasting machine can produce coffee beans with consistent quality according to the specified standards.

2.1. Diagram Block

In this study, two block diagrams were used to describe the workflow of the automatic coffee roasting machine system. In Figure 1, the block diagram explains the *input* part, namely there are temperature sensors, rpm sensors and *switches* or *pushbuttons* which are then processed with a microcontroller and continued with the *output of* actuators such as *DC motors* controlled by motor drivers, 12V DC fans regulated by *relay* modules, and *servo motors* or *control valves* that regulate the *burner* or heater section.

JURNAL ECOTIPE
Electronic, Control, Telecommunication, Information, and Power Engineering
Volume 12, Issue 1, April 2025, pp. 43-53
ISSN 2355-5068 ; e-ISSN 2622-4852
DOI: 10.33019/jurnalecotipe.v12i1.4551

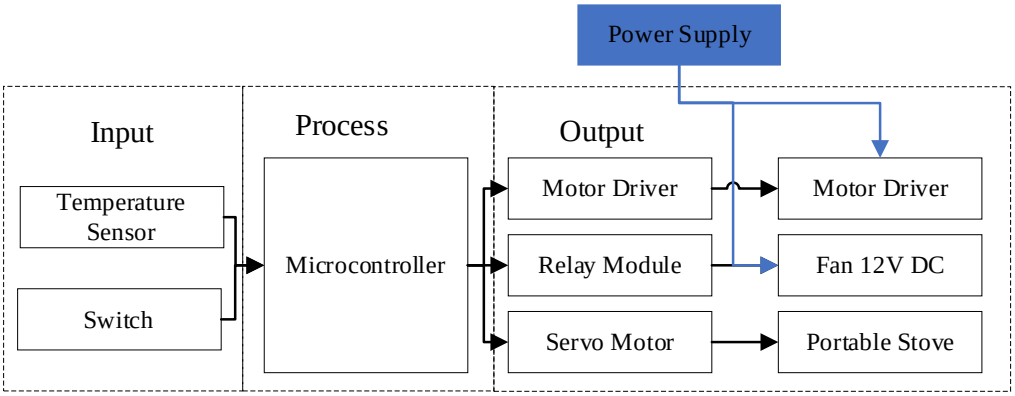

Figure 1. Actuator systems block diagram

The use of two microcontrollers, Arduino Uno and ESP32, in this system is made to take advantage of their respective strengths. Arduino Uno functions to read data from the temperature sensor and display it directly on the LCD with a fast response. Meanwhile, the ESP32 is responsible for sending temperature data to the Blynk platform, enabling remote monitoring and control via a mobile application. By dividing these tasks, each microcontroller can focus on its respective role, namely Arduino Uno for local data processing and ESP32 for wireless communication. This separation also provides redundancy and reliability, so that if one of the microcontrollers has a problem, the system can still run properly. This structure also opens opportunities to develop the system further in the future without changing many parts of the overall system.

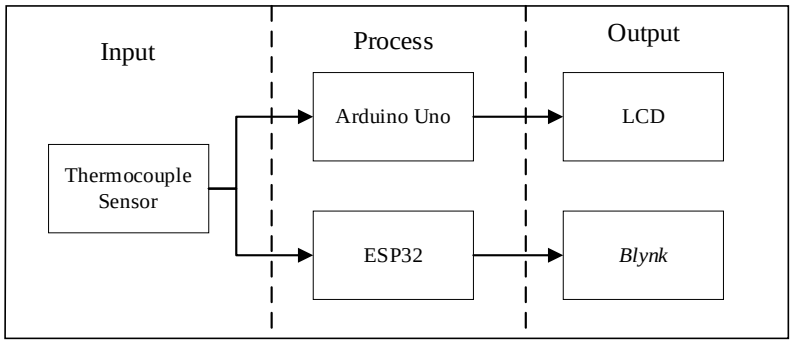

Figure 2. monitoring system

2.2. Research Flowchart

Flowcharts in this study are used to describe the system workflow systematically and facilitate understanding of the processes that occur in automatic coffee roasting machines. Flowcharts are used to describe the overall workflow of the system, which includes the process of designing, testing, and controlling an automatic coffee roasting machine. The system starts with problem identification and literature study, followed by system design, assembly, and testing. The machine is then activated by selecting the roasting option (light, medium, or dark roast), followed by reading the input from the pushbutton and setting the temperature using a servo motor. Once the temperature reaches the desired setpoint, the blower activates to keep the temperature stable, and the roasting process continues until the coffee beans are inserted. In addition, the real-time temperature monitoring system uses a thermocouple sensor, with temperature readings displayed on the LCD and the Blynk app for remote monitoring.

The process starts with turning on the system and selecting a roasting option *(light, medium,* or *dark roast*). Once the option is selected, the system reads the input from the *push button* and the Arduino controls the DC motor and servo to regulate the gas flow and ignite the lighter. The temperature will rise until it reaches the respective set point: 180°C for *light roast*, 220°C for *medium roast*, and 250°C for *dark roast*. Once the temperature is reached, the *blower* activates to maintain the temperature, and the coffee beans are inserted. After that, the system will automatically shut down.

JURNAL ECTIPE
Electronic, Control, Telecommunication, Information, and Power Engineering
Volume 12, Issue 1, April 2025, pp. 43-53
ISSN 2355-5068 ; e-ISSN 2622-4852
DOI: 10.33019/jurnalecotipe.v12i1.4551

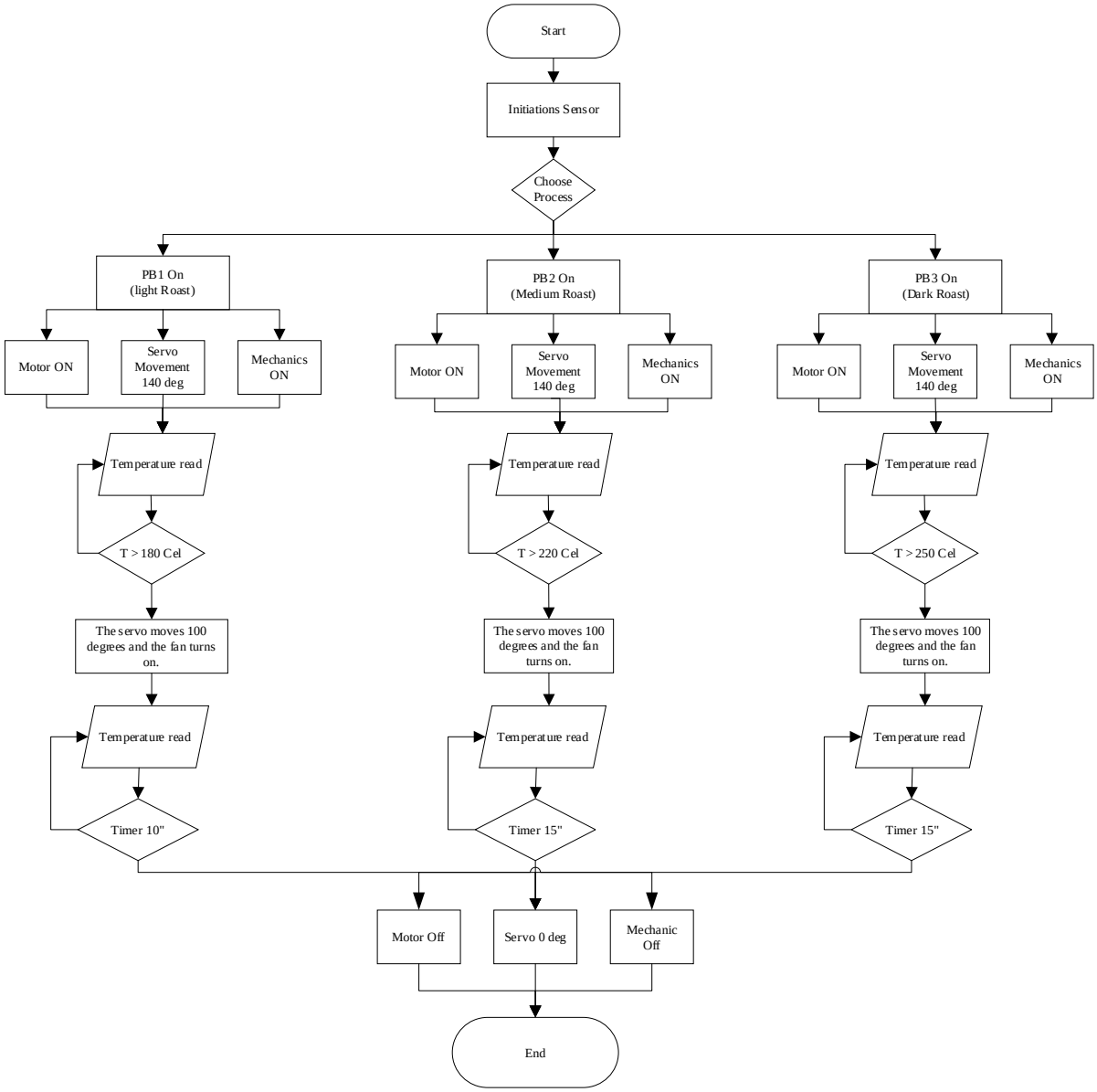

Figure 3. Shows how the coffee *roasting* machine works

2.3. Data Collection Method

Data collection in this study was carried out through a series of tests to analyze the performance of the automatic system in controlling temperature and ensuring consistent coffee roasting results. The first test involved comparing the thermocouple sensor with a manual thermometer to measure the temperature inside the coffee roasting machine. The thermocouple was positioned at the same point as the manual thermometer, with temperature recorded every 10 seconds for 60 seconds. Next, a comparison was made between the temperature readings displayed on the LCD and the Blynk application for real-time temperature monitoring. The temperature was measured and displayed every 10 seconds for 60 seconds. A servo test was also conducted to determine the effect of the motor servo rotation on temperature increase, with tests performed at 5, 10, and 15-minute intervals to observe the temperature changes. Additionally, a test was carried out to assess the temperature decrease by varying the servo motor rotation at different intervals (5, 10, and 15 minutes) to measure the effective decrease in temperature after exceeding the setpoint. Lastly, a temperature stabilization test was conducted where the machine was operated with the gas valve open at a 140° angle, and the servo continuously opened to maintain the temperature below 180°C. Once the temperature reached or exceeded the setpoint, the servo closed by 40°, and the DC fan was activated to dissipate heat.

JURNAL ECOTIPE
Electronic, Control, Telecommunication, Information, and Power Engineering
Volume 12, Issue 1, April 2025, pp. 43-53
ISSN 2355-5068 ; e-ISSN 2622-4852
DOI: 10.33019/jurnalecotipe.v12i1.4551

2.4. Model Design

The design of the hardware model aims to ensure efficient placement of the system components in order to function optimally. The main components in this system include thermocouple temperature sensors, servo motors, DC fans, and Arduino Uno as the microcontroller, as well as ESP32 for IoT communication. All components are placed with an eye towards ease of access and maintenance, as well as ensuring efficient energy and data flow between each component. The components are connected with appropriate cables and modules to support stable functionality during the coffee roasting process. This design also ensures that each part can be easily installed and accessed for replacement or maintenance, if required.

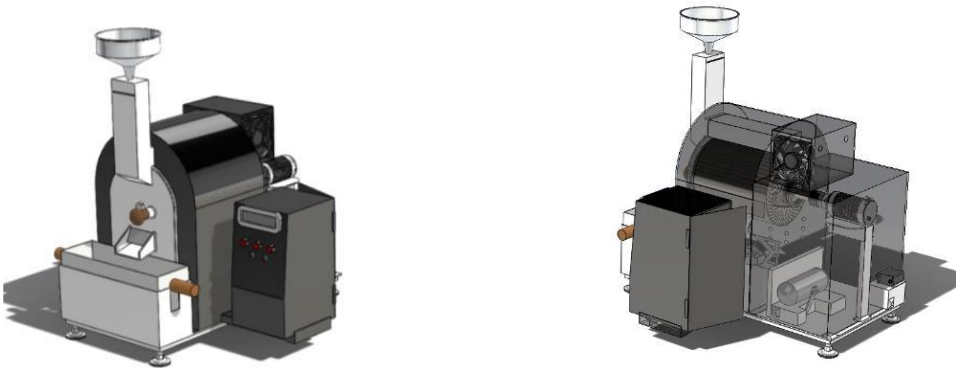

Figure 4. Design of a small-scale roasting machine model

2.5. Blynk App Design

The Blynk app is designed to provide remote control of the coffee roasting machine system. The Blynk app interface allows users to select the roasting type (light, medium, or dark roast) and monitor the temperature of the machine in real-time. The app displays a temperature indicator that shows the current temperature in the machine, as well as the status of active roasting. Users can control the system directly from the app, such as starting or stopping the roasting process, as well as adjusting the temperature settings when necessary. The interface design uses contrasting colors for easy reading, with a simple yet informative look to ensure a comfortable user experience.

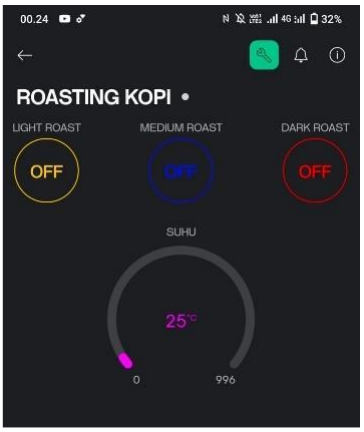

Figure 5. Coffee roasting application

3. RESULTS AND DISCUSSION

The results of designing and making an automatic system and monitoring system that can be controlled through the Blynk application. Furthermore, testing is carried out after the system has been designed. This test aims to determine and analyze the level of success, weaknesses, and the process of making this system. Data management in this system aims to produce good roasting results based on predetermined standards.

3.1 Sensor Analysis

3.1.1 Comparison of Thermocouple and Thermometer Sensors

JURNAL ECOTIPE
Electronic, Control, Telecommunication, Information, and Power Engineering
Volume 12, Issue 1, April 2025, pp. 43-53
ISSN 2355-5068 ; e-ISSN 2622-4852
DOI: 10.33019/jurnalecotipe.v12i1.4551

Temperature testing using a thermocouple and a manual thermometer was conducted to measure and compare the temperature in the coffee roasting machine. The thermocouple is installed inside the machine in the same position as the manual thermometer. The coffee roasting machine was turned on with a servo rotation of 60°. Every 10 seconds for 60 seconds, the temperature was recorded using both measuring instruments. The data obtained was used to calculate the error between the thermocouple and the manual thermometer, with the aim of ensuring the accuracy and consistency of temperature measurement in the roasting process. The results of this test can be seen in Table 1.

Table 1. Sensor Testing Results

Time (s)	Thermocouple (°C)	Thermometer (°C)	Error (°C)
0	29.25	29.00	0.25
10	29.25	29.00	0.25
20	29.50	29.00	0.50
30	29.50	29.00	0.50
40	29.50	29.00	0.50
50	30.25	30.00	0.25
60	31.00	30.00	1.00
Average error			0.46

Analysed from Table 1, the comparison temperature using the thermocouple shows an average error of 0.46°C compared to the manual measurement using a thermometer. Despite the slight error, with the highest error of 1.00°C at 60 seconds, the thermocouple sensor still shows good accuracy in temperature measurement. Overall, the thermocouple proved to be feasible for use in the coffee roasting machine monitoring system, although it needs periodic calibration to maintain its accuracy.

3.1.2. Comparison of LCD and Display

The display comparison test between LCD and Blynk application was conducted to monitor and display the temperature in the coffee roasting machine. The coffee roasting machine was turned on with a servo rotation of 60°. Every 10 seconds for 60 seconds, the temperature is recorded using both measuring instruments, which is then displayed on the LCD screen and also on the Blynk application connected via a smartphone. The data obtained from these measurements were used to compare the suitability and accuracy of the temperature display between the LCD screen and the Blynk application. This comparison aims to ensure that both display methods are able to show temperature data consistently and accurately, making it easier for users to monitor the coffee roasting process. The results of this test can be seen in Table 2.

Table 2. Comparison of LCD and Blynk Display

Time (s)	LCD (°C)	Blynk (°C)	Error (°C)
0	30.75	30.75	0
10	32.50	32.5	0
20	35.00	35.00	0
30	36.25	36.25	0
40	37.75	37.75	0
50	39.50	39.50	0
60	41.25	41.25	0
Average error			0

After testing and analyzing the temperature measurement using a thermocouple sensor displayed on the I2C LCD and Blynk application which can be seen in Table 2. The temperature displayed on the LCD display has a very fast response time because the data is sent directly from the thermocouple to the LCD. This is the same as the temperature displayed on the Blynk application, which has no delay even though it goes through the process of sending via the internet network.

Volume 12, Issue 1, April 2025, pp. 43-53
ISSN 2355-5068 ; e-ISSN 2622-4852
DOI: 10.33019/jurnalecotipe.v12i1.4551

3.2 Servo Turn Analysis

3.2.1. Servo Testing Against Rise

This test was conducted to show the relationship between the servo motor rotation and the time required in increasing the effective temperature. Tests were carried out at time intervals of 5 minutes, 10 minutes, 15 minutes to see the temperature increase at each different time interval. The data can be used as a heating controller properly which can be seen in Figure 11.

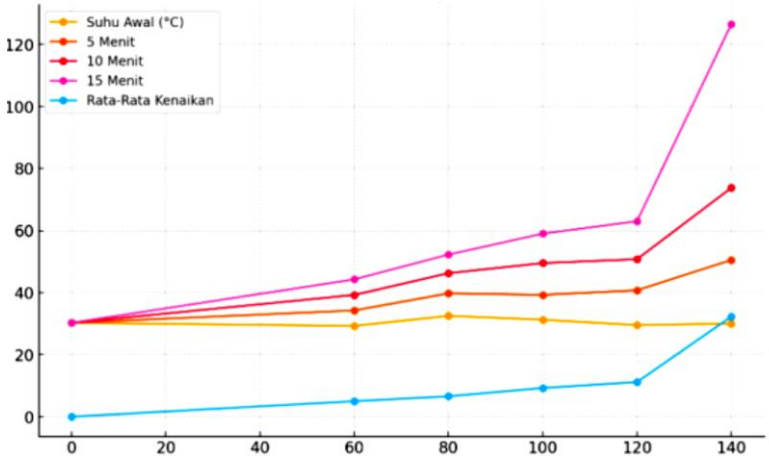

Figure 6. Rise graph The X-axis represents the rotation of the servo and the Y-axis represents the temperature

The test results displayed in Figure 6 show that the larger the servo rotation, the faster the temperature increase in various time intervals. Larger servo turns result in a more significant temperature increase in less time, indicating better heating efficiency. The results of this test were incorporated into the program using a servo angle of 140° for a rapid and optimal temperature increase.

3.2.2. Servo to Drop Testing

This test is carried out to show the relationship between servo motor rotation and the time required for effective temperature reduction. Tests are carried out at time intervals of 5 minutes, 10 minutes, 15 minutes to see the temperature drop at each different time interval.

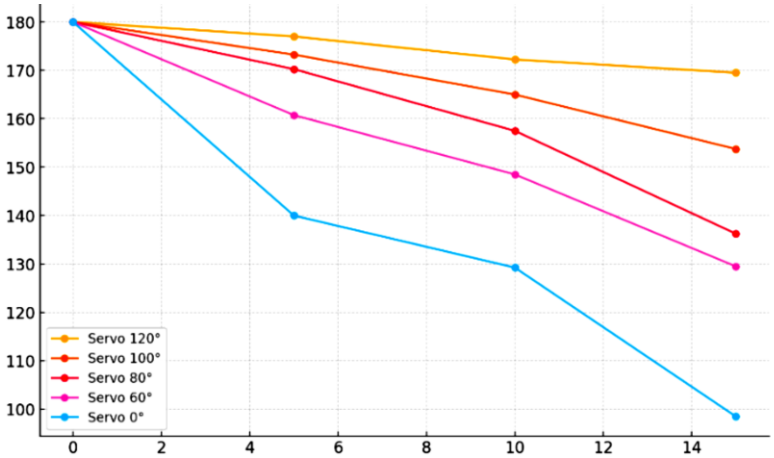

Figure 7. Drop graph The X-axis represents the time (minute) and the Y-axis represents the temperature

The data in Figure 7 shows the temperature drop over a given time for various servo angles, with an initial temperature of 180°C. This test shows that the smaller the servo angle, the greater the average temperature drop, with a more significant temperature drop at longer time intervals. The results of this test were entered into the program using a servo angle of 100° to reduce the temperature if it exceeded the setpoint in the roasting process.

JURNAL ECOTIPE
Electronic, Control, Telecommunication, Information, and Power Engineering
Volume 12, Issue 1, April 2025, pp. 43-53
ISSN 2355-5068 ; e-ISSN 2622-4852
DOI: 10.33019/jurnalecotipe.v12i1.4551

3.2.3 Stabilization Analysis

The temperature stabilization test of the coffee roasting machine aims to assess the system's ability to maintain a consistent temperature during the roasting process. This test was conducted by monitoring the temperature at various levels of heating intensity to ensure the system could maintain the target temperature of 180°C. The machine is operated with the gas valve opening at an angle of 140°, and the servo will continue to open at that angle as long as the temperature is below 180°C. When the temperature reaches or exceeds the setpoint, the servo will close by 40°, and the DC fan will turn on to dissipate the heat inside the engine. These steps aim to keep the temperature stable around the setpoint. The data from this test is used to assess the efficiency of the temperature control as well as identify and correct potential unwanted temperature fluctuations.

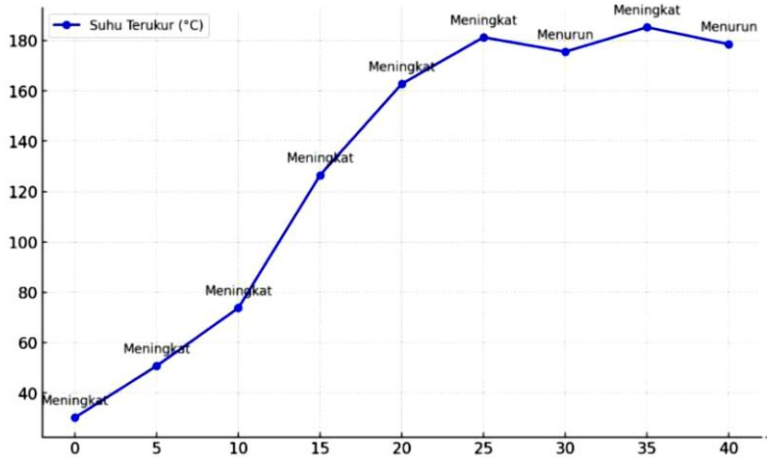

Figure 8. Stabilization Chart The X-axis represents the time (minute) and the Y-axis represents the temperature

Figure 8 shows the change in measured temperature against time during the heating process. From the data provided, the measured temperature continues to increase from the beginning (30.25°C) until it reaches a peak at the 35th minute (185.25°C), before finally decreasing at the 40th minute (178.50°C). So that the temperature can be maintained at approximately 180°C.

3.2.4 Motor Rotation Testing for Roasting

In this test, experiments were carried out with DC motors at two different speeds, namely 68 RPM and 136 RPM, to see the relationship between the motor rotation speed and the time required to achieve optimal roasting results. Table 3 below shows the test data of the motor rotation with speeds of 68 RPM and 136 RPM, as well as the optimal roasting time at 7 minutes, which resulted in the smallest percentage of failure.

Table 3. Motor Rotation Testing Against Time

Motor Speed (RPM)	Set Point (°C)	Time (Minutes)	Present Fail (%)
68	Light Roast	4	10,7%
		5	7,1%
		6	4,3%
		7	3,9%
	Medium Roast	4	6,6%
		5	9,5%
		6	4,5%
		7	3,1%
	Dark Roast	4	6,4%
		5	5,4%
		6	8,8%
		7	4,3%
136	Light Roast	4	53,1%

Volume 12, Issue 1, April 2025, pp. 43-53
ISSN 2355-5068 ; e-ISSN 2622-4852
DOI: 10.33019/jurnalecotipe.v12i1.4551

		5	6,3%
		6	4,1%
		7	3,3%
	Medium Roast	4	5,8%
		5	8,7%
		6	4,3%
		7	2,4%
	Dark Roast	4	5,5%
		5	4,7%
		6	7,2%
		7	3,3%

Table 3. it shows test results at motor speeds of 68 RPM and 136 RPM for three temperature point sets: Light Roast (180°C), Medium Roast (220°C), and Dark Roast (250°C). The smallest failure percentage is recorded at the 7th minute time, which is the optimal roasting time to produce the best quality coffee beans with minimal losses. To get a good analysis of roasting results, the next sub-chapter uses 4", 5" and 10" times as the best roasting results of the coffee color form.

3.2.5 Analysis of Roasting Results

This research is a coffee bean roasting process that includes the length of the process time, the temperature required, the type of coffee produced and the characteristics of the coffee roasting results using 140° servo rotation opening. The results of the type of coffee roasting obtained will be adjusted to the color according to the SCAA (Specialty Coffee Association of America) standard [9]. In the analysis below, 4 types of coffee are shown consisting of light roast with a temperature of 180 °C, medium roast with a temperature of 220 °C and dark roast 250 °**C** to find out the success of roasting results seen in color and displayed in RGB.

Table 4. Coffee Roasting Color Results

Type	**Roasting Temperature (°C)**	**Time (Minutes)**	**Color Code (RGB)**
Light Roast	180	4"	(248,221,136)
		5"	(251,206,109)
		10"	(120,88,63)
Medium Roast	220	5"	(249,185,91)
		7"	(240,142,62)
		15"	(98,76,66)
Dark Roast	250	5"	(203,126,37)
		7"	(160,83,30)
		15"	(70,67,66)

The results of the coffee process can be seen in Table 4, explained based on the variables of temperature, time, and color of the coffee beans produced. Light Roast process with temperature between 160°C to 180°C, showing changes in coffee beans. The colour code in the light roast process that is closest to the SCAA standard is at minute 10. Medium Roast, with temperatures between 200°C and 220°C, shows changes in coffee beans. The colour code in the medium roast process that is closest to the SCAA standard is at minute 15. While Dark Roast, at a temperature of 230 ° C to 250 ° C, shows changes in coffee. These results reflect the effect of temperature and time on the colour development of coffee beans, which directly affects the flavour profile and characteristics of the coffee produced from each type.

4. CONCLUSION

This research successfully developed a small-scale automatic coffee roasting machine with precise temperature control using a thermocouple and servo mechanism, which allows automatic temperature and roast time setting. Tests showed that the thermocouple had good temperature accuracy with an average error of 0.46°C, and that the LCD and Blynk app were able to display the temperature accurately

Volume 12, Issue 1, April 2025, pp. 43-53
ISSN 2355-5068 ; e-ISSN 2622-4852
DOI: 10.33019/jurnalecotipe.v12i1.4551

and consistently. Servo motor testing revealed that the larger servo rotation angle accelerates the temperature increase, improving the heating efficiency. This machine shows that the optimal roasting time for Light Roast, Medium Roast, and Dark Roast occurs at 7 minutes with the smallest failure percentage. Although the roasting results show quality consistent with the taste characteristics as standard, the maximum temperature achieved is still around 130°C, which is lower than the optimal temperature for Light Roast. Therefore, while these machines offer a consistent and economical solution for small businesses, improvements are needed to achieve higher temperatures to produce better quality coffee roasts.

Acknowledgments

This research was supported by the Research and Community Service Centre (P3M) of the Cilacap State Polytechnic. We would like to thank all those who have provided support and contributed to the implementation of this research. The support we received was very meaningful in realizing the technological development that we are studying.

REFERENCES

[1] N. Núñez, C. Martínez, J. Saurina, and O. Núñez, "High-performance liquid chromatography with fluorescence detection fingerprints as chemical descriptors to authenticate the origin, variety and roasting degree of coffee by multivariate chemometric methods," *J Sci Food Agric*, vol. 101, no. 1, pp. 65–73, 2021, doi: 10.1002/jsfa.10615.

[2] E. Bertone, A. Venturello, A. Giraudo, G. Pellegrino, and F. Geobaldo, "Simultaneous determination by NIR spectroscopy of the roasting degree and Arabica/Robusta ratio in roasted and ground coffee," *Food Control*, vol. 59, pp. 683–689, 2016, doi: 10.1016/j.foodcont.2015.06.055.

[3] E. Dybkowska, A. Sadowska, R. Rakowska, M. Dębowska, F. Świderski, and K. Świąder, "Assessing polyphenols content and antioxidant activity in coffee beans according to origin and the degree of roasting," *Rocz Panstw Zakl Hig*, vol. 68, no. 4, pp. 347–353, 2017, [Online]. Available: https://www.scopus.com/inward/record.uri?eid=2-s2.0-85043395098&partnerID=40&md5=33b81ec5ec9c95140b01914b5da2d6e6

[4] L. Febvay *et al.*, "Identification of markers of thermal processing ('roasting') in aqueous extracts of Coffea arabica L. seeds through NMR fingerprinting and chemometrics," *Magnetic Resonance in Chemistry*, vol. 57, no. 9, pp. 589–602, 2019, doi: 10.1002/mrc.4834.

[5] M. Basile and I. Kikic, "A lumped specific heat capacity approach for predicting the non-stationary thermal profile of Coffee during roasting," *Chem Biochem Eng Q*, vol. 23, no. 2, pp. 167–177, 2009, [Online]. Available: https://www.scopus.com/inward/record.uri?eid=2-s2.0-70450237315&partnerID=40&md5=64cc8668bed1e7afe15dc1100b8e601d

[6] H. Yohanes *et al.*, "Blue Ocean Strategy Approach and Canvas Business Model for New Technology: Case Study of a Spouted Bed Coffee Roaster System," in *AIP Conference Proceedings*, 2024. doi: 10.1063/5.0183894.

[7] S. A. Putra, U. Hanifah, and M. A. Karim, "Theoretical study of fluidization and heat transfer on fluidized bed coffee roaster," in *AIP Conference Proceedings*, 2019. doi: 10.1063/1.5098287.

[8] S. Sulistyo and R. M. N. Aulia, "Design and manufacturing of portable coffee roaster," in *AIP Conference Proceedings*, 2023. doi: 10.1063/5.0143259.

[9] O. A. Ogunjirin, M. Olayinka, A. J. Farounbi, J. A. Oyedokun, and O. A. Ola, "Instrumentation of NCAM developed coffee roasting machine," in *IOP Conference Series: Earth and Environmental Science*, 2020. doi: 10.1088/1755-1315/445/1/012004.

Volume 12, Issue 1, April 2025, pp. 43-53
ISSN 2355-5068 ; e-ISSN 2622-4852
DOI: 10.33019/jurnalecotipe.v12i1.4551

[10] Y. Pratama, I. G. E. Dirgayussa, P. F. Simarmata, and M. H. Tambunan, "Detection roasting level of lintong coffee beans by using euclidean distance," *Bulletin of Electrical Engineering and Informatics*, vol. 10, no. 6, pp. 3072–3082, 2021, doi: 10.11591/eei.v10i6.3153.

[11] O. A. Ogunjirin, O. M. Odeniyi, A. S. Olubo, A. J. Farounbi, O. A. Ola, and S. A. Adeleke, "Design and construction of an electrically powered coffee roasting machine," in *IOP Conference Series: Earth and Environmental Science*, 2020. doi: 10.1088/1755-1315/445/1/012009.

[12] R. Wulandari, M. A. Mizar, A. Aminnudin, I. G. R. S. Dirgantara, A. D. N. Luthfianto, and P. Sihassaleh, "Heat transfer through a clay furnace in a coffee roasting machine to produce coffee with a distinctive aroma," in *AIP Conference Proceedings*, 2023. doi: 10.1063/5.0150485.

[13] L. E. Yulianti, D. P. Putri, I. F. Azizah, S. Witman, M. A. Karim, and A. Rahayuningtyas, "Physicochemical Properties of " Cisalak'Robusta Coffee With Hot Air Based Roasting Method," in *BIO Web of Conferences*, 2023. doi: 10.1051/bioconf/20236903014.

[14] A. Rahayuningtyas *et al.*, "Evaluation of Fluidized-Bed and Drum Roaster Performance in Roasting of Robusta Green Bean," in *BIO Web of Conferences*, 2023. doi: 10.1051/bioconf/20236903006.

[15] T. H. Nasution, A. Putramas, and I. Siregar, "Automatic coffee roaster design using Arduino," in *AIP Conference Proceedings*, 2018. doi: 10.1063/1.5080068.

[16] T. Inovan, A. I. Cahyadi, and O. Wahyunggoro, "Implementation of Adaptive-PID Based Temperature Trajectory Tracking Control to Improve Repeatability in Coffee Roasting," in *Proceedings of the 2023 IEEE International Conference on Industry 4.0, Artificial Intelligence, and Communications Technology, IAICT 2023*, 2023, pp. 162–167. doi: 10.1109/IAICT59002.2023.10205885.

[17] A. H. Falah, M. Rivai, and D. Purwanto, "Implementation of Gas and Sound Sensors on Temperature Control of Coffee Roaster Using Fuzzy Logic Method," in *Proceedings - 2019 International Seminar on Intelligent Technology and Its Application, ISITIA 2019*, 2019, pp. 80–85. doi: 10.1109/ISITIA.2019.8937148.

[18] P. C. Ayu, M. R. Machrizailani, A. Rohanah, K. N. Sinamo, and N. U. W. Sebayang, "Design of coffee roaster with controlled temperature system to maintain the sustainability of coffee roasting process," in *IOP Conference Series: Earth and Environmental Science*, 2024. doi: 10.1088/1755-1315/1302/1/012116.

[19] B. Purwantana, R. P. Alamsyah, and H. D. Prawira, "Design of Portable Coffee Roaster for Home Industry," in *IOP Conference Series: Earth and Environmental Science*, 2019. doi: 10.1088/1755-1315/327/1/012019.

[20] B. Samodro, B. Mahesworo, T. Suparyanto, D. B. Surya Atmaja, and B. Pardamean, "Maintaining the Quality and Aroma of Coffee with Fuzzy Logic Coffee Roasting Machine," in *IOP Conference Series: Earth and Environmental Science*, 2020. doi: 10.1088/1755-1315/426/1/012148.

JURNAL ECOTIPE
Electronic, Control, Telecommunication, Information, and Power Engineering

Volume 12, Issue 1, April 2025, pp. 54-64
ISSN 2355-5068 ; e-ISSN 2622-4852
DOI: 10.33019/jurnalecotipe.v12i1.4545

Autonomous Camera Tracking System Using Image Processing for Dynamic Educational Content Creation

Valina Sinka[1], Sri Gunawan[2], Muhammad Mustajib[3], Muhammad Rafi Solakhudin[4]
[1,2,3]Management Department, Airlangga University, Surabaya 60115, Indonesia
[4]Automation Engineering, Shipbuilding Institute of Polytechnic Surabaya, Surabaya 60111, Indonesia

ARTICLE INFO

Article historys:

Received : 10/02/2025
Revised : 17/02/2025
Accepted : 30/03/2025

Keywords:

Camera Tracking; Image Processing; MediaPipe; Online Learning Activity

ABSTRACT

In the context of the Online Learning activity, where video content plays a crucial role in educational materials, the demand for effective video production systems has become essential. Traditionally, at least two people are needed to operate cameras, which poses a challenge due to limited human resources. This study addresses this issue by developing a Camera Position Tracking System using image processing, specifically utilizing the MediaPipe framework for real-time tracking of presenters. The system's mechanics enable a DSLR camera to automatically adjust its position based on the presenter's movement, detected within a range of 1.5 to 8 meters. The light intensity required for optimal operation is between 125 and 190 lux. The system's success lies in converting detected position data into motor stepper pulses that move the camera, ensuring efficient, cost-effective video production with minimal human intervention.

Corresponding Author:

Valina Sinka
Management Department, Airlangga University, Surabaya 60115, Indonesia
Email: valinasinka28@gmail.com

1. INTRODUCTION

The increasing reliance on video-based education has revolutionized the way knowledge is delivered, particularly in online learning environments[1]. High-quality educational videos enhance engagement, improve comprehension, and provide flexibility for both instructors and students. However, traditional video production methods require multiple camera operators, leading to increased costs and inefficiencies[2]. Manual camera handling also introduces inconsistencies in framing, limiting the overall quality of educational content.

To address these challenges, this study proposes a autonomous camera tracking system using image processing for dynamic educational content creation[3]. By leveraging image processing techniques and artificial intelligence, the system can autonomously track and follow the movement of presenters without the need for human intervention. Utilizing the MediaPipe framework, the system processes real-time video data to detect and track human positions, ensuring smooth and professional video capture[4]. This innovation is particularly beneficial for educational institutions, online academies, and training centers, where high-quality instructional videos are essential yet often constrained by budget and manpower[5].

The integration of automation in video production not only reduces costs but also enhances efficiency by allowing educators to focus solely on delivering content rather than managing camera operations[6]. With real-time tracking capabilities and adaptive camera positioning, the system ensures that presenters remain in the optimal frame throughout the recording process[7]. This research

JURNAL ECOTIPE
Electronic, Control, Telecommunication, Information, and Power Engineering
Volume 12, Issue 1, April 2025, pp. 54-64
ISSN 2355-5068 ; e-ISSN 2622-4852
DOI: 10.33019/jurnalecotipe.v12i1.4545

contributes to the advancement of smart educational technology by providing a scalable, cost-effective, and intelligent solution for modern video-based learning environments[8].

2. RESEARCH METHOD

In This study employs an experimental and system development approach to design and evaluate an autonomous camera tracking system for educational video production[9]. The methodology consists of several key stages, including system design, data collection, system testing, and data analysis

2.1. Hardware System Design

The proposed automated camera tracking system consists of both hardware and software components that work together to enable real-time presenter tracking and dynamic camera positioning. The system is designed to optimize video production for educational purposes by automating camera movement based on the detected position of the presenter[10].

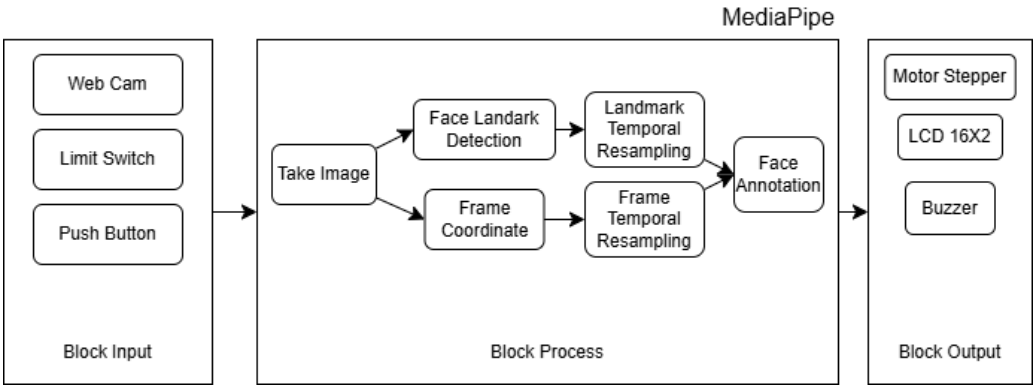

Figure 1 Block Diagram System

The hardware system consists of three main components: imaging devices, a motion control system, and a processing unit. The system employs two cameras a DSLR camera for high-quality video recording and a webcam for real-time presenter tracking. The webcam continuously captures video input, which is processed to determine the presenter's position. To ensure accurate camera movements, a NEMA 17 stepper motor, controlled by a Raspberry Pi 4, is used to adjust the camera's position along two axes (X and Y)[11]. The motor system is integrated with a lead screw mechanism and timing belts, allowing smooth and precise adjustments to keep the presenter within the optimal frame. The Raspberry Pi 4 serves as the central control unit, processing video data and converting detected movements into motor control commands.

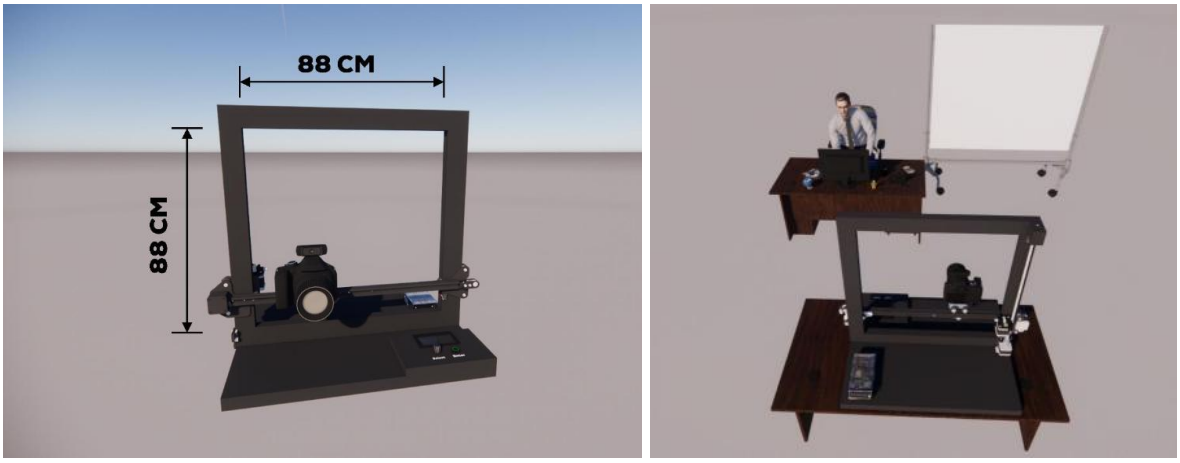

Figure 2 Mechanical Design and Application

JURNAL ECTIPE
Electronic, Control, Telecommunication, Information, and Power Engineering
Volume 12, Issue 1, April 2025, pp. 54-64
ISSN 2355-5068 ; e-ISSN 2622-4852
DOI: 10.33019/jurnalecotipe.v12i1.4545

The mechanical design of the autonomous camera tracking system features a rigid aluminum frame with dimensions 88 cm × 88 cm, ensuring stable and precise movement of the mounted DSLR camera. The camera is positioned on a linear rail system driven by a NEMA 17 stepper motor, which enables smooth horizontal tracking based on real-time image processing data. A timing belt and pulley mechanism facilitate motion transmission, ensuring minimal lag in response to presenter movement. This lightweight yet durable structure supports efficient tracking while maintaining stability, making it suitable for dynamic educational content creation[12].

The mechanical system of the automated camera tracking setup relies on precise stepper motor control to ensure smooth movement along both horizontal and vertical axes. The number of pulses required to move the camera is determined by the mechanical components used. For horizontal movement, which utilizes a timing belt and pulley system, the total required pulses are calculated using the formula:

$$Pulse\ max = (belt\ length)/(Pulley\ circumference) \times Pulse\ Stepper \quad (1)$$

for vertical movement, controlled by a lead screw mechanism, the required pulses follow the equation

$$Pulse\ max = (belt\ length\ Screw)/(Pulley\ circumference\ Screw) \times Pulse\ Stepper \quad (2)$$

Given the system specifications, where the timing belt spans 88 cm with a pulley circumference of 4 cm, and the lead screw moves 0.8 cm per revolution, the calculated pulseMax values are 4,400 pulses for horizontal movement and 22,000 pulses for vertical movement. These calculations ensure that the system maintains accurate and stable tracking, allowing the camera to follow the presenter seamlessly[7].

2.2. Software System Design

The software system is responsible for presenter detection, tracking, and camera movement control. The MediaPipe framework is employed for real-time human pose estimation, enabling the system to detect key landmarks on the presenter's body and track movements accurately. The system is programmed using Python and OpenCV, which process video input from the webcam, extract positional data, and translate it into stepper motor commands. The tracking algorithm ensures smooth transitions and minimal delay, optimizing accuracy while preventing sudden or unstable movements[13].

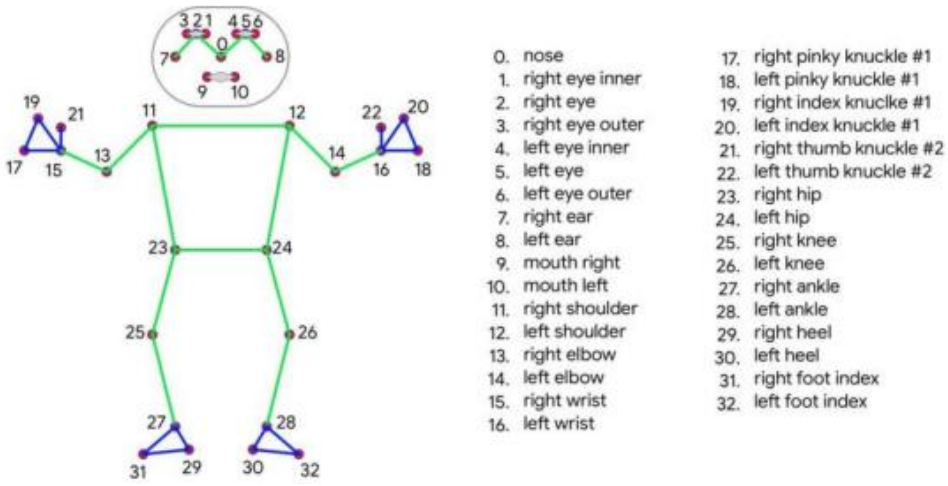

Figure 3 Key Points/Markers of each body part of the MediaPipe Holistic framework

By integrating AI-based image processing with automated hardware control, this system provides an intelligent, cost-effective solution for educational video production. It reduces the need for manual camera operation while improving video quality and consistency, making it highly beneficial for institutions, online learning platforms, and training centers[14].

Volume 12, Issue 1, April 2025, pp. 54-64
ISSN 2355-5068 ; e-ISSN 2622-4852
DOI: 10.33019/jurnalecotipe.v12i1.4545

2.3. Mediapipie Framework

MediaPipe is an open-source framework developed by Google for machine learning-based image processing. This framework is designed to operate in real time with low latency and is compatible with various platforms, including desktop and mobile devices. In this study, MediaPipe Holistic is utilized as it combines face, hand, and body detection models simultaneously to support presenter tracking in educational video production.

MediaPipe employs several key algorithms for image processing. One of the primary models is BlazePose, a Convolutional Neural Network (CNN)-based algorithm capable of recognizing 33 keypoints of the human body in 3D with high accuracy. Additionally, the system incorporates Face Mesh Detection, which uses landmark regression techniques to detect up to 468 facial keypoints, and the Hand Tracking Model, which operates with a multi-stage pipeline to accurately recognize hand and finger positions. In this study, MediaPipe Holistic leverages these techniques to ensure stable and accurate presenter tracking under various lighting conditions and camera angles.

Once the image is captured by the camera, MediaPipe applies pose estimation techniques to analyze the presenter's position and movement. The process begins with pose detection, where the system identifies the presence of a human figure in the frame using deep learning-based models. Subsequently, the system performs keypoint localization, mapping the body's landmarks using Heatmap Regression techniques. To maintain tracking stability, the system integrates the Kalman Filter, which predicts the presenter’s position based on previous data, reducing noise and enhancing movement accuracy. The resulting coordinate data is then converted into X, Y, and Z references, which serve as input for automatic camera movement control.

In this system’s implementation, MediaPipe processes data from a webcam through several key stages. First, the camera captures images at a resolution of 1280×720 pixels. The system then extracts the presenter's keypoints using the BlazePose model. Next, the body’s coordinates are analyzed to determine movement direction. Finally, the extracted coordinate data is converted into stepper motor control commands via a Raspberry Pi 4, allowing the camera to automatically follow the presenter and ensure optimal framing throughout the recording session.

2.4. Data Collection

To evaluate the performance of the automated camera tracking system, data was collected through a series of controlled experiments focusing on detection range, lighting conditions, and tracking accuracy. The detection range was tested by placing the presenter at varying distances from the camera, ranging from 1.5 meters to 8 meters, to determine the system’s optimal operational range. Additionally, lighting conditions were analyzed by adjusting the intensity between 125 to 190 lux, as this range was identified as ideal for maintaining accurate detection and reducing errors in tracking. The system’s tracking accuracy was evaluated by monitoring its responsiveness to different movement speeds and directions of the presenter. The ability of the system to consistently follow the presenter without lag or misalignment was assessed to ensure reliable real-time tracking. These experiments provided crucial insights into the system’s effectiveness and helped refine its ability to maintain smooth, automatic adjustments in educational video production[15].

3. RESULTS AND DISCUSSION

To evaluate the performance of the Autonomous Camera Tracking System, a series of tests were conducted focusing on sensor accuracy, motion detection, tracking responsiveness, framework efficiency, and training improvements. The results are categorized into multiple sections for a detailed analysis.

3.1. System Performance Evaluation

The automated camera tracking system was tested under various conditions to evaluate its overall performance in tracking a presenter for educational video production. The evaluation focused on real-time detection accuracy, response time, motor control precision, and system stability. The system was deployed in an indoor environment with controlled lighting conditions ranging between 125 and 190 lux, as this range was identified as optimal for accurate tracking. The presenter moved within a 1.5 to 8-meter range, and the system successfully adjusted the camera's position to maintain proper framing.

JURNAL ECOTIPE
Electronic, Control, Telecommunication, Information, and Power Engineering
Volume 12, Issue 1, April 2025, pp. 54-64
ISSN 2355-5068 ; e-ISSN 2622-4852
DOI: 10.33019/jurnalecotipe.v12i1.4545

Figure 4 Mechanical of the Automatic Camera System

Figure 4 illustrates the mechanical structure of an automatic camera tracking system designed for presenter tracking. The system features a horizontal rail that allows the camera to move autonomously, enabling smooth tracking of the presenter within a designated area. Stepper motors are likely employed to control the camera's movement with high precision. This structure ensures stability and smooth motion, which is crucial for maintaining clear and consistent video recording

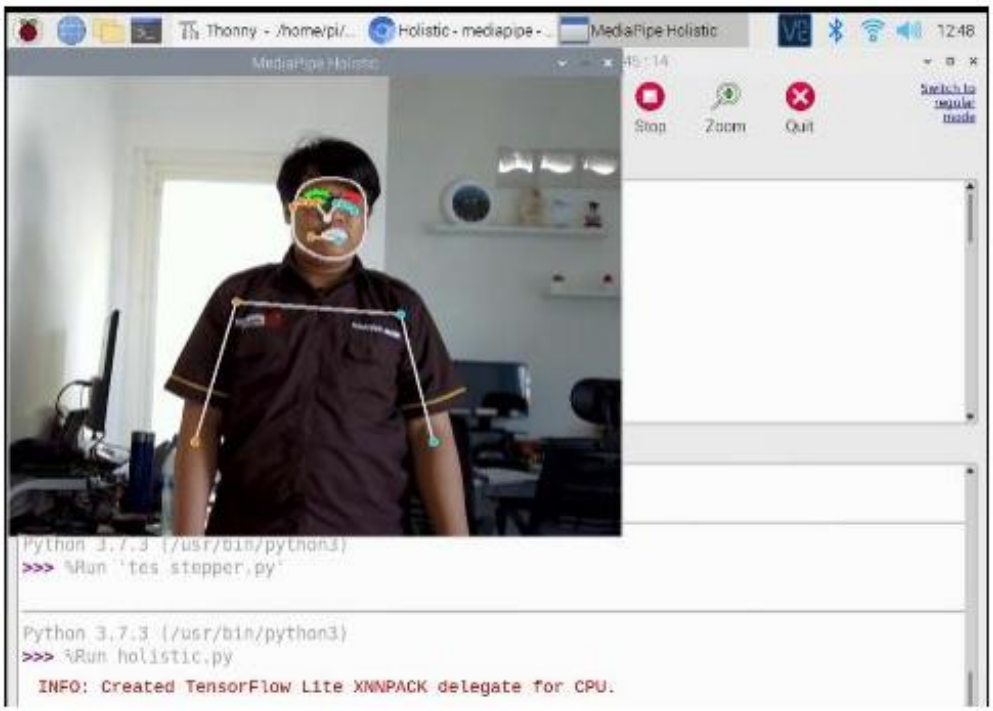

Figure 5 MediaPipe Implementation for Presenter Tracking

Figure 5 demonstrates the MediaPipe Holistic framework in action, effectively recognizing and tracking the presenter's movement in real-time. During testing, the system exhibited high accuracy and minimal lag, ensuring precise detection of facial and body landmarks. The stepper motor's precision was evaluated to assess the system's ability to adjust the camera position dynamically. The camera smoothly followed the presenter along both horizontal and vertical axes, keeping the subject centered within the frame. Additionally, response time analysis revealed that the system quickly detected movement and adjusted accordingly, maintaining stable and seamless tracking. These results highlight the system's reliability in automated educational video production, offering a real-time, AI-driven solution for intelligent camera control.

JURNAL ECTIPE
Electronic, Control, Telecommunication, Information, and Power Engineering
Volume 12, Issue 1, April 2025, pp. 54-64
ISSN 2355-5068 ; e-ISSN 2622-4852
DOI: 10.33019/jurnalecotipe.v12i1.4545

3.2. Detection Accuracy Analysis

The accuracy of the automated camera tracking system was evaluated based on its ability to detect and track the presenter at varying distances, angles, and lighting conditions. The system's performance was tested within a range of 1.5 to 8 meters, where accuracy gradually declined as distance increased. At 1.5 to 4.5 meters, the system achieved an accuracy of 98–93%, ensuring stable tracking and precise framing. However, at 6 meters and beyond, accuracy decreased, reaching 85% at 7.5 meters and at 8 meters. This drop is attributed to lower resolution of the detected features and increased background noise, which affects the system's ability to maintain reliable tracking.

Table 1 Detection Accuracy Based on Distance

Distance (m)	Detection Accuracy (%)	Remarks
1,5	98	Optimal detection, clear landmarks
3	96	High accuracy, stable tracking
4,5	93	Slight decrease in accuracy
6	90	Moderate tracking accuracy
7,5	85	Still detectable, stable tracking
8	85	Presenter fully detected

Figure 6 Framework MediaPipie Distance Testing

In addition to distance, the angle of detection also played a significant role in accuracy. The system performed best when the presenter was facing the camera directly, but accuracy slightly decreased when the presenter turned 30° to 60° from the camera, as some facial and body landmarks became partially obscured. At extreme angles (above 75°), tracking errors increased due to occlusions and incomplete landmark detection.

Table 2 Detection Accuracy Based on Angle Presenter

Presenter Angle (°)	Detection Accuracy (%)	Remarks
0° (Front-facing)	98	Ideal detection, all landmarks visible
30°	95	Slight accuracy drop, minor occlusion
60°	88	Partial occlusion of facial landmarks
75°	80	Significant tracking loss in side view
90° (Side view)	70	Poor detection, many landmarks missing

JURNAL ECOTIPE
Electronic, Control, Telecommunication, Information, and Power Engineering
Volume 12, Issue 1, April 2025, pp. 54-64
ISSN 2355-5068 ; e-ISSN 2622-4852
DOI: 10.33019/jurnalecotipe.v12i1.4545

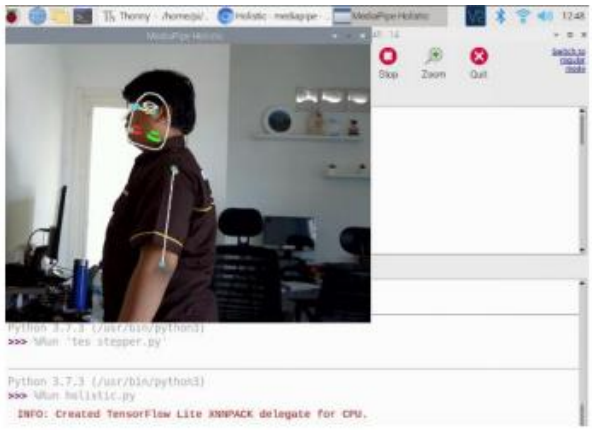

Figure 7 Angle Testing

Lighting conditions also impacted detection accuracy. The system was tested under different illumination levels, where the optimal detection range was observed between 125 to 190 lux. At lower light levels (below 100 lux), tracking performance degraded, leading to occasional misalignment in framing. Conversely, excessive brightness (above 250 lux) caused overexposure, reducing the contrast needed for effective landmark detection. These results indicate that maintaining a well-lit environment within the recommended lux range is essential for ensuring optimal tracking performance.

Table 3 Detection Accuracy Light Intensity

Light Intensity (lux)	Detection Accuracy (%)	Remarks
50	72	Too dark, poor landmark visibility
100	85	Low brightness, minor tracking errors
125	93	Optimal range, stable tracking
150	96	Optimal range, high accuracy
190	98	Ideal lighting conditions

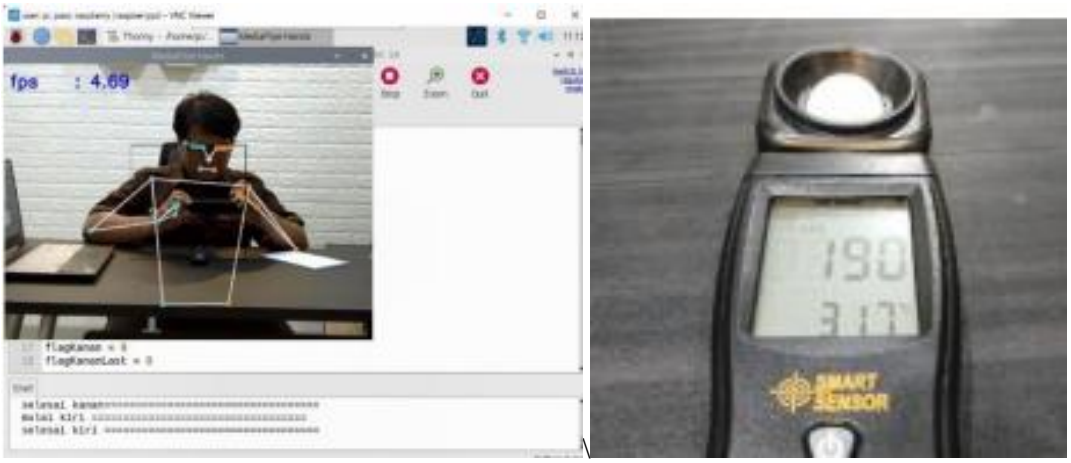

Figure 8 Light Intensity Testing

Overall, the system demonstrated high accuracy within ideal distance, angle, and lighting conditions, confirming its effectiveness for automated educational video production. Future improvements, such as adaptive lighting adjustments and multi-angle tracking, could further enhance its robustness in diverse recording environments.

3.3. Response Time and Processing Speed

The performance of the automated camera tracking system relies on two critical factors: response time and image processing speed, both of which determine the system's ability to track a presenter smoothly in real-time. The response time was measured as the delay between the presenter's movement and the corresponding camera adjustment, ensuring that the tracking remained fluid and accurate. Based

Volume 12, Issue 1, April 2025, pp. 54-64
ISSN 2355-5068 ; e-ISSN 2622-4852
DOI: 10.33019/jurnalecotipe.v12i1.4545

on experimental results, the system achieved an average response time of 253.1 milliseconds, which is fast enough to maintain stable tracking. However, response time tends to increase when the presenter moves beyond 6 meters, where detection becomes less reliable due to reduced image resolution and increased background noise.

In terms of processing speed, the system's frame rate (FPS) was tested under different lighting conditions to evaluate its ability to process and update tracking data in real time. Under optimal lighting conditions (125–190 lux), the system operated efficiently at an average of 30 FPS, ensuring smooth and continuous detection of the presenter's movement. However, when exposed to low-light conditions (below 100 lux), the frame rate dropped to 25 FPS, resulting in slight tracking delays. This reduction was caused by increased noise in the video feed, requiring more computational time for the MediaPipe framework to correctly identify key landmarks.

To further refine the system's real-time tracking, the motor response delay was tested to determine the ideal time interval for stepper motor adjustments. The results showed that the optimal delay for motor movement ranged between 0.005 and 0.1 seconds, providing a balance between accuracy and movement smoothness. If the delay was too low, the motor movements became jerky, whereas a delay that was too high introduced noticeable lag in tracking.

Figure 9 Sample Testing Respons Time with 2,78 Second

Overall, the system demonstrated fast response times and reliable processing speeds, making it suitable for automated educational video production. The findings suggest that maintaining optimal lighting conditions and presenter positioning within 1.5 to 6 meters results in the best tracking performance. Future improvements could focus on hardware acceleration, optimized tracking algorithms, and adaptive lighting compensation to further reduce latency and improve real-time tracking accuracy.

3.4. Motor Control and Camera Movement Precision

The accuracy and stability of the automated camera tracking system rely heavily on the motor control system that adjusts the camera's position in response to the presenter's movements. The system uses a NEMA 17 stepper motor with a lead screw mechanism for vertical movement and a timing belt with a pulley system for horizontal movement. The stepper motor is controlled by the Raspberry Pi 4, which translates tracking data from the MediaPipe framework into precise movement commands.

To evaluate camera movement precision, tests were conducted by measuring the accuracy of motor steps per unit movement. The number of pulses required for movement was calculated using the following formulas:

$$\text{Pulse max} = (\text{belt length})/(\text{Pulley circumference}) \times \text{Pulse Stepper} \quad (3)$$

$$\text{Pulse max} = (\text{belt length Screw})/(\text{Pulley circumference Screw}) \times \text{Pulse Stepper} \quad (4)$$

Volume 12, Issue 1, April 2025, pp. 54-64
ISSN 2355-5068 ; e-ISSN 2622-4852
DOI: 10.33019/jurnalecotipe.v12i1.4545

Based on system specifications the horizontal movement used a timing belt system with a pulley circumference of 4 cm and a belt length of 88 cm, resulting in 4,400 pulses for full horizontal travel. The vertical movement used a lead screw with an 8 mm pitch, requiring 22,000 pulses for full travel of 88 cm.

During testing, the system demonstrated smooth and stable camera movements, ensuring that the presenter remained centered in the frame. However, minor vibrations were observed at higher motor speeds, which could be mitigated by optimizing the motor acceleration profile. The stepper motor delay was fine-tuned to 0.005–0.1 seconds, balancing tracking responsiveness and movement smoothness.

The results confirm that the motor control system effectively maintains precise camera positioning, allowing the system to dynamically adjust the frame in real-time without noticeable lag or jitter. Future improvements may include damping mechanisms to reduce vibrations and the use of brushless DC motors for smoother transitions in high-speed tracking scenarios.

3.5. Comparative Analysis with Manual Camera Operation

To evaluate the effectiveness of the automated camera tracking system, a comparative analysis was conducted against manual camera operation. The comparison focuses on tracking accuracy, response time, movement stability, and operational efficiency, particularly in the context of educational video production.

Tracking Accuracy: The automated system, powered by the MediaPipe framework, maintained an accuracy of 93–98% within an optimal tracking range of 1.5 to 4.5 meters. In contrast, manual tracking depends on the operator's skill and reaction time, which can introduce inconsistencies in framing, especially during rapid presenter movements. At distances beyond 6 meters, the automated system showed a slight accuracy decline due to reduced image resolution and tracking stability, whereas a human operator could still make real-time adjustments.

Response Time: The automated system demonstrated an average response time of 253.1 milliseconds, ensuring fast and seamless camera adjustments. In comparison, manual tracking introduces human reaction delays, which typically range from 500 milliseconds to over 1 second, depending on the operator's experience. The automation significantly reduces latency and human error, improving real-time tracking efficiency.

Movement Stability: The automated system, utilizing stepper motors and optimized motion delay (0.005–0.1 seconds), provided smooth and stable camera movements without noticeable jitter. Manual tracking, however, is prone to sudden shifts and inconsistencies, especially during frequent camera adjustments. Although the automated system performed well under standard conditions, minor vibrations at higher tracking speeds suggest that further optimization could improve motion stability.

Operational Efficiency: Unlike manual camera operation, which requires a dedicated operator, the automated system eliminates human dependency, allowing educators to focus entirely on delivering content. This makes it an ideal solution for e-learning platforms, lecture recordings, and self-produced instructional videos. Additionally, automation reduces production costs and labor requirements, making video creation more scalable and accessible for educational institutions.

4. CONCLUSION

This study successfully developed an automated camera tracking system for educational video production, integrating image processing and motorized camera positioning to enhance efficiency and reduce the need for manual operation. By utilizing the MediaPipe framework, the system effectively detects and tracks the presenter's movements in real time, ensuring smooth and professional video framing. The implementation of stepper motors with lead screw and timing belt mechanisms enables precise camera adjustments along the horizontal and vertical axes, maintaining stable and accurate positioning. Through extensive testing, the system demonstrated a high detection accuracy within an optimal range of 1.5 to 8 meters, with ideal lighting conditions between 125 and 190 lux. The stepper motor control algorithm effectively converted position data into movement pulses, ensuring that the camera seamlessly followed the presenter's position. Additionally, performance evaluations showed that the system maintained a fast response time, minimizing tracking delays and enhancing video quality. Overall, this research contributes to the advancement of automated educational content creation,

Volume 12, Issue 1, April 2025, pp. 54-64
ISSN 2355-5068 ; e-ISSN 2622-4852
DOI: 10.33019/jurnalecotipe.v12i1.4545

providing a cost-effective, scalable, and intelligent solution for modern video-based learning environments. Future improvements may include multi-camera tracking, integration with AI-based speech recognition, and enhanced tracking algorithms to further optimize performance and expand its applications in various educational settings.

REFERENCES

[1] N. Kumar *et al.*, "Educational technology and libraries supporting online learning," *AI-Assisted Libr. Reconstr.*, hal. 209–237, 2024, doi: 10.4018/979-8-3693-2782-1.ch012.

[2] N. Peimani dan H. Kamalipour, "Online education and the covid-19 outbreak: A case study of online teaching during lockdown," *Educ. Sci.*, vol. 11, no. 2, hal. 1–16, 2021, doi: 10.3390/educsci11020072.

[3] A. Khumaidi, "Sistem Tracking Posisi Kamera Menggunakan Pengolahan Citra Untuk Pemusatan Posisi Pengambilan Video di Automation Academy," *J. Tek. Elektro dan Komput. TRIAC*, vol. 9, no. 2, hal. 103–108, 2022, doi: 10.21107/triac.v9i2.16021.

[4] U. Anitha, R. Narmadha, D. R. Sumanth, dan D. N. Kumar, "Robust Human Action Recognition System via Image Processing," *Procedia Comput. Sci.*, vol. 167, no. 2019, hal. 870–877, 2020, doi: 10.1016/j.procs.2020.03.426.

[5] W. Rahmaniar dan A. Hernawan, "Real-time human detection using deep learning on embedded platforms: A review," *J. Robot. Control*, vol. 2, no. 6, hal. 462-468Y, 2021, doi: 10.18196/jrc.26123.

[6] Julham Comaro, I. Malik, M. Mesin Produksi dan Perawatan, P. Negeri Sriwijaya, dan J. Teknik Mesin, "Perancangan Dan Pengembangan Alat Uji Tarik Mini Berbasis Arduino Untuk Spesimen Non-Ferro," *Agustus*, vol. 1, no. 1, hal. 2723–3359, 2020, [Daring]. Tersedia pada: http://dx.doi.org/10.5281/zenodo.4540926.

[7] W. Chamorro, J. Andrade-Cetto, dan J. Solà, "High-speed event camera tracking," *31st Br. Mach. Vis. Conf. BMVC 2020*, no. 2, hal. 1–12, 2020.

[8] V. Bazarevsky, I. Grishchenko, K. Raveendran, T. Zhu, F. Zhang, dan M. Grundmann, "BlazePose: On-device Real-time Body Pose tracking," 2020, [Daring]. Tersedia pada: http://arxiv.org/abs/2006.10204.

[9] T. J. Sánchez-Vicinaiz, E. Camacho-Pérez, A. A. Castillo-Atoche, M. Cruz-Fernandez, J. R. García-Martínez, dan J. Rodríguez-Reséndiz, "MediaPipe Frame and Convolutional Neural Networks-Based Fingerspelling Detection in Mexican Sign Language," *Technologies*, vol. 12, no. 8, hal. 1–22, 2024, doi: 10.3390/technologies12080124.

[10] N. H. M. DHUZUKI *et al.*, "Design and Implementation of a Deep Learning Based Hand Gesture Recognition System for Rehabilitation Internet-of-Things (Riot) Environments Using Mediapipe," *IIUM Eng. J.*, vol. 26, no. 1, hal. 353–372, 2025, doi: 10.31436/IIUMEJ.V26I1.3455.

[11] A. Amarudin, D. A. Saputra, dan R. Rubiyah, "Rancang Bangun Alat Pemberi Pakan Ikan Menggunakan Mikrokontroler," *J. Ilm. Mhs. Kendali dan List.*, vol. 1, no. 1, hal. 7–13, 2020, doi: 10.33365/jimel.v1i1.231.

[12] A. D. Agustiani, S. M. Putri, P. Hidayatullah, dan M. R. Sholahuddin, "Penggunaan MediaPipe untuk Pengenalan Gesture Tangan Real-Time dalam Pengendalian Presentasi," vol. 16, no. 2, 2024.

[13] S. Shriram, B. Nagaraj, J. Jaya, S. Shankar, dan P. Ajay, "Deep Learning-Based Real-Time AI Virtual Mouse System Using Computer Vision to Avoid COVID-19 Spread," *J. Healthc. Eng.*, vol. 2021, 2021, doi: 10.1155/2021/8133076.

JURNAL ECTIPE
Electronic, Control, Telecommunication, Information, and Power Engineering
Volume 12, Issue 1, April 2025, pp. 54-64
ISSN 2355-5068 ; e-ISSN 2622-4852
DOI: 10.33019/jurnalecotipe.v12i1.4545

[14] A. Specker, "ReidTrack : Reid-only Multi-target Multi-camera Tracking," hal. 5442–5452.

[15] R. Hartmann, F. Al MacHot, P. Mahr, dan C. Bobda, "Camera-based system for tracking and position estimation of humans," *2010 Conf. Des. Archit. Signal Image Process. DASIP2010*, no. April 2014, hal. 62–67, 2010, doi: 10.1109/DASIP.2010.5706247.

JURNAL ECOTIPE
Electronic, Control, Telecommunication, Information, and Power Engineering

Volume 12, Issue 1, April 2025, pp. 65-76
ISSN 2355-5068 ; e-ISSN 2622-4852
DOI: 10.33019/jurnalecotipe.v12i1.4550

Improving the Effectiveness of Help Desk Service Management in the Self-Service System at the UIN Sunan Ampel Surabaya Academic Library

Muhammad Fawaid Al Ghifary[1], Faris Mushlihul Amin[2], Mujib Ridwan[3], Muhammad Rafi Solakhudin[4]

[1,2,3]Departement of Information System, State Islamic University of Surabaya, Surabaya, Indonesia
[4]Automation Engineering, Shipbuilding Institute of Polytechnic Surabaya, Surabaya 60111, Indonesia

ARTICLE INFO

Article historys:

Received : 14/02/2025
Revised : 28/02/2025
Accepted : 30/03/2025

Keywords:

ITIL V4; Service Desk Management; Self-Service Systems; Library Services

ABSTRACT

The increasing reliance on self-service systems in academic libraries necessitates robust service desk man-agement to ensure user satisfaction and operational efficiency. At the UIN Sunan Ampel Library, self-service systems provide convenient access to various services, but their performance remains underexplored. Evaluat-ing the library's service desk management using the ITIL V4 framework reveals critical insights into its effec-tiveness and areas for improvement. The framework's Service Desk Practice Success Factors (PSF)—Acknowledge, Classify, Own, and Act—are used to assess how well self-service systems align with ITIL best practices. This research adopts a qualitative descriptive methodology, utilizing interviews and data analysis to evaluate service desk processes. The findings indicate significant benefits in accessibility and user empower-ment through self-service features. However, challenges persist, including manual acknowledgment workflows, insufficient SLA implementation, and limited real-time monitoring capabilities. These issues hinder optimal service delivery and responsiveness. To address these gaps, the study recommends integrating automation for acknowledgment tasks, developing measurable SLA policies, and implementing comprehensive training for library staff. Additionally, real-time tracking tools should be incorporated to enhance system efficiency and user experience. Despite these challenges, the study underscores the potential of ITIL V4 to improve library service desk management, ultimately fostering better user satisfaction and operational excellence.

Corresponding Author:

Muhammad Fawaid Al Ghifary
Departement of Information System, State Islamic University of Surabaya, Surabaya, Indonesia
Email: fawaidalghifary99@gmail.com

1. INTRODUCTION

Libraries are essential facilities in supporting academic and research activities, providing access to relevant information and literature for their users[1]. With advancements in information technology, library services have undergone a transformation, including the implementation of self-service systems to enhance accessibility and operational efficiency[2, 3]. These self-service systems allow users to perform various activities, such as literature searches, book borrowing, and returns, without requiring direct interaction with library staff[4].

JURNAL ECOTIPE
Electronic, Control, Telecommunication, Information, and Power Engineering
Volume 12, Issue 1, April 2025, pp. 65-76
ISSN 2355-5068 ; e-ISSN 2622-4852
DOI: 10.33019/jurnalecotipe.v12i1.4550

At the Library of the State Islamic University (UIN) Sunan Ampel Surabaya, self-service systems have been implemented as part of efforts to improve service quality[5]. However, the success of this implementation is closely tied to the effectiveness of service desk management[6]. The service desk plays a crucial role in ensuring the smooth operation of self-service systems, addressing user complaints, and providing necessary technical support[7].

The ITIL V4 (Information Technology Infrastructure Library) framework offers a systematic and standardized approach to managing IT services[8]. Within this context, service desk practices focusing on Acknowledge, Classify, Own, and Act serve as a reference for evaluating the effectiveness of service management in libraries[9]. This evaluation is essential to determine the extent to which self-service systems meet user needs and how existing challenges can be addressed.

This study aims to evaluate the management of the service desk in self-service systems at the UIN Sunan Ampel Library using the ITIL V4 framework[10]. Employing a descriptive qualitative approach, this research analyzes the strengths and weaknesses of the existing system while providing recommendations to improve the quality of IT services in the library. The findings are expected to contribute to the development of more effective and efficient technology-based library services.

2. RESEARCH METHOD

This study employs a mixed-method approach, integrating qualitative and quantitative methods to provide a comprehensive understanding of the self-service system at the UIN Sunan Ampel Surabaya Library. The combination of these methods ensures a more holistic evaluation of the effectiveness of Service Desk Management and allows for a deeper exploration of user experiences, challenges, and operational efficiency [11].

2.1. Research Approach

The research is structured around a descriptive qualitative approach with supplementary quantitative data analysis. The qualitative component focuses on in-depth interviews and observations, while the quantitative aspect relies on structured surveys and data analytics to measure system performance and user satisfaction [12].

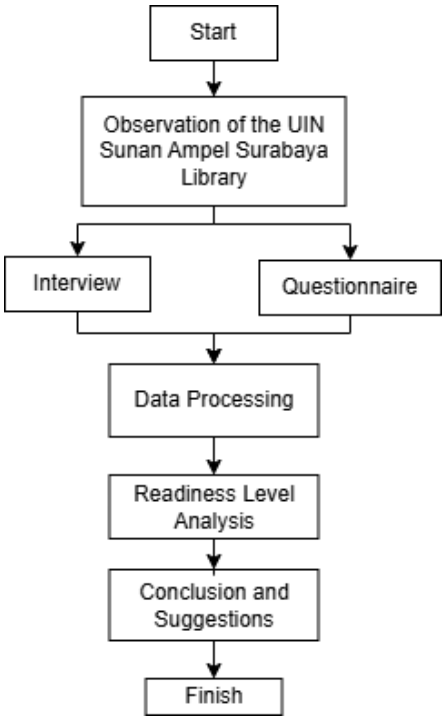

Figure 1 Research Flow

Volume 12, Issue 1, April 2025, pp. 65-76
ISSN 2355-5068 ; e-ISSN 2622-4852
DOI: 10.33019/jurnalecotipe.v12i1.4550

Qualitative Method:

1. Direct Observation: The research team conducted structured observations within the library environment to document real-time service operations, identify workflow inefficiencies, and evaluate user interactions with self-service systems.
2. In-Depth Interviews: Semi-structured interviews were conducted with library staff and service desk personnel to gain insights into the existing challenges, service expectations, and operational bottlenecks. The interview process covered aspects such as system usability, issue resolution efficiency, and staff preparedness for handling technical issues.

Quantitative Method:

1. User Surveys: Structured surveys were distributed to 200 library users, including students and faculty members, to assess their satisfaction with the self-service system. The survey included a mix of Likert-scale questions (to quantify user satisfaction levels) and open-ended questions (to collect qualitative feedback on service challenges).
2. Performance Metrics Analysis: System transaction logs were analyzed over a six-month period, focusing on parameters such as the average number of transactions, error rates, and resolution times. These data points provided quantifiable measures of the system's efficiency.

This approach ensures that the research findings are not only descriptive but also provide a data-driven overview of the library's readiness to adopt and enhance technology-based services. By integrating subjective perspectives (through qualitative methods) and objective metrics (through quantitative methods), this mixed-method approach strengthens the validity of the conclusions drawn.

2.2. Method of Collecting Data

The research was conducted in several stages to systematically collect and analyze data. These stages aim to provide a comprehensive understanding of the operational processes and user experiences within the UIN Sunan Ampel Surabaya Library[13]. Data collection followed a multi-stage process to ensure accuracy and reliability:

1. Preliminary Observation Phase: Initial observations were conducted to familiarize researchers with system workflows and user behaviors.
2. Interview and Survey Distribution: Library staff interviews were conducted over a four-week period, while user surveys were distributed electronically over eight weeks.
3. Data Integration and Triangulation: Qualitative findings from interviews were cross-referenced with quantitative survey data to validate key themes and ensure consistency in the research conclusions.

These stages are designed to capture both qualitative and quantitative aspects of the library's operations, ensuring a holistic analysis of its readiness for improvement.

2.3. Evaluation Framework

The evaluation framework in this study adopts the ITIL V4 framework, focusing on the Practice Success Factors (PSF) to assess and evaluate the performance and readiness of library services. The framework provides a structured approach to managing and improving service processes by addressing key operational aspects[14]. The evaluation is carried out through four primary components:

1. Acknowledge

This aspect focuses on recognizing requests or incidents reported by users or staff. In the context of library services, it includes acknowledging user feedback, service requests, and potential issues in a timely manner. The effectiveness of this step is measured by the responsiveness of the library in handling initial reports or inquiries.

2. Classify

The classification process involves grouping and prioritizing reported issues or requests based on their nature and urgency. This step is crucial to ensure that resources are allocated efficiently, and high-

Volume 12, Issue 1, April 2025, pp. 65-76
ISSN 2355-5068 ; e-ISSN 2622-4852
DOI: 10.33019/jurnalecotipe.v12i1.4550

priority issues are addressed promptly. In library operations, classification may include distinguishing between technical issues, user complaints, or service improvement requests.

3. Own

This component emphasizes assigning responsibility for resolving the issues or fulfilling the requests. Clear ownership ensures accountability and proper follow-through in addressing user needs. In the library context, this may involve assigning tasks to specific staff members or departments to handle reported incidents or implement improvements.

4. Act

The final aspect involves taking concrete actions to resolve the issues or fulfill the requests. This step focuses on implementing practical solutions and ensuring that corrective measures are effectively carried out. It includes monitoring the progress and evaluating the outcomes to ensure the issues are fully resolved and user satisfaction is achieved.

By applying the ITIL V4 framework, this evaluation provides a systematic approach to understanding the effectiveness of library service operations. The framework ensures that the library's processes align with best practices in service management, facilitating continuous improvement.

2.4. Research Location and Subjects

This research was conducted at the UIN Sunan Ampel Surabaya Library, a higher education institution library committed to providing advanced information and technology-based services. The library serves as a crucial facility for academic resources, offering various services, including a Service Desk and self-service library systems.

The research focuses on two primary subjects to comprehensively analyze the library's service readiness and operational effectiveness.

1. Service Desk Staff

The Service Desk staff plays a pivotal role in managing and delivering library services. They are responsible for handling user inquiries, addressing technical issues, and ensuring smooth daily operations. This group provides valuable insights into internal processes, operational challenges, and readiness to adopt service improvements or new technologies.

2. Library Self-Service Users

This group comprises library patrons, including students, faculty members, and general visitors, who utilize the self-service systems provided by the library. These users contribute quantitative and qualitative feedback on their experiences, satisfaction levels, and perceived ease of use. Their input is essential to evaluating the effectiveness and usability of the library's self-service technology. By involving both internal (staff) and external (users) stakeholders, the study ensures a holistic approach to understanding the library's service delivery and identifying potential areas for enhancement.

2.5. Data Analysis Process

The data analysis process in this research is conducted in several stages to ensure the validity and relevance of findings. These stages integrate results from observations, interviews, and documentation, aligning them with the ITIL V4 framework to evaluate performance and formulate actionable recommendations[15]. The process begins with data processing from observations, interviews, and documentation. Observational data are systematically categorized to identify patterns, bottlenecks, and operational strengths. Interview data, gathered from Service Desk staff, are transcribed, thematically coded, and analyzed to extract qualitative insights on challenges, workflows, and service readiness. Additionally, supporting documentation, such as internal reports, service logs, and user feedback records, is reviewed and cross-referenced with observational and interview data to ensure a comprehensive understanding.

The next stage involves analysis using ITIL V4 indicators, focusing on Practice Success Factors (PSF). The evaluation assesses several key aspects: Acknowledge, which measures the speed and consistency of recognizing user requests and incidents; Classify, which examines the accuracy and efficiency of grouping and prioritizing service requests or issues; Own, which evaluates the delegation of responsibilities and accountability in resolving issues; and Act, which determines the effectiveness of actions taken to address requests and their impact on user satisfaction. Through this structured

JURNAL ECOTIPE
Electronic, Control, Telecommunication, Information, and Power Engineering
Volume 12, Issue 1, April 2025, pp. 65-76
ISSN 2355-5068 ; e-ISSN 2622-4852
DOI: 10.33019/jurnalecotipe.v12i1.4550

approach, the research identifies areas for improvement in library operations and provides evidence-based recommendations to enhance service quality and operational readiness.

2.6. Expected Outcomes

The research aims to deliver tangible outcomes that address operational challenges and enhance library services at UIN Sunan Ampel Surabaya. These outcomes are designed to improve efficiency, user satisfaction, and technological adoption. One of the key outputs is the identification of challenges, where data analysis and evaluation using the ITIL V4 framework help uncover operational inefficiencies, delays in handling user requests, and limitations in the current technological infrastructure.

Based on these findings, the research provides recommendations for technological implementation to address the identified challenges. These recommendations include the establishment of a Service Level Agreement (SLA) to set clear performance standards for library services, ensuring accountability and consistency in meeting user expectations. Additionally, the study suggests the implementation of Radio-Frequency Identification (RFID) technology to streamline inventory management, improve book lending and return processes, and enhance tracking capabilities. Furthermore, the development and integration of real-time monitoring systems are proposed to oversee library operations, track service usage, and enable proactive issue resolution.

These outcomes aim to create a sustainable framework for continuous improvement, fostering a modern, efficient, and user-centric library environment.

2.7. Expected Outcomes

While this research provides valuable insights into Service Desk Management, certain limitations must be acknowledged.

1. Limited sample size: The study is based on 200 respondents, which may not fully capture the diverse experiences of all library users.
2. Potential response bias: Surveys and interviews rely on self-reported data, which may introduce subjective bias.
3. Technology constraints: The assessment focuses on the existing IT infrastructure, meaning findings may not fully generalize to other libraries with different technological capabilities.

3. RESULTS AND DISCUSSION

This chapter discusses the findings of the evaluation of Service Desk Management on the self-service system at the UIN Sunan Ampel Surabaya Library using the ITIL V4 framework. The analysis focuses on the Acknowledge, Classify, Own, and Act aspects and their contributions to the service value chain.

3.1. Description of Research Object

This study focuses on the Service Desk Management service in the self-service system implemented in the Sunan Ampel Surabaya State Islamic University (UIN) Library. This library acts as an information and learning center that provides various technology-based services to support the academic needs of the academic community. One of the innovations that has been implemented is the self-service system for borrowing and returning books, which allows users to make transactions independently through available computer devices. This self-service service is designed to improve the efficiency and convenience of users in accessing library facilities. Users can use this service by using a library membership card or Student Identity Card (KTM) which is integrated with the library system. In addition, this service is also supported by additional features such as online loan extensions, access to loan history, and late fine notifications

JURNAL ECOTIPE
Electronic, Control, Telecommunication, Information, and Power Engineering
Volume 12, Issue 1, April 2025, pp. 65-76
ISSN 2355-5068 ; e-ISSN 2622-4852
DOI: 10.33019/jurnalecotipe.v12i1.4550

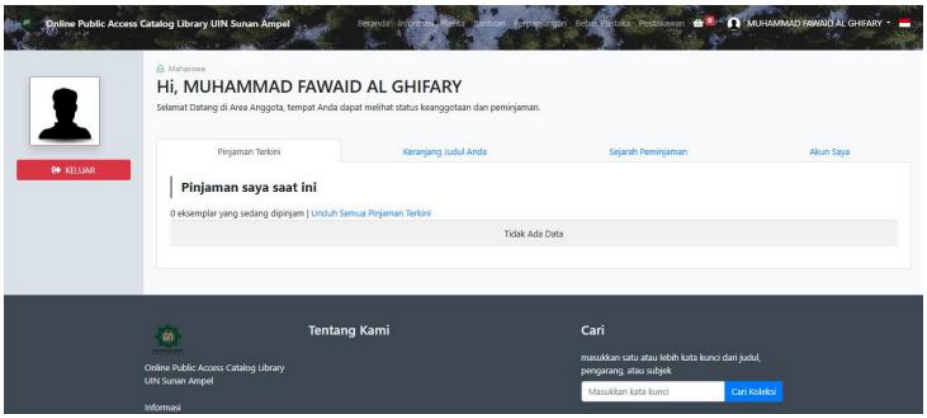

Figure 2 Library Member Loan History View

Although this innovation has provided significant benefits, there are several obstacles that need to be considered. One of the main challenges is the acknowledgment process which is still carried out manually, so it has the potential to slow down the response to user requests. In addition, the lack of communication integration in the service flow and the inconsistency of the implementation of standard operating procedures (SOPs) are obstacles in ensuring smooth services.

The ITIL V4 framework is used in this study to evaluate the performance of Service Desk Management. This framework provides a holistic approach that includes technical and non-technical aspects, such as Service Value Chain, Practice Success Factors (PSF), and maturity level. The focus of the evaluation includes the acknowledge, classify, own, and act aspects, which are important elements in ensuring the success of technology-based IT services. With this study, it is expected to obtain a comprehensive picture of the effectiveness of Service Desk Management services at the UIN Sunan Ampel Surabaya library, as well as strategic recommendations to improve efficiency and sustainable service quality.

3.2. Result and Data Analysis

Based on the results of observations and interviews, the following data were obtained regarding the performance of self-service services at the UIN Sunan Ampel Surabaya Library.

Table 1. Identification of Self Service Performance

Evaluation Aspect	FINDINGS	Percentage
Average Number of Transaction	Total Transaction for borrowing and returning books in the last six months	1.200 Transaction/month
Service success rate	Successful transaction recorded without technical problem	85 %
Main technical constraints	Errors in inputting transaction data (Manual Acknowledgment)	15 %
Real-time Monitoring feature	Not available to staff in the system	-

Self-service services show good performance with a transaction success rate of 85%. However, technical constraints such as manual acknowledgment processes and lack of real-time monitoring features hinder efficiency. Based on the ITIL V4 framework, the solution to this requires improvements in the Information and Technology and Value Stream and Processes dimensions.

Challenges in Request Management and Incident Resolution Interviews with users and library staff revealed the following challenges:

JURNAL ECTIPE
Electronic, Control, Telecommunication, Information, and Power Engineering
Volume 12, Issue 1, April 2025, pp. 65-76
ISSN 2355-5068 ; e-ISSN 2622-4852
DOI: 10.33019/jurnalecotipe.v12i1.4550

Table 2. Challenges in Request Management and Incident Resolution

Challenge Category	DESCRIPTION	Frequency
System technical errors	Transaction data not synchronized between user devices and the main system.	25% of total incidents
User procedure misalignment	Users lack understanding of system usage steps.	20% of total incidents
Slow response to incidents	Staff takes a long time to respond to user reports.	40% of users feel the response is slow

The table highlights that most challenges arise from technical issues and a lack of user guidance. The Engage and Deliver and Support dimensions of ITIL V4 need to be strengthened through clear user guidelines, staff training, and automated incident status notifications.

The maturity level assessment based on the ITIL V4 framework yielded the following results:

Table 3. Evaluation of Maturity Levels

Aspect Evaluated	Maturity Level	Findings
Incident management	Level 2 (*Repeatable*)	Processes are structured but not fully documented.
Service request management	Level 3 (*Defined*)	Clear operational procedures, but execution lacks consistency.
Service communication	Level 2 (*Repeatable*)	Relies on manual I interactions between staff and users.

The current maturity levels indicate that services are relatively well-organized but require improvements in documentation, automation, and communication integration. The *Continual Improvement* dimension of ITIL V4 is relevant to support ongoing enhancements.

Based on the analysis, the following recommendations are proposed to address the identified challenges:

Table 4. Recommendation for ITIL V4

Recommendation	Implementation Steps	Recommendation
Automating acknowledgment	Integrating automation features to ensure transactions are directly recorded	Automating acknowledgment
Real-time monitoring	Developing a real-time dashboard to monitor transaction and incident statuses.	Real-time monitoring
Staff training	Providing intensive training to staff to improve response speed and quality.	Staff training
Developing Service Level Agreements (SLAs)	Setting response time targets for each reported incident.	Developing Service Level Agreements (SLAs)

The above recommendations align with ITIL V4 principles, particularly in the Continual Improvement, Deliver and Support, and Engage dimensions. Implementing these measures is expected to enhance operational efficiency, improve user experience, and add value to the library services

JURNAL ECTIPE
Electronic, Control, Telecommunication, Information, and Power Engineering
Volume 12, Issue 1, April 2025, pp. 65-76
ISSN 2355-5068 ; e-ISSN 2622-4852
DOI: 10.33019/jurnalecotipe.v12i1.4550

3.3. Identifying Challenges and Issues

Based on the results of observations, interviews, and data analysis, several challenges and issues were identified in the implementation of *Service Desk Management* in the self-service system at the UIN Sunan Ampel Library. These challenges affect the efficiency and effectiveness of service delivery. The details are summarized in the following table.

Table 5. Identifying Challenge and Issues

Challenge Category	Description	Impact
Manual Acknowledgment process	The acknowledgment process for transactions (e.g., book borrowing/returning) is still performed manually by staff.	Slows down transaction processing and increases the risk of errors in recording transactions.
Lack of real-time monitoring	No realtime dashboard for staff to monitor transaction statuses or detect pending issues in the system.	Limits the ability of staff to quickly identify and resolve system problems.
Inconsistent application of SOPs	Standard Operating Procedures (SOPs) are not consistently implemented across all staff handling the system.	Results in varying service quality and response times for similar issues.
Delayed response to incidents	Staff response to user-reported incidents (e.g., failed transactions) is often delayed due to high workload or unclear prioritization.	Reduces user satisfaction and creates frustration among users.
Limited user guidance	Users often lack understanding of how to operate the self-service system effectively.	Leads to frequent errors during transactions, increasing the burden on support staff.

The challenges faced in the *Service Desk Management* at the UIN Sunan Ampel Library highlight several areas for improvement. From a technical perspective, the manual acknowledgment process and the absence of real-time monitoring reveal a significant gap in the system's technological capability. These issues hinder efficiency and increase the risk of errors in transaction handling. To address these gaps, automating processes and implementing a monitoring system would be critical steps, aligning with the ITIL V4 dimensions of *Information and Technology* and *Value Streams and Processes*.

User-related challenges also emerge due to limited guidance provided to users, which often leads to procedural errors during self-service transactions. These errors increase the workload of support staff and reduce the overall effectiveness of the system. Creating user-friendly manuals, providing on-site assistance, or conducting workshops can significantly improve user comprehension and minimize mistakes, supporting the *Engage* dimension of ITIL V4.

Operational challenges further compound the issues, including inconsistent application of Standard Operating Procedures (SOPs) and delayed responses to incidents. These issues indicate the need for clearer workflows and improved staff training. Establishing a Service Level Agreement (SLA) can standardize response times and ensure consistent service quality, aligning with ITIL V4's focus on *Deliver and Support*.

To overcome these challenges, several measures are recommended. First, automating acknowledgment processes and transaction recording can reduce manual errors and expedite service delivery. Second, the development of a real-time monitoring dashboard would enable staff to track system statuses and resolve issues proactively. Third, enhancing user education through step-by-step guides and workshops would empower users to navigate the self-service system effectively, reducing the frequency of procedural errors. Fourth, standardizing SOP implementation across all staff through regular training sessions would ensure uniformity in service delivery. Finally, introducing SLAs with measurable targets for response times would improve the timeliness of incident resolution and enhance user satisfaction.

JURNAL ECTIPE
Electronic, Control, Telecommunication, Information, and Power Engineering
Volume 12, Issue 1, April 2025, pp. 65-76
ISSN 2355-5068 ; e-ISSN 2622-4852
DOI: 10.33019/jurnalecotipe.v12i1.4550

By addressing these challenges systematically, the UIN Sunan Ampel Library can significantly enhance its *Service Desk Management* processes. These improvements would result in better service quality, increased operational efficiency, and higher levels of user satisfactions.

3.4. Evaluation of ITIL V4 Framework

The ITIL V4 framework plays a crucial role in analyzing and addressing the challenges identified in the Service Desk Management system at the UIN Sunan Ampel Library. By providing a structured approach to managing IT services, ITIL V4 ensures that processes align with organizational goals and user needs, enabling efficient and effective service delivery. The implementation of ITIL V4 in this study helps evaluate key aspects of the library's service management processes, particularly in the context of its self-service system. ITIL V4 emphasizes flexibility and adaptability, which are essential for addressing technical, user-related, and operational challenges in a dynamic library environment. By leveraging its principles, the framework provides actionable insights into areas such as service acknowledgment, incident resolution, and system monitoring. Implementation of ITIL V4 Dimensions.

1. Value Stream and Processes

This dimension focuses on creating value through seamless and coordinated workflows. In the library's self-service system, the acknowledgment process, user interactions, and incident handling were analyzed using this dimension. The lack of automation and real-time monitoring highlighted inefficiencies in the current processes, prompting recommendations to streamline workflows and improve service efficiency.

2. Service Value Chain (SVC)

The SVC model, which outlines six interconnected activities (Plan, Improve, Engage, Design and Transition, Obtain/Build, Deliver and Support), was applied to evaluate the lifecycle of service delivery. Specifically (Engage) Emphasized user interactions and feedback mechanisms to identify gaps in user support and communication, (Deliver and Support) Evaluated the effectiveness of daily operations, such as transaction recording and incident resolution, identifying the need for SLAs to standardize response times, (Improve) Addressed continuous improvement opportunities, such as enhancing user education and training staff to ensure consistent SOP implementation.

3. Practice Success Factors (PSF)

The PSF component of ITIL V4 was used to measure the maturity level of various service management practices, such as incident management and service request fulfillment. This analysis revealed that the library operates at a repeatable level (Level 2) in several areas, indicating structured but incomplete processes. Recommendations were made to elevate these practices to the defined level (Level 3) through documentation, automation, and process standardization.

4. Information and Technology

This dimension was critical in assessing the technological gaps in the self-service system. The absence of real-time monitoring tools and reliance on manual acknowledgment were key issues identified. Recommendations included implementing a dashboard for real-time monitoring and automating transaction processes to enhance efficiency and reduce errors.

5. Continual Improvement

ITIL V4's continual improvement principle was applied to identify opportunities for ongoing enhancements. The study proposed iterative evaluations and feedback loops to monitor the impact of implemented changes, ensuring that services remain aligned with user expectations and organizational objectives.

The ITIL V4 framework provides a comprehensive approach to evaluating and improving the *Service Desk Management* processes in the library. By leveraging its dimensions and principles, the library can address its current challenges and achieve a higher level of operational excellence. Future efforts should focus on fully implementing the recommended changes, ensuring continuous alignment with the ITIL V4 practices to deliver value-driven and user-centric service.

JURNAL ECTIPE
Electronic, Control, Telecommunication, Information, and Power Engineering
Volume 12, Issue 1, April 2025, pp. 65-76
ISSN 2355-5068 ; e-ISSN 2622-4852
DOI: 10.33019/jurnalecotipe.v12i1.4550

3.5. Impact of Research Findings

The findings of this research have brought significant positive impacts on improving services, enhancing system efficiency, and increasing user satisfaction at the UIN Sunan Ampel Surabaya Library. These impacts align with the research objectives and recommended best practices based on the ITIL V4 framework.

1. Service Improvement

Recommendations such as automating the acknowledgment process and developing a real-time monitoring dashboard enable the library to deliver faster, more accurate, and responsive services. These improvements provide users with not only more efficient services but also enhanced quality in every interaction with the self-service system. Relation to Research Objectives: The research objective of improving the effectiveness of Service Desk Management is achieved through the integration of technology and workflow optimization supported by the Information and Technology and Value Streams and Processes dimensions in ITIL V4.

2. Operational System Efficiency

Automation and consistent implementation of SOPs as recommended allow library staff to reduce time spent on manual tasks such as transaction verification. This enables staff to allocate more time to strategic tasks, such as managing collections and engaging directly with users. The implementation of SLAs also provides clarity in task prioritization, helping the organization manage resources more effectively. Relation to ITIL V4 Best Practices: This operational efficiency aligns with the Deliver and Support principle, which emphasizes the importance of maintaining service availability and functionality as per user requirements.

3. Enhanced User Satisfaction

With improved user education through guides and training, along with SLAs that ensure quicker response times, users experience a better service experience. A more transparent process and consistent service standards increase user trust in the system. Relation to ITIL V4 Dimensions: The Engage dimension is the focus here, where user feedback is integrated into the system to create a better and more relevant service experience.

4. Application of Best Practices

The recommendations derived from this research reflect the application of ITIL V4 best practices, such as the Service Value Chain, which guides every step of service delivery from planning to improvement. Continuous improvement processes are also implemented to ensure that every enhancement step is regularly evaluated and adjusted to organizational needs. Relation to Research Objectives: This research successfully connects the application of ITIL V4 dimensions to the specific context of the library, resulting in a more adaptive and relevant service model.

5. Long-Term Contribution

The long-term impacts of this research include fostering a culture of continuous improvement in managing the library's IT services. By leveraging these recommendations, the library can continuously innovate in delivering modern, user-focused services while enhancing staff capabilities in addressing evolving technological challenges Relation to ITIL V4 Practices: The Continual Improvement principle in ITIL V4 ensures that services are not only improved in the short term but are continuously developed to meet future demands.

The impacts of this research demonstrate great potential in transforming Service Desk Management at the UIN Sunan Ampel Library. By following the ITIL V4-based recommendations, the library can not only meet its research objectives but also create a service system that is more efficient, measurable, and user-centered. This positions the library as a model for modern service management that can be applied to other educational institutions.

3.6. Recommendations for Service Development

Based on the findings, several strategies are proposed to enhance the quality and efficiency of the Service Desk Management system at the UIN Sunan Ampel Library. Automating transaction processes, particularly the acknowledgment system, can significantly reduce manual errors and speed up service delivery. By integrating automation technologies, transactions for book borrowing and returning can be recorded automatically, allowing staff to focus on more strategic tasks. Additionally, the implementation

Volume 12, Issue 1, April 2025, pp. 65-76
ISSN 2355-5068 ; e-ISSN 2622-4852
DOI: 10.33019/jurnalecotipe.v12i1.4550

of a real-time monitoring dashboard will enable staff to track system statuses and address issues proactively, minimizing downtime and improving responsiveness. To ensure consistent and reliable service delivery, establishing Service Level Agreements (SLAs) is recommended. SLAs will define clear response time targets for resolving incidents, providing users with measurable expectations and fostering trust in the system.

User education is also a critical component of the proposed improvements. Creating user-friendly guides and conducting workshops will help users navigate the self-service system effectively, reducing procedural errors and enhancing the overall user experience. At the same time, staff training is essential to ensure consistent application of Standard Operating Procedures (SOPs) and to improve problem-solving capabilities. Regular training sessions and scenario-based simulations will prepare staff to handle common issues efficiently. Finally, integrating a continual improvement process into the management system will ensure that services remain adaptive and aligned with user needs. This involves regular evaluations of service performance, gathering feedback, and implementing incremental changes to address emerging challenges. By adopting these strategies, the library can deliver a more user-centric, efficient, and sustainable service system.

4. CONCLUSION

The evaluation of Service Desk Management in the self-service library system at UIN Sunan Ampel Surabaya using the ITIL V4 framework highlights several key findings. While the self-service system provides adequate accessibility for users, there are notable challenges, such as the manual acknowledgment process, inconsistent incident classification, and the lack of sufficient monitoring tools. User satisfaction is generally positive, with an average score of 3.8 out of 5, though issues such as interface usability and delays in addressing technical problems were raised. The analysis using ITIL V4—focusing on Acknowledge, Classify, Own, and Act—identifies areas for improvement. To address these issues, the study recommends implementing automation technologies like RFID for inventory management, integrating real-time monitoring systems, and establishing Service Level Agreements (SLAs). Additionally, staff training programs are essential to enhance readiness for technological advancements. By adopting these solutions, the self-service library system is expected to provide a better user experience, improve operational efficiency, and support the library's mission as a modern, responsive, and user-centric information hub.

.

REFERENCES

[1] L. Sa'diyah dan M. F. Adli, "Perpustakaan Di Era Teknologi Informasi," *AL Maktab.*, vol. 4, no. 2, hal. 142, 2019, doi: 10.29300/mkt.v4i2.4042.

[2] R. I. Fachriz, Y. E. Nugroho, dan A. D. Cahyaningtyas, "Layanan Peminjaman dan Pengembalian Otomatis Berbasis Self Service di UPT Perpustakaan Rumah Ilmu Universitas Negeri Semarang," *J. Penelit. Pendidik.*, vol. 39, no. 2, hal. 87–92, 2022, doi: 10.15294/jpp.v39i2.40300.

[3] A. M. F. Thaha, A. Tenriawaru, dan G. Gunawan, "Implementasi Content Management System Pada Layanan Digitalisasi Perpustakaan Menggunakan Senayan Library Management System," *AnoaTIK J. Teknol. Inf. dan Komput.*, vol. 1, no. 2, hal. 59–67, 2023, doi: 10.33772/anoatik.v1i2.14.

[4] Suryani dan Nur Madinah Yandriswan, "Digitalisasi Sistem Perpustakaan Multi Level Akses Berbasis Web (Studi Kasus : Sma Negeri 04 Makassar)," *J. Inform. Polinema*, vol. 9, no. 2, hal. 201–206, 2023, doi: 10.33795/jip.v9i2.1238.

[5] Manulu, "SENTRI : Jurnal Riset Ilmiah," *SENTRI J. Ris. Ilm.*, vol. 2, no. 4, hal. 1275--1289, 2023.

[6] M. Mursyidah, S. Sukirman, dan D. Hidayati, "Pemanfaatan Sistem Informasi Manajemen Perpustakaan Dalam Menumbuhkan Minat Baca Siswa Di SMAN 1 Berau," *J. Inov. Dan Manaj. Pendidik.*, vol. 3, no. 1, hal. 61–75, 2023, doi: 10.12928/jimp.v3i1.9366.

Volume 12, Issue 1, April 2025, pp. 65-76
ISSN 2355-5068 ; e-ISSN 2622-4852
DOI: 10.33019/jurnalecotipe.v12i1.4550

[7] M. Mambang *et al.*, "Evaluasi Maturity Level Tata Kelola Teknologi Informasi di Perpustakaan Perguruan Tinggi Menggunakan Cobit 5," *J. Nas. Komputasi dan Teknol. Inf.*, vol. 5, no. 4, hal. 652–658, 2022, doi: 10.32672/jnkti.v5i4.4546.

[8] Fajar Nugraha Wahyu, "Pengembangan Sistem Service Desk Uin Syarif Hidayatullah Jakarta Menggunakan Metode User Centered Design (UCD) Berdasarkan Itil V3 Framework," 2023.

[9] N. B. Utomo dan M. A. Syamsuddin, "Evaluasi Implementasi Service Desk Pada Direktorat Informasi Kepabeanan Dan Cukai Menggunakan Itil V3," *J. Perspekt. Bea Dan Cukai*, vol. 4, no. 1, hal. 86–96, 2020, doi: 10.31092/jpbc.v4i2.766.

[10] B. A. Sekti dan S. N. Kholifah, "Analisis Tingkat Kematangan Aplikasi Tangerang LIVE dalam Mengelola Incident Management , Problem Management , dan Service Desk Menggunakan Framework ITIL V4 meningkatkan pelayanan kepada penduduknya . Salah satu upaya yang mereka lakukan Tangerang . Tang," vol. 10, no. 1, hal. 187–202, 2024.

[11] A. Aulia Zahra D, I. Santosa, dan W. Agustika Nurtrisha, "Asesmen dan Peningkatan Manajemen Layanan Teknologi Informasi Pada Practice Service Request Management dan Change Control Menggunakan ITIL 4 (Studi Kasus : Unit RiYanTI Telkom University)," *e-Proceeding Eng.*, vol. 10, no. 3, hal. 3165–3171, 2023, [Daring]. Tersedia pada: https://openlibrarypublications.telkomuniversity.ac.id/index.php/engineering/article/view/20572.

[12] J. F. Andry dan K. Christianto, "Evaluating Maturity Level Using Framework ITIL: A Case Study of Service Desk's," *Int. J. Inf. Technol. Bus.*, vol. 1, no. 1, hal. 16–23, 2018, doi: 10.24246/ijiteb.112018.16-23.

[13] J. A. Ayuh dan H. P. Chernovita, "Analisis Incident Management E-Court Pada Pengadilan Negeri Salatiga Menggunakan Framework ITIL V4," *JATISI (Jurnal Tek. Inform. dan Sist. Informasi)*, vol. 8, no. 2, hal. 585–598, 2021, doi: 10.35957/jatisi.v8i2.901.

[14] R. Andriani, "Analisis Kualitas Self Service Perpanjangan Online Peminjaman Koleksi Di Upt Perpustakaan Institut Teknologi Bandung," *Shaut Al-Maktabah J. Perpustakaan, Arsip dan Dokumentasi*, vol. 12, no. 1, hal. 60–71, 2020, doi: 10.37108/shaut.v12i1.228.

[15] D. Ditasman, R. Hartono, dan N. Saputra, "Inovasi Layanan Pojok Brailie Dan Kualitas Layanan Perpustakaan Dan Kearsipan Provinsi Bengkulu," *J. Gov. Public Adm.*, vol. 1, no. 1, hal. 106–129, 2023, doi: 10.59407/jogapa.v1i1.392.

JURNAL ECOTIPE
Electronic, Control, Telecommunication, Information, and Power Engineering

Volume 12, Issue 1, April 2025, pp. 77-86
ISSN 2355-5068 ; e-ISSN 2622-4852
DOI: 10.33019/jurnalecotipe.v12i1.4547

Effect of Tilt Angle on Solar Cell Efficiency and Electrical Energy of Nanofluid-Filled Photovoltaic-Thermal (PV/T) Systems

Fadilla Ananda[1], Marhama Jelita[2]
[1,2] Department of Electrical Engineering, Universitas Islam Negeri Sultan Syarif Kasim Riau, Pekanbaru 28293, Indonesia

ARTICLE INFO

Article historys:

Received : 10/02/2025
Revised : 02/03/2025
Accepted : 30/03/2025

Keywords:

Energy Efficiency; Finite Element Method; Nanofluid; PV/T System; Tilt Angle

ABSTRACT

This study aims to investigate the impact of nanofluid concentration and panel tilt angle on the efficiency of photovoltaic-thermal (PV/T) systems, with the goal of optimizing energy performance. Numerical simulations were conducted using the Finite Element Method (FEM) to analyze the effects of varying nanofluid concentrations and panel inclination angles on PV/T system performance. The findings revealed that a nanofluid concentration of 20% provided the most uniform fluid flow. At an inclination angle of $\pi/6$, increasing the concentration to 20% reduced the PV cell temperature and enhanced photovoltaic efficiency to 12.04%, while also achieving the highest electrical power output of 36.71 W. The highest thermal efficiency of 69.5% was observed at a 20% concentration with a $\pi/6$ tilt angle, whereas the highest total efficiency of 81.7% was achieved at a $\pi/3$ tilt angle. The study demonstrates that optimizing the combination of nanofluid concentration and panel tilt angle significantly enhances the energy efficiency of PV/T systems. This advancement contributes to the development of more efficient renewable energy technologies.

Corresponding Author:

Marhama Jelita
Universitas Islam Negeri Sultan Syarif Kasim Riau, JL. HR. Soebrantas No.Km 15, Simpang Baru, Kota Pekanbaru
Email: marhamajelita@gmail.com

1. INTRODUCTION

Energy is the main pillar in driving economic development and social welfare, both in supporting economic activities and daily needs [1]. Most energy resources come from fossil fuels. Dependence on fossil fuels causes challenges in the form of depletion of reserves, a global energy crisis, and negative environmental impacts such as global warming, excess carbon emissions, and significant climate change [2]. The development of renewable energy sources, especially solar energy, is a solution to overcome dependence on fossil fuels [3]. The main technology for converting solar energy into electricity is photovoltaic (PV) panels, which convert solar energy into electricity. However, only about 20% can be converted, while 80% is wasted as heat [4]. The accumulation of heat can decrease the efficiency and performance of PV cells. An increase in temperature above 25°C can degrade the performance of PV modules resulting in reduced power output and efficiency decreasing by about 0.5% per degree Celsius against temperature increase [5]. The reduction in PV efficiency caused by rising temperatures can be mitigated by incorporating a cooling system into the PV panel. This technology, known as a photovoltaic-thermal (PV/T) system, converts solar energy into both electricity and thermal energy at the same time [6].

Because of the high efficiency of PV/T systems, extensive research has been conducted to further develop and improve them [7]. Many studies have explored ways to improve electrical efficiency, as well as designing and optimizing the operational parameters of PV/T systems. Previous research shows

JURNAL ECTIPE
Electronic, Control, Telecommunication, Information, and Power Engineering
Volume 12, Issue 1, April 2025, pp. 77-86
ISSN 2355-5068 ; e-ISSN 2622-4852
DOI: 10.33019/jurnalecotipe.v12i1.4547

that the temperature reduction of PV cells evaluated using PV/T technology with water as the cooling medium, results in a temperature reduction of up to 2°C, which contributes to a 3% increase in efficiency [8]. Furthermore, another investigation revealed that a PV/T cooling system employing water fluid in a laminar arrangement could decrease the PV cell temperature is reduted drop of 2°C [9]. The research additionally discovered that the base fluid (water) used in the solar collector outperforms the air system, the water temperature within the PV/T collector remains more stable despite variations in solar radiation levels, whereas the air-based collector is more prone to temperature fluctuations [10].

Cooling systems in PV/T can use various types of fluids, one of which is nanofluids. Nanofluids are fluids that have added nanoparticles with sizes between 1 and 100 nanometers, which can improve their thermal properties. Prior studies investigated the application of CuO-water nanofluids for cooling, resulting in a 51.22% overall efficiency and a 72.58% energy accumulation efficiency, surpassing that of Al_2O_3-water [11]. Moreover, additional studies discovered that CuO/water nanofluids exhibited superior performance compared to Al_2O_3/water and pure water [12]. Meanwhile, another study said that nanoparticles in nanofluids improve thermal conductivity and heat transfer, resulting in more optimal performance in PV/T systems [13]. The other research analyzed the combination of nanofluid flow rate and nanoparticle concentration to obtain maximum thermal efficiency [14].

In PV/T systems, the use of nanofluids shows a positive impact on the efficiency of panels installed with various tilt angles [15]. The amount of solar radiation received is significantly influenced by the tilt angle, which directly affects system performance. Previous research revealed that at optimal tilt angles, the use of nanofluids can increase thermal efficiency by up to 35% compared to systems using plain water as the cooling medium [16]. In addition, the optimal tilt angle is important to maximize the energy received, as it affects the heat transfer and performance of the PV/T system. When the inclination angle is not optimal, the received solar radiation decreases, thus lowering the electrical and thermal energy conversion efficiency [17]. This suggests that optimization of the inclination angle of solar cell panels, along with the use of nanofluids, can make a significant contribution to the efficiency of renewable energy systems.

A literature review indicates that utilizing nanofluids as a cooling medium in PV/T systems enchances thermal conductivity and energy efficiency compared to plain water, especially in the CuO/water nanofluid type [11, 12]. It was noted in earlier studies that the tilt angle of the panel influences the quantity of solar radiation it receives, thereby affecting system efficiency [16]. This research focuses on improving solar cell efficiency and electrical energy applied to PV/T systems through assessing the effects of nanofluid concentration and tilt angle variation. The Finite Element Method (FEM) was chosen for its ability to solve complex thermal analysis. The evaluation of the PV cell efficiency, electrical energy, thermal capability, and overall system efficiency will be grounded in the Second Law of Thermodynamics. This law elucidates that energy transitions from high to low states, offering insights into the system's overall efficiency.

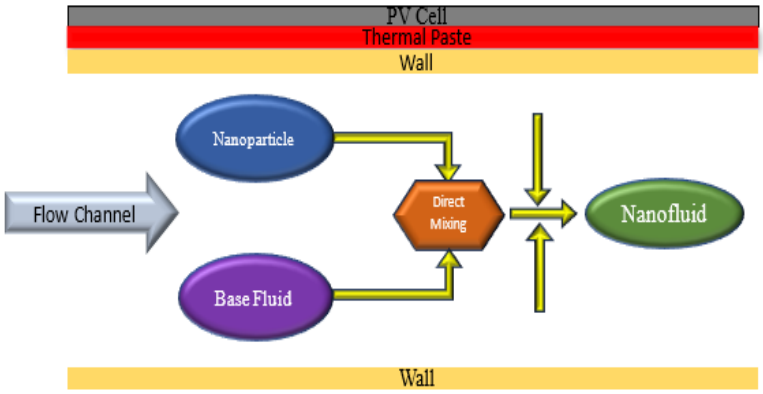

Figure 1. Schematic Model of PV/T Solar Panels and Flow Channels Filled with Nanofluids

2. RESEARCH METHOD

Figure 1 illustrates the photovoltaic-thermal (PV/T) solar panel model used in this study. The PV/T system consists of multiple layers: the PV cell layer, a thermal paste layer, the reservoir wall, and a flow

Volume 12, Issue 1, April 2025, pp. 77-86
ISSN 2355-5068 ; e-ISSN 2622-4852
DOI: 10.33019/jurnalecotipe.v12i1.4547

channel within the reservoir that contains the nanofluid. The solar panel design features a side length of 30.5 cm and a thickness of 0.27 mm. Monocrystalline silicon (c-Si) was chosen for the PV cell layer due to its superior heat absorption capacity compared to polycrystalline silicon (p-Si). Typically, c-Si cells exhibit a photovoltaic conversion efficiency of approximately 13% and a heat coefficient of 0.54. The thermal paste layer, a conductive material, measures 30.5 cm in length and 0.3 mm in thickness. The reservoir wall is constructed from aluminum, with a length of 30.5 cm and a thickness of 1 mm. The flow channel within the reservoir, designed for fluid circulation, has a length of 30.5 cm and a thickness of 15 mm. The nanofluid was prepared using a direct mixing method, combining a base fluid (water) with nanoparticles (solid) to achieve a stable mixture. The nanofluid flow was assumed to be laminar, with a velocity of 0.01 m/s. The reservoir wall thickness was set at 0.015 m for simulation purposes. This study investigates the effects of varying tilt angles ($\pi/6$, $\pi/4$, and $\pi/3$) and nanoparticle concentrations (1%, 10%, and 20%) on the fluid velocity profile within the channel. These parameters were systematically analyzed to asses their effect on the total efficiency of the PV/T system.

The conjugate heat transfer approach has been used to develop heat transfer equations for the PV cell layer, thermal paste layer, reservoir structure, and flow channel. The temperature at the PV surface is considered fixed and uniform. In the analysis, the sky is assumed to be a black body that emits long-wave radiation according to the environmental conditions. In addition, it is assumed that the environment is dust-free allowing full transmission of solar energy. Table 1 lists the physical properties of solar radiation as well as the relevant environmental condition parameters.

Table 1. Nature of Incoming Energy from the Sun and Environmental Conditions

Quantity Name	Value	Distance (m)
Solar Irradiance	1.000	G (kg/m^2)
Heat Transfer Coefficient	6.5	Hc(W/(m2K))
Ambient Temperature	298.15	T_{amb} (K)
Radiation Emissivity	0.3	ε (kg/m^2)

PV panels, as shown in Figure 1, receive energy from sunlight. A portion of the radiative energy is transformed into electrical power through the photovoltaic process, whereas the remaining energy is converted into thermal energy. Radiation affects the entire surface of the plate. Thermal paste applied under the PV array serves to effectively distribute the heat, thereby helping to improve the efficiency of electrical conversion. The following formula describes the convection heat transfer process at the PV panel's top and bottom interfaces.:

$$q\_conv = -hc\,A + Tpv - Tamb \quad (1)$$

Hc represents the heat loss caused by convection, while A represents the surface area. Heat transfer at the PV/T panel's top and bottom interfaces as well as the energy carried by the nanofluid flow inside the reservoir are both included in the total conjugate convection. The following formula can be used to describe heat loss from infrared radiation, which is electromagnetic radiation released by the atmosphere and surface:

$$q_{lw} = \varepsilon.\sigma + \left(T^4{}_{pv} \_ T^4{}_{amb}\right) \quad (2)$$

Where σ stands for electrical conductivity and ε for radiation emissivity. An important consideration for modeling heat in participating media is the assessment of extinguishing, absorption, and scattering coefficients. The media extinguishing coefficient can be formulated as follows:

$$K_e = \frac{1.5\phi Q_e}{d} + (1 - \phi)\,\frac{4\pi K_{bf}}{\lambda} \quad (3)$$

Where Q is the nanoparticle attenuation coefficient, λ is the wavelength of radiation, and d denotes the diameter of the nanoparticle. The attenuation coefficient of water can be calculated using the following equation:

$$K_{bf} = K_a + K_s \quad (4)$$

Table 2. Basic Thermophysical Properties of Nanofluids

Volume 12, Issue 1, April 2025, pp. 77-86
ISSN 2355-5068 ; e-ISSN 2622-4852
DOI: 10.33019/jurnalecotipe.v12i1.4547

Properties	Water	Copper
Cp (J/kgK)	4.179	383
ρ (kg/m^3)	997.1	8954
K (W/mK)	0.605	400
μ (Ns/m^2)	0.00108	-

Table 3. Nanofluid Physical Properties

Properties	Copper
Cp (J/kgK)	4027.2
ρ (kg/m^3)	1315.4
K (W/mK)	0.608027
μ (pas)	0.001196

In all layers, heat transfer occurs from the nanofluid to the solid, from the solid to the nanofluid, or flows through the solid layer via a conjugate convection mechanism. The nanofluid at the inlet is assumed to have a uniform temperature. This hybrid approach is applied to enable solar cells to convert transform solar radiation into electrical energy under optimal conditions. Most of the absorbed fraction of incident solar radiation is transformed into thermal energy, resulting in a rise in the solar cell temperatur. The increase in temperature is utilized through a cooling mechanism for the PV/T module using nanofluids, with the aim of maximizing the generated electricity. To calculate the efficiency, various equations are used. When PVs are exposed to solar radiation, the energy that is not fully utilized turns into thermal energy on the panel surface. The heat transfer across the PV cell, thermal paste, and reservoir wall is expressed by the following equation:

$$\nabla . (k \nabla T) = 0 \tag{5}$$

Inside the duct, heat transfer takes place through convection and conduction. The flow, at both inlet and outlet velocities, is assumed to be constant, incompressible, Newtonian, and laminar. The solid nanoparticles are assumed to have a uniform shape and size and maintain thermal equilibrium with the host fluid. The utilized particles are nano-sized aluminum oxide, with thermophysical values listed in Table 2. The difference in density versus temperature in relation to the gravitational force is considered linear according to the Boussinesq model. This model applies accurately when the density variation is small enough that it does not affect the convective flow, except for the gravitational effect. Taking these elements into account, the equations for continuity, momentum, and energy are articulated as follows:

$$\frac{\partial U}{\partial X} + \frac{\partial V}{\partial Y} = 0 \tag{6}$$

$$U\frac{\partial U}{\partial X} + V\frac{\partial U}{\partial Y} = -\frac{1}{\rho_{nf}}\frac{\partial P}{\partial X} + \frac{\mu_{nf}}{\rho_{nf}}\left(\frac{\partial^2 U}{\partial X^2} + \frac{\partial^2 U}{\partial Y^2}\right) - \frac{1}{\rho_{nf}}(\rho\beta)_{nf} g \sin\varphi\,(T - T_C) \tag{7}$$

$$U\frac{\partial V}{\partial X} + V\frac{\partial V}{\partial Y} = -\frac{1}{\rho_{nf}}\frac{\partial P}{\partial Y} + \frac{\mu_{nf}}{\rho_{nf}}\left(\frac{\partial^2 V}{\partial X^2} + \frac{\partial^2 V}{\partial Y^2}\right) - \frac{1}{\rho_{nf}}(\rho\beta)_{nf} g \cos\varphi\,(T - T_c) \tag{8}$$

$$U\frac{\partial T}{\partial X} + V\frac{\partial T}{\partial Y} = \alpha_{nf}\left(\frac{\partial^2 T}{\partial X^2} + \frac{\partial^2 T}{\partial Y^2}\right) + \frac{1}{(\rho C_\rho)nf}\nabla . Q_r \tag{9}$$

Here, (U, V) refers to the velocity vector, T denotes the temperature, and P signifies the pressure. The subscript none indicates the bulk properties of the nanofluid, while g represents gravitational acceleration. Furthermore, μ, ρ, β, and α represent the dynamic viscosity, density, thermal expansion value, and thermal diffusion rate of the nanofluid at ambient temperature, correspondingly. The nanofluid density is expressed as the combined relationship between water and dispersed particles,

$$\rho_{nf} = (1 - \phi)\,\rho_{bf} + \phi\rho_{sp} \tag{10}$$

Where φ is the volume fraction of nanoparticles. The symbol bf refers to the base fluid or water. The viscosity of the base fluid affected by the addition of nanoparticles can be written:

Volume 12, Issue 1, April 2025, pp. 77-86
ISSN 2355-5068 ; e-ISSN 2622-4852
DOI: 10.33019/jurnalecotipe.v12i1.4547

$$\mu_{nf} = \frac{\mu_{bf}}{(1-\phi)^{2.5}} \tag{11}$$

The thermal diffusivity of nanofluids, which is a measure of how quickly heat can spread through a material:

$$\alpha_{nf} = \frac{k_{nf}}{(\rho C_p)_{nf}} \tag{12}$$

Nanofluids' specific heat capacity is a combination of their base fluid and nanoparticles:

$$(\rho C_p)_{nf} = (1-\phi)\,(\rho C_P)_{bf} + \phi(\rho C_P)_{sp} \tag{13}$$

The thermal expansion coefficient of the nanofluid, which describes how much the volume of the nanofluid changes as the temperature changes, can be calculated:

$$\beta_{nf} = (1-\phi)\,\beta_{bf} + \phi\beta_{sp} \tag{14}$$

The heat transfer capability of the nanofluid was calculated based on Maxwell's equations:

$$k_{nf} = k_{bf}\left[\frac{k_p+2k_{bf}-2(k_p-k_f)\phi}{k_p+2k_{bf}+(k_p+k_p)\phi}\right] \tag{15}$$

Equations (5) to (15) are analyzed using the finite element method (FEM). After solving these equations, the power conversion efficiency of the PV cell is evaluated using the following equation:

$$\eta_{pv} = \eta_{ref}\left[1-\beta_{ref}\left(T_{pv}-T_{ref}\right)\right] \tag{16}$$

The electrical energy produced is the total electrical potential energy transformed into dynamic energy in SI units of Joules per second (Watt). For PV/T (Photovoltaic/Thermal) systems, the electrical energy output can be calculated with the following formula:

$$E_{pv} = \eta_{pv} \times A_m \times G \tag{17}$$

PV cell efficiency, surface area, and solar radiation intensity all affect the electrical output. The following formula can be used to express the electricity generated by a PV module under exposure to sunlight:

$$E_{in} = G.A_m \tag{18}$$

The thermal energy obtained by using nanofluid serving as a heat dissipation agent in the PV/T system is calculated by:

$$E_{nf} = m_{nf}C_p(T_{out}-T_{in}) \tag{19}$$

The percentage of thermal energy successfully converted into electrical energy can be calculated using:

$$\eta_{th} = \frac{E_{nf}}{E_{in}} \times 100\% \tag{20}$$

Total electrical and thermal energy output divided by total electrical energy received is the PV/T system's overall or global efficiency, and it is calculated as follows:

$$\eta_{glob} = \frac{E_{nf}+E_{PV}}{E_{in}} \times 100\% \tag{21}$$

The Finite Element Method (FEM) is used to numerically solve the continuity, momentum, and energy equations. This method operates by breaking down the problem domain into multiple smaller subdomains, making the computational process more manageable. In this study, the flow inside the solar collector is assumed to be an incompressible and laminar flow (spf) to solve equations (6)–(8), as well as heat transfer in fluids (ht) for equation (9). Irradiation is calculated assuming a constant heat flux as the boundary condition.

As a validation step, the temperature values obtained were compared with the research data of Fontenault and Gutierrez-Miravete (2012), as shown in Figure 2.

JURNAL ECTIPE
Electronic, Control, Telecommunication, Information, and Power Engineering
Volume 12, Issue 1, April 2025, pp. 77-86
ISSN 2355-5068 ; e-ISSN 2622-4852
DOI: 10.33019/jurnalecotipe.v12i1.4547

(a) experiments conducted

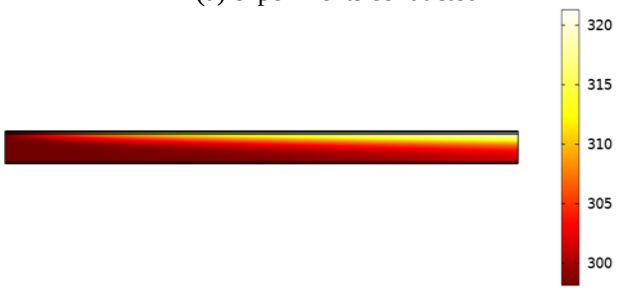

(b) Fontenault dan Gutierrez-Miravete (2012)

Figure 2. Validation of current isotherms (a) with published work (b)

3. RESULTS AND DISCUSSION

Numerical calculations are carried out by considering an inlet temperature that is assumed to be uniform, which is equivalent to room temperature. This temperature selection aims to represent the condition the working fluid reached room temperature to facilitate heat transfer from the solar panel. Parametric studies were performed to examine different factors, such as PV cell temperature, efficiency PV cell, output electrical energy, efficiency thermal, and overall energy efficiency. The analysis was carried out with nanoparticle concentrations of 1%, 10%, and 20%.

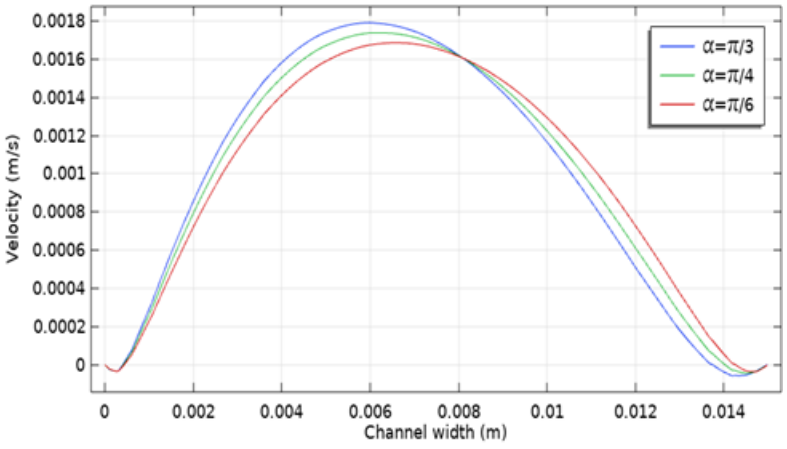

Figure 3. Fluid Velocity Profile

Figure 3. velocity profile of laminar flow in a closed channel, according to Navier-Stokes theory. The fluid velocity is zero at the walls due to the no-slip effect and increases parabolically towards the center, where the maximum velocity is reached. The variation in velocity profiles for the three angle variations reflects changes in pressure gradient, viscosity or channel geometry. Larger angle values result in higher peak velocities, while smaller angle values result in lower peak velocities but wider flow profiles, indicating a more even distribution of kinetic energy.

Volume 12, Issue 1, April 2025, pp. 77-86
ISSN 2355-5068 ; e-ISSN 2622-4852
DOI: 10.33019/jurnalecotipe.v12i1.4547

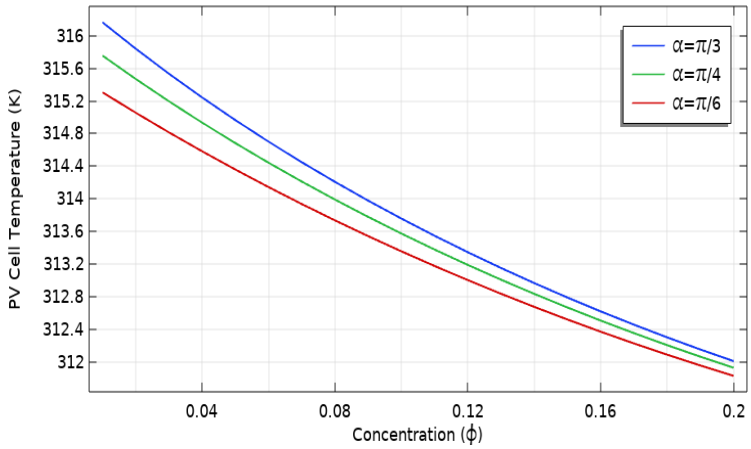

Figure 4. PV Cell Average Temperature

Figure 4. shows the correlation between concentration and PV cell temperature (Kelvin) for three angle values. Overall, the PV cell temperature decreases with increasing concentration values. This decrease in temperature is in accordance with heat transfer theory, where an increase in concentration ϕ often increases the efficiency of cooling or heat distribution, thereby reducing the heat trapped in the PV cell. Smaller α angles result in lower temperatures, which can be attributed to a more optimized radiation distribution, favoring thermal stability and improving PV cell performance. A slight drop in temperature will lead to a significant difference in thermal performance.

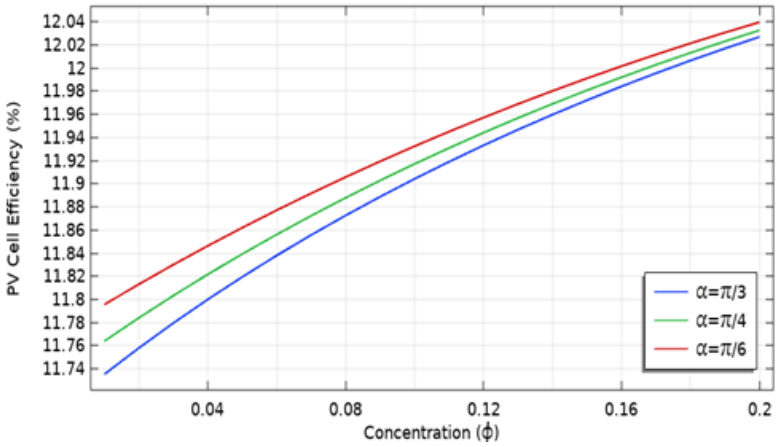

Figure 5. PV Efficiency

Figure 5. shows the correlation between concentration (ϕ) and photovoltaic (PV) cell efficiency in percent for three angle values. In general, the PV efficiency increases as the concentration increases reflecting that an increase in concentration enhances the conversion of light energy into electricity due to more optimized light absorption. In the three variations of tilt angle, it is seen that smaller angles result in higher efficiency. Thus, the efficiency of the PV cell is affected by the increase in nanoparticle concentration and the value of the flow inclination angle, where smaller angles provide more optimal efficiency.

JURNAL ECTIPE
Electronic, Control, Telecommunication, Information, and Power Engineering
Volume 12, Issue 1, April 2025, pp. 77-86
ISSN 2355-5068 ; e-ISSN 2622-4852
DOI: 10.33019/jurnalecotipe.v12i1.4547

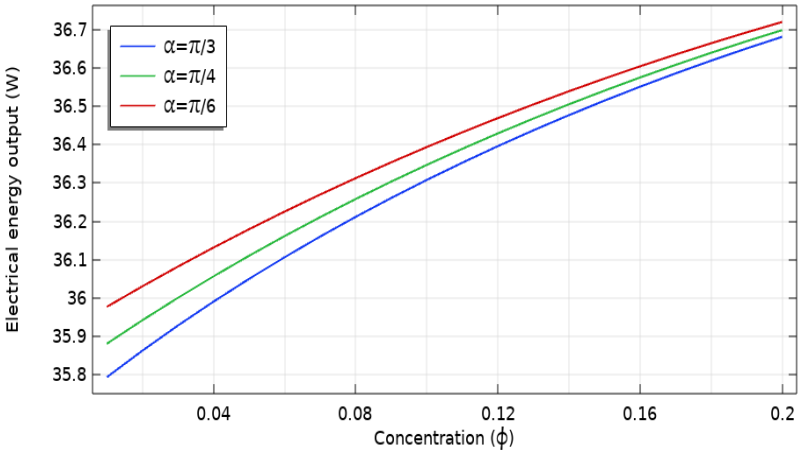

Figure 6. Electrical energy output of PV/T

Figure 6. shows the correlation between concentration (ϕ) and electrical power output (watts) of the PV cell for three angle values. The electrical power increases with increasing concentration. This increase in electrical power reflects that higher concentration allows more light energy to be converted into electrical energy. In addition, smaller angle α produces more power, this angle setting increases the efficiency of light incidence and heat distribution, supporting the theory that optical and thermal design have a significant impact on the performance of the PV system.

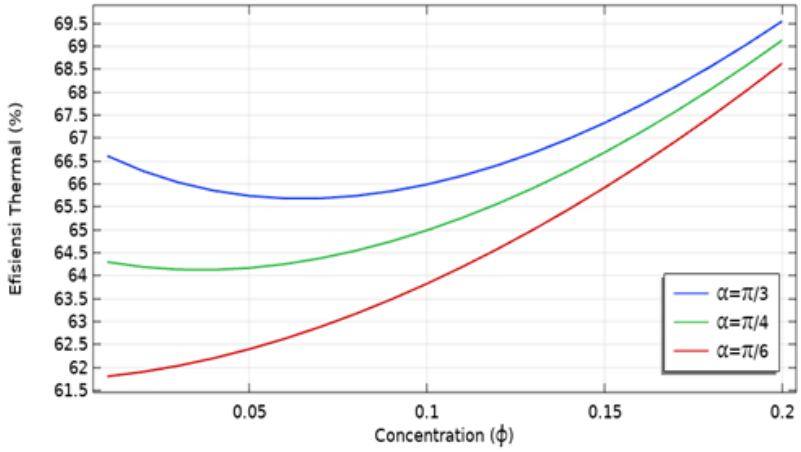

Figure 7. Thermal Efficiency

Figure 7. reflects that a higher concentration of ϕ allows for more optimal utilization of thermal energy, increasing the thermodynamic process efficiency. The higher efficiency at smaller angles α is in accordance with heat transfer theory, where a more focused energy path or optimal angle arrangement favors more effective heat transfer, thereby enhancing the system thermal efficiency.

Volume 12, Issue 1, April 2025, pp. 77-86
ISSN 2355-5068 ; e-ISSN 2622-4852
DOI: 10.33019/jurnalecotipe.v12i1.4547

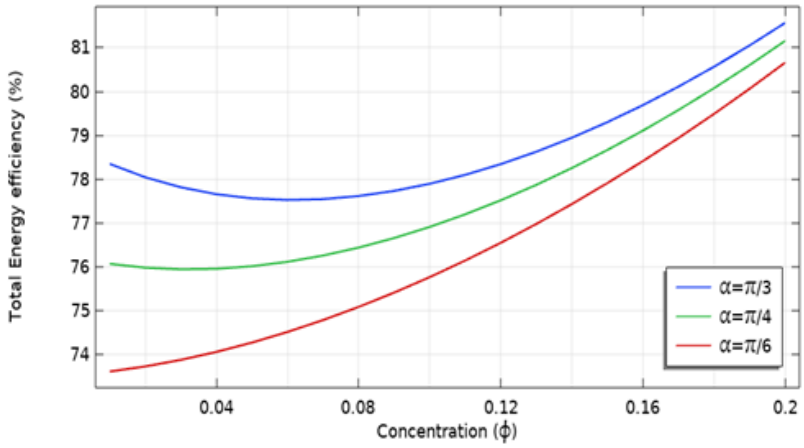

Figure 8. Total Efficiency of PV/T System

Figure 8. this increase in efficiency is in line with the theory of energy conversion, where higher concentration (ϕ) increases the density of energy converted into work. In addition, smaller values of angle α indicate more optimal thermodynamic performance, consistent with the theory that certain geometric arrangements angles can maximize efficient energy transfer and improve total thermal performance.

4. CONCLUSION

The main conclusion of this study shows that nanofluid concentration and panel tilt angle significantly impact the efficiency and performance of PV/T systems. An optimal concentration of 0.02 results in an even distribution of fluid flow, while increasing the concentration to 0.2 at an inclination angle of π/6 lowers the panel temperature, increases the photovoltaic efficiency by 12.04%, and produces the best electrical power of 36.71 W. The system thermal and overall efficiencies improve with higher nanofluid concentration and optimal inclination angle, reaching the highest total efficiency of 81.7% at an angle of π/3. This study shows a significant effect of nanofluid concentration and tilt angle on PV/T performance, but is limited to low concentration variations and has not considered environmental factors, long-term durability, and economic analysis. Future research needs to explore and test the system in real-world conditions for more optimized efficiency.

Acknowledgments

The authors sincerely extend their deepest appreciation to their parents for their moral support, encouragement, and prayers throughout the completion of this research. The authors wish to extend their gratitude to Marhama Jelita for providing facilities and support during the research. In addition, appreciation is given to Kenny, Furqon and Rejita for their valuable suggestions, constructive discussions, and technical assistance.

REFERENCES

[1] L. Akbar, I. Mafruhah, and E. Gravitiani, "Determinants of Variables That Affect Electrical Energy Consumption in Indonesia 2011-2020," *International Journal of Energy Economics and Policy*, vol. 14, no. 1, pp. 165–171, Jan. 2024, doi: 10.32479/ijeep.11069.

[2] Ula Tajul and Affandi, "Dampak Konsumsi Energi Terbarukan Terhadap Pertumbuhan Ekonomi: Studi di Asia Tenggara," *Journal of Economics Science*, vol. 5, no. 2, pp. 26–34, Oct. 2019.

[3] A. Rahma Wardhana and W. H. Marifatullah, "TRANSISI INDONESIA MENUJU ENERGI TERBARUKAN," *Jurnal Tashwirul Afkar*, vol. 38, no. 02, pp. 269–283, 2020, [Online]. Available: http://tashwirulafkar.net/index.php/afkar/index.

Volume 12, Issue 1, April 2025, pp. 77-86
ISSN 2355-5068 ; e-ISSN 2622-4852
DOI: 10.33019/jurnalecotipe.v12i1.4547

[4] M. B. Hayat, D. Ali, K. C. Monyake, L. Alagha, and N. Ahmed, "Solar energy—A look into power generation, challenges, and a solar-powered future," Mar. 10, 2019, *John Wiley and Sons Ltd*. doi: 10.1002/er.4252.

[5] P. Dwivedi, K. Sudhakar, A. Soni, E. Solomin, and I. Kirpichnikova, "Advanced cooling techniques of P.V. modules: A state of art," *Case Studies in Thermal Engineering*, vol. 21, 2020, doi: 10.1016/j.csite.2020.100674.

[6] M. Herrando and A. Ramos, "Photovoltaic-Thermal (PV-T) Systems for Combined Cooling, Heating and Power in Buildings: A Review," May 01, 2022, *MDPI*. doi: 10.3390/en15093021.

[7] C. A. F. Ramos, A. N. Alcaso, and A. J. M. Cardoso, "Photovoltaic-thermal (PVT) technology: Review and case study," in *IOP Conference Series: Earth and Environmental Science*, Institute of Physics Publishing, Oct. 2019. doi: 10.1088/1755-1315/354/1/012048.

[8] S. Diwania, S. Agrawal, A. S. Siddiqui, and S. Singh, "Photovoltaic–thermal (PV/T) technology: a comprehensive review on applications and its advancement," *International Journal of Energy and Environmental Engineering*, vol. 11, no. 1, pp. 33–54, Mar. 2020, doi: 10.1007/s40095-019-00327-y.

[9] O. El Manssouri, B. Hajji, G. M. Tina, A. Gagliano, and S. Aneli, "Electrical and thermal performances of Bi-fluid PV/thermal collectors," *Energies (Basel)*, vol. 14, no. 6, Mar. 2021, doi: 10.3390/en14061633.

[10] A. N. Al-Shamani *et al.*, "Nanofluids for improved efficiency in cooling solar collectors - A review," 2014, *Elsevier Ltd*. doi: 10.1016/j.rser.2014.05.041.

[11] H. A. M. Alsalame, J. H. Lee, and G. H. Lee, "Performance evaluation of a photovoltaic thermal (Pvt) system using nanofluids," *Energies (Basel)*, vol. 14, no. 2, Jan. 2021, doi: 10.3390/en14020301.

[12] S. Diwania, A. S. Siddiqui, S. Agrawal, and R. Kumar, "Modeling and assessment of the thermo-electrical performance of a photovoltaic-thermal (PVT) system using different nanofluids," *Journal of the Brazilian Society of Mechanical Sciences and Engineering*, vol. 43, no. 4, Apr. 2021, doi: 10.1007/s40430-021-02909-6.

[13] S. K. Gupta and S. Pradhan, "A review of recent advances and the role of nanofluid in solar photovoltaic thermal (PV/T) system," in *Materials Today: Proceedings*, Elsevier Ltd, 2021, pp. 782–791. doi: 10.1016/j.matpr.2020.10.708.

[14] M. Jelita and H. Saleh, "Improvement of Solar Cell Efficiency and Electrical Energy of a Photovoltaic-Thermal System by Using Nanofluid," *Jurnal Kejuruteraan*, vol. 35, no. 3, pp. 735–745, May 2023, doi: 10.17576/jkukm-2023-35(3)-21.

[15] D. Wang *et al.*, "A method for evaluating both shading and power generation effects of rooftop solar PV panels for different climate zones of China," *Solar Energy*, vol. 205, pp. 432–445, Jul. 2020, doi: 10.1016/j.solener.2020.05.009.

[16] A. Barbón, C. Bayón-Cueli, L. Bayón, and C. Rodríguez-Suanzes, "Analysis of the tilt and azimuth angles of photovoltaic systems in non-ideal positions for urban applications," *Appl Energy*, vol. 305, Jan. 2022, doi: 10.1016/j.apenergy.2021.117802.

[17] H. D. Kambezidis and B. E. Psiloglou, "Estimation of the optimum energy received by solar energy flat-plate convertors in Greece using typical meteorological years. Part I: South-oriented tilt angles," *Applied Sciences (Switzerland)*, vol. 11, no. 4, pp. 1–27, Feb. 2021, doi: 10.3390/app11041547.

JURNAL ECTIPE
Electronic, Control, Telecommunication, Information, and Power Engineering

Volume 12, Issue 1, April 2025, pp. 87-94
ISSN 2355-5068 ; e-ISSN 2622-4852
DOI: 10.33019/jurnalecotipe.v12i1.4533

Review on Innovative DC-DC Converter Design for High Efficiency and High Voltage Gain Applications

Andi M. Nur Putra[1], Adrianti[2], Muhammad Imran Hamid[3]
[1,2,3]Department of Electrical Engineering, Universitas Andalas, Padang 25163, Indonesia

ARTICLE INFO

Article historys:

Received : 17/01/2025
Revised : 30/01/2025
Accepted : 13/03/2025

Keywords:

DC-DC Converters; Energy Efficiency; High Voltage Gain; Hybrid Topology

ABSTRACT

This paper reviewed the advancements in DC-DC converter technologies, emphasizing their role in addressing the demands of high efficiency and high voltage gain in renewable energy systems, electric vehicles (EVs), and distributed energy networks. Advanced topologies, including hybrid, quadratic, triple-boost, coupled inductor, and voltage multiplier designs, were evaluated for their ability to overcome the limitations of traditional converters. Key findings highlighted significant improvements in energy efficiency, exceeding 95%, and a substantial reduction in voltage ripple. Performance metrics such as scalability, thermal management, and component stress were analyzed, demonstrating the suitability of these designs for diverse applications. Comparative analyses illustrate the superiority of innovative designs in meeting the energy needs of emerging technologies. Applications in renewable energy, EV infrastructure, and distributed networks underscore the transformative potential of these converters in optimizing power delivery and enhancing system reliability. This review bridged the gap between theoretical advancements and practical implementations, showcasing the pivotal contribution of DC-DC converter to modern energy systems.

Corresponding Author:
Andi M. Nur Putra
Student of Electrical Engineering, Universitas Andalas, Padang 25163, Indonesia
Email: andimnurputra@gmail.com

1. INTRODUCTION

DC-DC converters represent a cornerstone in modern power electronics, offering indispensable functionality as intermediaries between generation systems and their load. Their critical role in regulating voltage ensures the seamless integration of renewable energy sources, electric vehicles (EVs), and DC microgrids. As the global adoption of photovoltaic (PV) arrays, fuel cells, and battery systems accelerates, the demand for efficient, reliable DC-DC converters has grown substantially. These converters must not only provide the necessary voltage step-up for low and variable input levels but also maintain high efficiency under diverse and challenging caused by variable solar irradiance, ensuring stable output and efficient power delivery to storage or grid systems.

Traditional boost converters have been widely employed due to their simplicity and low cost. However, they face significant limitations in applications requiring high voltage gains and dynamic load regulation. As duty cycles approach extreme values, conduction and switching losses escalate, reducing efficiency and increasing thermal stress on components. These challenges highlight the need for advanced DC-DC converter topologies, including switched inductors, coupled inductors, voltage scalability, and significantly higher voltage gains, addressing the limitations of conventional design.

JURNAL ECTIPE
Electronic, Control, Telecommunication, Information, and Power Engineering
Volume 12, Issue 1, April 2025, pp. 87-94
ISSN 2355-5068 ; e-ISSN 2622-4852
DOI: 10.33019/jurnalecotipe.v12i1.4533

The innovations in DC-DC converter technology have far-reaching implications across multiple domains. High-efficiency converters in EV systems enable rapid charging, optimized energy utilization, and extended battery lifespan. In DC microgrids, the modular and scalable design facilitates stable voltage regulation and efficient power distribution, even under dynamic loading conditions. Advanced innovations such as coupled inductors, transformerless configurations, and hybrid topologies have not only improved efficiency but also reduced size and material costs, positioning these systems as vital components in next-generation energy architecture.

This comprehensive review explores the state-of-the-art in DC-DC converter technologies, focusing on their operational principles, innovative topologies, and key applications. Through detailed analyses of their performance metrics and design advancements, this paper offers insights into the current trends and identifies pathways for further development and optimization.

2. RESEARCH METHOD

DC-DC converters are critical tools in power electronics, designed to convert input voltage into levels suitable for specific applications. These converters are categorized into isolated and non-isolated types, each offering distinct advantages and applications. This section also explores advanced configurations such as switched inductors, coupled inductors, and voltage multipliers, highlighting their operational principles, performance benefits, and challenges.

2.1. Isolated and Non-isolated Converter

Isolated converters employ transformers to achieve electrical separation between the input and output, ensuring enhanced safety and fault isolation. This feature makes them indispensable in high-voltage and safety-critical applications, such as industrial power supplies, medical devices, and grid-tied renewable energy systems. The flyback topology, illustrated in **Figure 1a**, exemplifies this approach, storing energy in the transformer's primary winding during the switch-on phase and transferring it to the output during the switch-off phase. Despite their scalability issues, restricting their application to low-power systems [1].

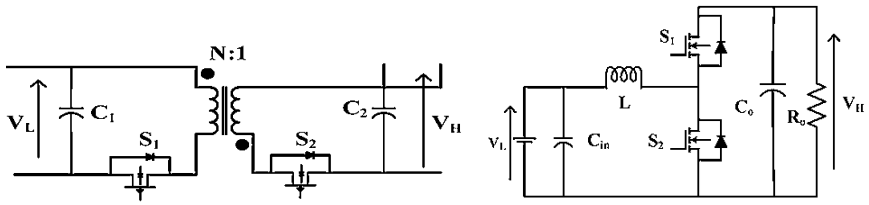

(a) (b)

Figure 2. Isolated and non-isolated converter topology, (a) Flyback converter; (b) Boost converter

Advanced isolated topologies such as push-pull, half-bridge, and full-bridge converters address the challenges. Push-pull converter, for instance, employs two switches to alternately drive the transformer windings, enhancing flux utilization and reducing core losses. Full-bridge converters, as depicted in [2], [3], leverage multiple switches and advanced control strategies to achieve superior efficiency and high-power capacity. The modular resonant topologies presented by [4] also highlight the improvement in energy transfer efficiency for grid-connected renewable systems.

Further research by [5] focuses on isolated bidirectional designs that ensure efficient energy transfer in high-frequency transformers in isolated designs, such as the work by [6], which enhances performance by reducing core size and improving power density in PV-fed microgrids. An isolated high-gain topology by [7] integrates magnetic flux balancing to mitigate transformer saturation, further enhancing efficiency and voltage regulation.

Non-isolated converters are compact, cost-effective, and efficient, making them ideal for applications where electrical isolation is necessary. Examples include boost, buck-boost, SEPIC, and Cuk converters. The boost converter, shown in **Figure 1b**, operates by storing energy in an inductor during the on-state and releasing it into the load during the off-state. While effective for basic step-up applications, boost converters exhibit limitations such as high ripple and restricted voltage gain under extreme duty cycles [8].

JURNAL ECTIPE
Electronic, Control, Telecommunication, Information, and Power Engineering
Volume 12, Issue 1, April 2025, pp. 87-94
ISSN 2355-5068 ; e-ISSN 2622-4852
DOI: 10.33019/jurnalecotipe.v12i1.4533

SEPIC converters address these constraints by enabling bidirectional energy flow and offering step-up and step-down capabilities, making the battery management systems versatile. Similarly, Cuk converter excels in minimizing input and output current ripple, which is crucial for applications such as LED drivers and portable electronics. Research by [9] demonstrated how transformerless configurations improve efficiency and compactness, addressing the traditional limitations of these topologies. Voltage boosting techniques using cascade networks in SEPIC and Cuk designs have also been explored, achieving high efficiency in renewable systems [10].

2.2. Switched Inductor

Switched inductor converters achieve substantial voltage gains by alternately configuring inductors for parallel charging and series discharging. This topology, illustrated in **Figure 2**, minimizes duty cycle requirements and optimizes transfer efficiency. These converters are particularly effective in medium-voltage renewable energy systems and microgrids, where robust voltage regulation is essential under load conditions.

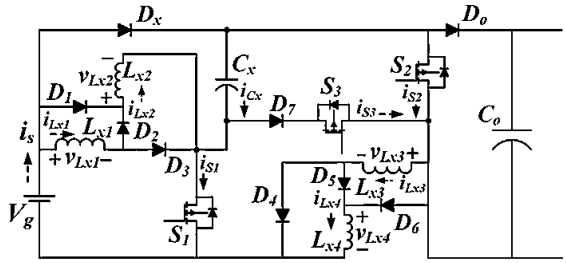

Figure 2. Switched inductor converter topology

Research [11] emphasizes the advantages of interleaved switched inductor designs in reducing ripple and thermal stress. Such configurations also improve power density and dynamic response, as highlighted by [12]. Advanced implementations like active clamping and dual-phase interleaving minimize switching applications such as EV charges and grid-connected PV [13]. Additional contributions by [14] showcase an optimized switched inductor topology integrating soft-switching mechanism to reduce noise and improve efficiency under high power loads.

2.3. Coupled Inductor

Coupled inductor topologies leverage magnetic coupling to achieve high voltage gain within compact designs. By integrating primary and secondary windings into a single core, these converters reduce core losses and enhance flux utilization [15]. **Figure 3** depicts a coupled inductor-based boost converter with clamping circuits to suppress leakage inductance and improve efficiency [15]. Such designs are particularly advantageous in high-power applications such as grid-tied renewable systems, EV fast chargers, and DC microgrids [16].

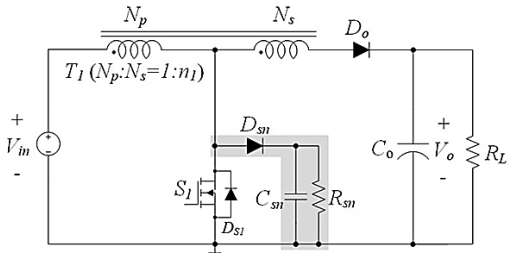

Figure 3. Conventional boost converter using a coupled inductor

Advanced coupled inductor configuration distributed power across multiple phases, reducing ripple and electromagnetic interference. Research by [17] explores the integration of high-saturation magnetic materials, enabling these converters to accommodate higher power densities. In [18], the researcher reviewed active flux balancing techniques, which ensure reliable performance in high-demand scenarios such as multi-source renewable energy setups. Recent contribution by [19] have expanded the applicability of coupled inductors in hybrid microgrid configurations, demonstrating their capability to handle variable renewable inputs while maintaining high system stability.

JURNAL ECTIPE
Electronic, Control, Telecommunication, Information, and Power Engineering
Volume 12, Issue 1, April 2025, pp. 87-94
ISSN 2355-5068 ; e-ISSN 2622-4852
DOI: 10.33019/jurnalecotipe.v12i1.4533

2.4. Voltage Multiplier

Voltage multipliers amplify output voltage incrementally through cascaded diodes and capacitors. **Figure 4** illustrates this approach, where each stage adds discrete voltage increments, achieving high gains in compact configurations [20]. Transfomerless designs address the complexity of traditional voltage multipliers, enhancing efficiency and reducing component counts. The designs are particularly effective in low-power applications, such as portable electronics, LED drivers, and compact renewable systems [21].

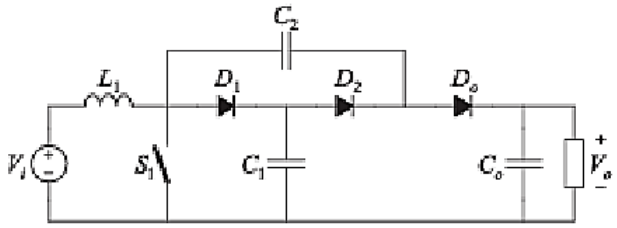

Figure 4. Non-isolated dc-dc converters based on the voltage multiplier

A hybrid voltage multiplier combines switched capacitors and inductors to achieve higher gains and improve stability under dynamic loads. In [22] demonstrate these configurations in high-frequency applications, highlighting their adaptability and cost-effectiveness for compact systems. In other ways, [23] further analyzed a modular voltage multiplier design integrated into multi-input systems, enabling enhanced energy sharing and fault tolerance across diverse energy sources.

2.5. Innovative Topologies

Innovative DC-DC converter designs integrated features from multiple topologies to maximize performance. Quadratic and triple-boost converters, depicted in **Figure 5a**, utilize multi-stage inductor-capacitor networks to achieve voltage gains exceeding 20x. These designs, evaluated by [24], are particularly effective for PV systems, energy storage, and PV power management, where high step-up ratios and low losses are paramount.

Quadratic converter leverage cascaded inductor and capacitor arrangements to minimize component stress and increase energy transfer efficiency [25]. By employing stages, quadratic converter achieves stable output with reduced ripple, making them ideal for a renewable system. Triple-boost converter, on the other hand, expands upon this concept by integrating an additional stage, further enhancing voltage gain while maintaining a compact form factor. These designs have been pivotal in grid-connected applications where scalability and reliability are critical [26].

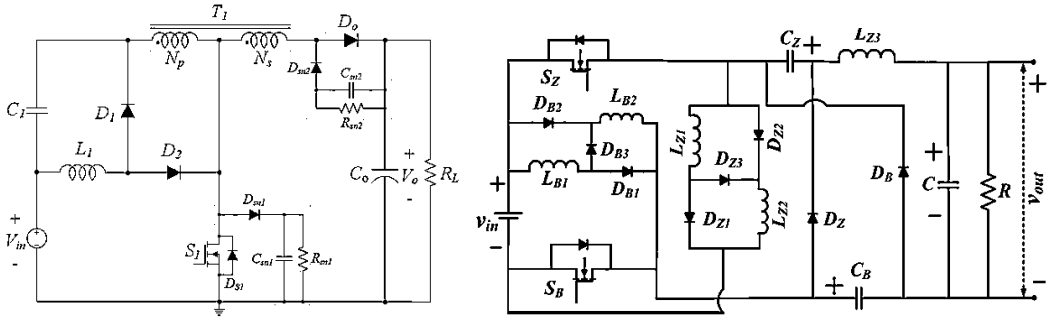

(a) (b)

Figure 5. Innovative DC-DC converter, (a) Quadratic boost DC-DC converter using a coupled-inductor, (b) Hybrid zeta-boost converter

A hybrid converter combines switched inductors, coupled inductors, and voltage multiplier elements, creating modular, scalable configurations. **Figure 5b** illustrates the hybrid topology's ability to balance efficiency, fault tolerance, and adaptability, making it ideal for high-voltage DC applications and grid-connected renewable systems [27]. Recent study by [28] has emphasized the potential of hybrid designs in adapting to load variability in microgrids, ensuring consistent performance under fluctuating demand.

JURNAL ECTIPE
Electronic, Control, Telecommunication, Information, and Power Engineering
Volume 12, Issue 1, April 2025, pp. 87-94
ISSN 2355-5068 ; e-ISSN 2622-4852
DOI: 10.33019/jurnalecotipe.v12i1.4533

Hybrid design also facilitates seamless integration with multi-source energy systems, such as PV arrays and battery storage units, providing superior fault tolerance and adaptability. Advanced implementations include high frequency switching techniques and active component balancing, further enhancing reliability and scalability. These features make hybrid converters particularly suitable for high demand applications, including EV fast chargers and large-scale renewable installations.

3. RESULTS AND DISCUSSION

Performance evaluation of DC-DC converters is crucial to understanding their efficacy in real-world applications. Metrics such as energy efficiency, voltage ripple, thermal management, scalability, and component stress are pivotal in determining their suitability for diverse applications. Each metric provides unique insights into how these converters perform under varying operational conditions.

3.1 Energy efficiency

Energy efficiency remains a cornerstone metric for DC-DC converters, particularly in renewable and battery-powered systems where energy conservation is paramount. Tradition boost converter typically achieve efficiencies around 85% - 90% under moderate load conditions [12]. However, advanced topologies, such as hybrid design, interleaved converters, and quadratic configurations, routinely exceed 95%. These high-efficiency designs leverage soft-switching mechanisms, optimized magnetic material, and reduce conduction losses to deliver superior energy utilization [29]. For instance, hybrid converter employing coupled inductors minimize switching losses and magnetic saturation, making the ideal for high-frequency applications.

3.2 Voltage Ripple

Voltage ripple, a measure of output voltage stability, significantly impacts the performance and reliability of DC-DC converters. Applications such as electric vehicle (EVs) and sensitive electronic systems require converter with minimal ripple to ensure stable operation. Coupled inductor and interleaved topologies demonstrate ripple reduction of up to 50% compared to conventional designs [30]. Voltage multiplier configurations, particularly in hybrid converters, offer ripple levels below 2%, making them indispensable for applications demanding high precision [31].

3.3 Thermal Management

Thermal performance is a critical aspect of converter design, influencing both efficiency and longevity. Advanced topologies incorporate features like interleaving, soft-switching, and active clamping to mitigate thermal buildup during high-power operations. Interleaved converters, for example, distribute power across multiple phases, reducing thermal hotspots and enhancing heat dissipation [32]. Hybrid designs integrate coupled inductors with advanced thermal management techniques to ensure consistent operation under high-load conditions [33].

3.4 Scalability and Component Stress

Scalability is a defining characteristic of modern DC-DC converter topologies. Design such as modular hybrid converters and quadratic configurations enable seamless integration into large systems, including renewable energy farm and microgrids [34]. These scalable design address dynamic power requirements while minimizing component stress. Stress on components, including switches and capacitors, is mitigated in advanced design through techniques like flux balancing and active control, enhancing reliability and reducing maintenance costs [14].

3.5 Comparative Analysis

Table 1 provides a detailed comparative analysis of converter performance metrics across different topologies. Each metric highlights the advantages and trade-offs associated with each design.

JURNAL ECTIPE
Electronic, Control, Telecommunication, Information, and Power Engineering
Volume 12, Issue 1, April 2025, pp. 87-94
ISSN 2355-5068 ; e-ISSN 2622-4852
DOI: 10.33019/jurnalecotipe.v12i1.4533

Table 1. Comparative analysis of different topologies converter performance

Topology	Efficiency (%)	Voltage Ripple (%)	Thermal Management	Scalability	Component Stress	Cost
Traditional Boost [35]	85-90	5-8	Basic	Moderate	High	Low
Hybrid Boost [36]	> 95	< 2	Advanced	High	Low	Moderate
Coupled inductor [37], [38]	> 92	< 3	Intermediate	Moderate-High	Moderate	Moderate
Voltage Multiplier [39]	90-93	< 3	Limited	High	Moderate	Low
Quadratic [40], [41], [42]	94-96	< 2.5	Advanced	High	Low	Moderate
Triple Boost [43], [44]	> 96	< 2	Advance	High	Low	High

3.6 Application In Emerging Energy Technologies

DC-DC converter plays a pivotal role in advancing modern energy systems, addressing a diverse range of applications across renewable energy, electric vehicles (EVs), and distributed energy networks. Their versatility and efficiency make them essential for emerging technological ecosystems.

In renewable energy, DC-DC converters are integral to photovoltaics (PV) and wind energy systems, here they regulate variable input voltage and optimize power extraction through maximum power poin tracking (MPPT). Advanced technologies such as hybrid and quadratic converters achieve high voltage gains with reduced losses ensuring efficient power delivery to storage systems or grids [45]. Interleaved design with coupled inductors improve power density and minimize thermal stress, making them ideal for residential and industrial installations. High-efficiency converters, such as those employing voltage multiplier techniques, enhance the performance of microgrids by stabilizing output under dynamic loading conditions [46].

In EV infrastructure, DC-DC converters facilitate rapid charging and efficient power distribution. High-efficiency converters like triple-boost and interleave coupled inductor designs enable faster charging by minimizing voltage ripple and thermal stress on battery systems [47]. Transformerless topologies are gaining prominence for their compact form factors, crucial for onboard EV applications. Coupled inductor-based designs also enable bidirectional energy transfer, a critical feature for vehicle-to-gris (V2G) applications, ensuring stability and efficiency in decentralized energy systems [48].

In distributed energy networks, the adaptability of DC-DC converter ensures seamless integration of multiple energy sources. Hybrid converters are particularly effective in managing diverse inputs, such as PV arrays and energy storage systems, optimizing power flow and enhancing fault tolerance [49]. Their modularity supports scalability, enabling efficient operation in large-scale renewable installations and microgrid configurations. Quadratic and triple-boost topologies have demonstrated exceptional performance in balancing high voltage gains and efficiency, critical for grid stabilization and energy storage management [50].

These advancements underline the transformative impact of DC-DC converter technologies in addressing future energy challenges. By offering scalable, efficient, and reliable solutions, the converter continues to drive innovation across multiple domains, supporting the transition toward a sustainable energy landscape.

4. CONCLUSION

This review underscores the critical role of DC-DC converters in enabling high-efficiency and high-gain applications across renewable energy, electric vehicles, and distributed networks. Advanced topologies, including hybrid, quadratic, and triple-boost designs, demonstrated significant performance improvements in energy efficiency, scalability, and thermal management. These innovations provide robust solutions to contemporary energy challenges, ensuring optimized power delivery and supporting the global transition toward sustainable energy systems.

Volume 12, Issue 1, April 2025, pp. 87-94
ISSN 2355-5068 ; e-ISSN 2622-4852
DOI: 10.33019/jurnalecotipe.v12i1.4533

Acknowledgments

We would like to express our heartfelt gratitude to the Institut Teknologi Padang (ITP) and Universitas Andalas (UNAND) for their invaluable support in facilitating this review research. The resources, guidance, and collaborative environment provided by both institutions played a pivotal role in the successful completion of this work. This review is a testament to their commitment to advancing research in power electronics and renewable energy systems.

REFERENCES

[1] Q. Huang, A. Q. Huang, R. Yu, P. Liu, "High-efficiency and high-density single-phase dual-mode cascaded buck–boost multilevel transformerless PV inverter with GaN AC switches," *IEEE Transactions*, 2018, [Online]. Available: https://ieeexplore.ieee.org/abstract/document/8514053/

[2] S. Sarani, A. Nikbahar, H. A. Zarchi, and X. Liang, "An Isolated High Boost Ratio DC-DC Converter With Very Low Input Current Ripples," *IEEE Transactions on Circuits and Systems II: Express Briefs*, 2024, doi: 10.1109/TCSII.2024.3386158.

[3] J. Lu, Y. Wang, X. Li, and C. Du, "High-Conversion-Ratio Isolated Bidirectional DC-DC Converter for Distributed Energy Storage Systems," *IEEE Trans Power Electron*, vol. 34, no. 8, pp. 7256–7277, Aug. 2019, doi: 10.1109/TPEL.2018.2881085.

[4] X. Zhu, L. Jiang, B. Zhang, and K. Jin, "The Resonant Modular Multilevel DC-DC Converter Adopting Switched-Inductor Cells for High Step-Up Ratio," *IEEE J Emerg Sel Top Power Electron*, vol. 10, no. 6, pp. 6634–6647, Dec. 2022, doi: 10.1109/JESTPE.2022.3157618.

[5] Y. E. Wu and B. H. Pan, "High Efficiency and Voltage Conversion Ratio Bidirectional Isolated DC-DC Converter for Energy Storage System," *IEEE Access*, vol. 10, pp. 55187–55199, 2022, doi: 10.1109/ACCESS.2022.3177206.

[6] B. Gu, J. Dominic, J. S. Lai, Z. Zhao, and C. Liu, "High boost ratio hybrid transformer DC-DC converter for photovoltaic module applications," *IEEE Trans Power Electron*, vol. 28, no. 4, pp. 2048–2058, Apr. 2013, doi: 10.1109/TPEL.2012.2198834.

[7] M. Kumar, M. Ashirvad, and Y. N. Babu, "An integrated Boost-Sepic-Ćuk DC-DC converter with high voltage ratio and reduced input current ripple," in *Energy Procedia*, Elsevier Ltd, 2017, pp. 984–990. doi: 10.1016/j.egypro.2017.05.219.

[8] Y. Zheng and K. M. Smedley, "Analysis and design of a single-switch high step-up coupled-inductor boost converter," *IEEE Transactions on Power …*, 2019, [Online]. Available: https://ieeexplore.ieee.org/abstract/document/8708262/

[9] A. Andrade, T. Faistel, R. Guisso, and A. Toebe, "Hybrid High Voltage Gain Transformerless DC-DC Converter," *IEEE Transactions on Industrial Electronics*, vol. 69, no. 3, pp. 2470–2479, Mar. 2022, doi: 10.1109/TIE.2021.3066939.

[10] A. Alzahrani, M. Ferdowsi, and P. Shamsi, "A family of scalable non-isolated interleaved DC-DC boost converters with voltage multiplier cells," *IEEE Access*, 2019, [Online]. Available: https://ieeexplore.ieee.org/abstract/document/8606084/

[11] S. Gopinathan, V. S. Rao, and S. Kumaravel, "Enhanced Voltage Gain Boost DC-DC Converter With Reduced Voltage Stress and Core Saturation," *IEEE Transactions on Circuits and Systems II: Express Briefs*, vol. 70, no. 8, pp. 3019–3023, Aug. 2023, doi: 10.1109/TCSII.2023.3252721.

[12] E. Babaei, H. M. Maheri, M. Sabahi, and ..., "Extendable nonisolated high gain DC–DC converter based on active–passive inductor cells," *IEEE transactions on …*, 2018, [Online]. Available: https://ieeexplore.ieee.org/abstract/document/8301592/

Volume 12, Issue 1, April 2025, pp. 87-94
ISSN 2355-5068 ; e-ISSN 2622-4852
DOI: 10.33019/jurnalecotipe.v12i1.4533

[13] P. Sharma and R. Chinnappa Naidu, "Optimization Techniques for Grid-Connected PV with Retired EV Batteries in Centralized Charging Station with Challenges and Future Possibilities: A review," 2022, *Ain Shams University*. doi: 10.1016/j.asej.2022.101985.

[14] S. M. NithyaDevi, V. Krishnasamy, and J. D. Navamani, "Transformerless high voltage gain Y-source converter with reduced switch stress," *e-Prime - Advances in Electrical Engineering, Electronics and Energy*, vol. 8, Jun. 2024, doi: 10.1016/j.prime.2024.100558.

[15] S. W. Lee and H. L. Do, "High step-up coupled-inductor cascade boost DC–DC converter with lossless passive snubber," *IEEE Transactions on Industrial Electronics*, 2018, [Online]. Available: https://ieeexplore.ieee.org/abstract/document/8286907/

[16] M. Das and V. Agarwal, "Design and analysis of a high-efficiency DC–DC converter with soft switching capability for renewable energy applications requiring high voltage gain," *IEEE Transactions on Industrial Electronics*, 2016, [Online]. Available: https://ieeexplore.ieee.org/abstract/document/7374681/

[17] A. Andrade, E. Mattos, L. Schuch, and ..., "Synthesis and comparative analysis of very high step-up DC–DC converters adopting coupled-inductor and voltage multiplier cells," *... on Power Electronics*, 2017, [Online]. Available: https://ieeexplore.ieee.org/abstract/document/8017435/

[18] R. Rajesh, N. Prabaharan, and T. K. Santhosh, "Design and Analysis of a Non-Isolated DC-DC Converter With a High-Voltage Conversion Ratio," *IEEE Transactions on Circuits and Systems II: Express Briefs*, vol. 70, no. 6, pp. 2036–2041, Jun. 2023, doi: 10.1109/TCSII.2022.3226187.

[19] H. C. Liu and F. Li, "Novel High Step-Up DC-DC Converter with an Active Coupled-Inductor Network for a Sustainable Energy System," *IEEE Trans Power Electron*, vol. 30, no. 12, pp. 6476–6482, Dec. 2015, doi: 10.1109/TPEL.2015.2429651.

[20] L. Schmitz, D. C. Martins, and ..., "Generalized high step-up DC-DC boost-based converter with gain cell," *IEEE Transactions on ...*, 2016, [Online]. Available: https://ieeexplore.ieee.org/abstract/document/7588175/

[21] T. Yao, Y. Cheng, Y. Guan, W. Wang, Y. Wang, and D. Xu, "A Family of High Step-Up DC-DC Converters Based on Enhanced Boost Cells With Coupled Inductor," *IEEE Trans Power Electron*, vol. 38, no. 10, pp. 12932–12945, Oct. 2023, doi: 10.1109/TPEL.2023.3298683.

[22] C. H. Lin, M. S. Khan, J. Ahmad, H. D. Liu, and T. C. Hsiao, "Design and Analysis of Novel High-Gain Boost Converter for Renewable Energy Systems (RES)," *IEEE Access*, vol. 12, pp. 24262–24273, 2024, doi: 10.1109/ACCESS.2024.3365705.

[23] A. Kumar and P. Sensarma, "Single Active Switch High Voltage Gain DC-DC Converter with Reduced Devices Stress," *2020 IEEE International Conference on ...*, 2020, [Online]. Available: https://ieeexplore.ieee.org/abstract/document/9379829/

[24] M. Samiullah, M. A. A. Hitmi, A. Iqbal, and S. Islam, "Novel Scalable Topologies of High Power Density Quadratic Converters with Low Voltage Stress on Power Diode," *IEEE Open Journal of the Industrial Electronics Society*, vol. 5, pp. 386–399, 2024, doi: 10.1109/OJIES.2024.3393757.

[25] S. W. Lee and H. L. Do, "Quadratic boost DC–DC converter with high voltage gain and reduced voltage stresses," *IEEE Trans Power Electron*, 2018, [Online]. Available: https://ieeexplore.ieee.org/abstract/document/8369098/

[26] S. N V, L. A, and D. N. J, "Dual input single Output quadratic Boost converter for DC microgrid," *e-Prime - Advances in Electrical Engineering, Electronics and Energy*, vol. 9, Sep. 2024, doi: 10.1016/j.prime.2024.100683.

JURNAL ECOTIPE
Electronic, Control, Telecommunication, Information, and Power Engineering

Volume 12, Issue 1, April 2025, pp. 95-102
ISSN 2355-5068 ; e-ISSN 2622-4852
DOI: 10.33019/jurnalecotipe.v12i1.4534

Analysis of Characteristics of Three Phase Transformer Using MATLAB

Fakhri Ramadhan[1], Sari Novalianda[2], Panangian Mahadi Sihombing[3], Yoga Tri Nugraha[4], Muhammad Irwanto[5], Syahrun Nizam Md Arshad[6], Mohd. Azlishah Othman[7]

[1,2,3,4]Department of Electrical Engineering, Universitas Al-Azhar Medan, Medan 20142, Indonesia
[5]Department of Electrical Engineering, Universitas Prima Indonesia, Medan 20118, Indonesia
[6]Department of Electrical Engineering, Universiti Malaysia Perlis (UniMAP), Perlis 02600, Malaysia
[7]Department of Electronic Engineering, Universiti Teknikal Malaysia Melaka (UTeM), Melaka 76100, Malaysia

ARTICLE INFO

Article historys:

Received : 18/01/2025
Revised : 30/01/2025
Accepted : 06/03/2025

Keywords:

Characteristic; Efficiency; Electromagnetic Field Radiation; MATLAB; Three Phase Transformer

ABSTRACT

Three-phase transformers are integral components of modern electrical power systems, serving as the backbone of energy transmission and distribution networks. Their primary purpose is to step up or step-down voltage levels efficiently, enabling the transfer of electrical power over long distances with minimal losses. Due to their widespread use in industrial, commercial, and residential applications, understanding the operational characteristics of three-phase transformers is crucial for improving energy efficiency, ensuring reliability, and optimizing performance. The analysis of transformer characteristics, such as efficiency, voltage regulation, power losses, and behavior under varying load conditions. This research aims to analyze the characteristics of three-phase transformers using MATLAB. The results of the analysis obtained in the research of the characteristics of 3-phase transformers produce an active power (P) of 6183.42 W, a reactive power (Q) of 3832.14 VAR, an apparent power (S) of 7274.61 VA and a transformer efficiency of 97.75% with a time of 0.02 s and produces losses in copper of 81.65 W which produces electromagnetic field radiation, with a polar graph representing the radiation pattern of the magnetic field (H field) and electric field (E field).

Corresponding Author:

Sari Novalianda
Department of Electrical Engineering, Universitas Al-Azhar Medan, Medan 20142, Indonesia
Email: sarivaldano4@gmail.com

1. INTRODUCTION

Three-phase transformers are vital components in the electric power system that function to transform voltage and current according to the needs of the distribution and transmission system. However, in its operation, three-phase transformers face various technical problems that can affect its performance. One of the main problems is power losses, which consist of copper losses due to winding resistance and core losses caused by hysteresis and eddy currents. These losses contribute to the decline in transformer efficiency, which needs to be analyzed to improve the performance of the electric power system [1][2][3]. In addition, the distribution of current and voltage in a three-phase transformer is often uneven due to load imbalance. This condition can cause power distortion which has an impact on the quality of the electrical power supplied. Therefore, it is necessary to analyze the characteristics of the transformer under balanced and unbalanced load conditions to understand how the system works under various operational conditions [4] [5]. Furthermore, modeling the equivalent circuit of a three-phase

JURNAL ECTIPE
Electronic, Control, Telecommunication, Information, and Power Engineering
Volume 12, Issue 1, April 2025, pp. 95-102
ISSN 2355-5068 ; e-ISSN 2622-4852
DOI: 10.33019/jurnalecotipe.v12i1.4534

transformer becomes an important aspect in the analysis of its characteristics. The equivalent circuit is used to determine key parameters such as impedance, leakage reactance, and winding resistance. However, manual calculations are often complex and require a more efficient method. By utilizing MATLAB, transformer characteristic analysis can be done more accurately and systematically through numerical modeling-based simulations.

To overcome these problems, validation is needed with simulation using MATLAB, which can help interpret the characteristics of three-phase transformers more effectively. MATLAB provides various functions and toolboxes for power system analysis, allowing modeling and simulation that are closer to actual operational conditions. Thus, this study aims to develop a more systematic analysis method in evaluating the characteristics of three-phase transformers and provide optimization recommendations based on simulation results [6][7][8]. This research aims to analyze the characteristics of three-phase transformers using MATLAB, focusing on theoretical concepts, simulation, and performance evaluation. By leveraging MATLAB's computational strengths, the research will explore key transformer characteristics, investigate the effects of operational conditions, and validate theoretical results through practical simulation models[9], [10], [11]. The insights gained from this research will contribute to a deeper understanding of transformer behavior and demonstrate the significance of computational tools in modern electrical engineering practices.

2. RESEARCH METHOD

A transformer is an electrical device that uses electromagnetic induction and magnetic coupling to change the alternating current voltage from one level to another. The primary coil and the secondary coil are the two coils that form the laminated iron core of the transformer. One of the main factors contributing to the widespread use of alternating current in the production and distribution of electricity is the ease and reliability of using transformers, which allows the selection of the most cost-effective and appropriate voltage for any need. This research uses an analytical approach and MATLAB-based simulation to analyze the characteristics of a three-phase transformer. The method used consists of several main stages, namely mathematical modeling, simulation of transformer characteristics, and validation of simulation results against theory and experimental data.

2.1 Voltage Transformation

The core principle of voltage transformation relies on electromagnetic induction. Alternating current (AC) produces a fluctuating magnetic flux in the core of a transformer when it passes through the primary winding. Depending on the turn's ratio, this flux causes a voltage to be induced in the secondary winding that may be more or lower than the primary voltage [12]. The relationship between primary and secondary voltages is given by the turn's ratio of the transformer can be calculate by equation 1 and despite changing the voltage, transformers conserve power (neglecting losses) between the primary and secondary circuits. This conservation of power is expressed as by equation 2.

$$\frac{V\ primary}{V\ secondary} = \frac{N\ primary}{N\ secondary} \tag{1}$$

$$V_{primary} \text{ x } I_{primary} = V_{secondary} \text{ x } I_{secondary} \tag{2}$$

2.2 Transformer Efficiency

A fundamental performance metric called transformer efficiency gauges how well a transformer minimizes losses when converting input electrical power into output electrical power. In an ideal transformer, the efficiency would be 100%, meaning that all the input power is transferred to the secondary side without any loss[13], [14]. The output power to input power ratio, represented as a percentage, is a transformer's efficiency (η).

$$\eta = \frac{P\ output}{P\ input} \text{ x } 100\% \tag{3}$$

2.3 Voltage Regulation

Voltage regulation refers to the percentage change in the secondary voltage of a transformer as the load changes from no load to full load. It is an indication of how much the voltage varies with the change in load. Mathematically, voltage regulation (V_R) is expressed as:

Volume 12, Issue 1, April 2025, pp. 95-102
ISSN 2355-5068 ; e-ISSN 2622-4852
DOI: 10.33019/jurnalecotipe.v12i1.4534

$$V_R = \frac{V\ no\ load - V\ full\ load}{V\ full\ load} \text{ x } 100\% \quad (4)$$

2.4 Losses

In transformers, losses are inevitable due to the inherent properties of the materials and components used. Understanding these losses is essential for optimizing transformer design and improving efficiency. The primary losses in a transformer can be categorized into core losses (also known as iron losses), copper losses, and stray losses. Each of these losses occurs due to specific factors such as resistance, magnetic flux, and leakage inductance.

A. Core Losses (Iron Losses)

Core losses, sometimes known as iron losses, occur in the transformer's magnetic core. The alternating magnetic field created by the current passing through the primary winding is what causes these losses. Energy is released as heat when the magnetic flow in the core shifts direction. Hysteresis loss and eddy current loss are the two primary components of core losses. As the transformer's alternating current (AC) reverses direction, the core material magnetizes and demagnetizes, causing hysteresis loss [15], [16]. The magnetic domains within the core material change direction in response to the applied magnetic field, which requires energy, causing heat to be generated. Circular currents called eddy currents are created inside the core material as a result of fluctuating magnetic flux. Energy losses result from the resistive heating caused by these currents flowing in loops within the core.

B. Copper Losses (Winding Losses)

The resistance in the transformer's primary and secondary windings is what causes copper losses. When current flows through the winding, energy is dissipated in the form of heat due to the resistance of the copper wire (or aluminum wire) used for the windings. These losses increase with the current, and therefore, are load dependent[17], [18]. The copper loss P_{copper} in either the primary or secondary winding is given by:

$$P_{copper} = I^2R \quad (4)$$

Copper losses are higher when the transformer is fully loaded and smaller when it is lightly loaded or not loaded at all because they are proportional to the square of the current. The resistance of the windings as current passes through them causes copper losses in transformers. The square of the current and the winding's resistance determines the copper loss exactly. The amount of copper loss in a transformer depends on a number of parameters. These variables mostly have to do with the transformer's windings' properties and the current passing through them.

2.5 Power Handling

The ability of a transformer to transfer electrical energy effectively and efficiently from the primary (input) side to the secondary (output) side is known as power handling. In AC circuits, transformers are used to increase or decrease voltage while maintaining power. However, its design, size, insulation, temperature limitations, and the load it handles are some of the elements that affect its power handling capacity. The voltage rating, current rating, frequency, and other characteristics of a transformer all affect how much power it can handle. The power handling capacity of a transformer is commonly measured in megavolt-amperes (MVA), kilovolt-amperes (kVA), or volt-amperes (VA). A transformer's ability to handle power is determined by its voltage and current ratings. The product of the maximum voltage and current determines the maximum power the transformer can handle.

$$S_{max} = V_{rated} \text{ x } I_{rated} \quad (5)$$

A. Active Power (P)

Active power in a transformer is the power used to do real work, that is, the power that can be used to drive a load connected to the electrical system, such as a motor, heater, or other electronic device. In a transformer, active power is calculated based on the relationship between voltage, current, and power factor, which reflects how the voltage and current are in phase with each other[19], [20],[21]. In a three-phase transformer, active power can be calculated using the equation:

$$P = \sqrt{3} \text{ x } V \text{ x } I \text{ x } \cos(\theta) \quad (6)$$

JURNAL ECTIPE
Electronic, Control, Telecommunication, Information, and Power Engineering
Volume 12, Issue 1, April 2025, pp. 95-102
ISSN 2355-5068 ; e-ISSN 2622-4852
DOI: 10.33019/jurnalecotipe.v12i1.4534

B. Reactive Power (Q)

Reactive power is the power component that does not do any actual work but is needed to support the operation of the transformer and inductive loads (such as electric motors, the transformer itself, and other inductive devices). This reactive power is important for maintaining the magnetic field in the transformer and other inductive devices. Reactive power in a three-phase system is calculated by

$$Q = \sqrt{3} \times V \times I \times \sin(\theta) \quad (7)$$

C. Apparent Power (S)

Apparent power is the total power supplied by an electrical system, which includes both active power (which does real work) and reactive power (which does no real work). In the context of transformers, apparent power describes the total amount of power received and used by the transformer to drive the load and maintain the magnetic field in the system. Apparent power in a three-phase system is calculated by

$$S = \sqrt{3} \times V \times I \quad (8)$$

2.6 MATLAB

MATLAB is a technical computing high-performance programming environment that is frequently used for method creation, data analysis, simulation, and numerical computing. It provides a vast range of tools and functions to help engineers, scientists, and researchers model systems, visualize data, and solve complex mathematical problems. For analyzing 3-phase transformers in MATLAB, MATLAB provides an easy interface to model and simulate electrical systems such as transformers. The analysis of 3-phase transformers typically involves simulating key characteristics like voltage regulation, load effect, efficiency, and losses.

3. RESULTS AND DISCUSSION

The results and discussion of the MATLAB simulation-based examination of a three-phase transformer's properties are presented in this part. The analysis involves computing and visualizing several key parameters of the transformer such as power, voltage regulation, efficiency, and losses. These results are obtained using MATLAB's built-in functions and custom code to model and simulate the behavior of the transformer under various operating conditions that can be seen in Figure 1 shows the three-phase voltage waveforms obtained from the MATLAB simulation. In this graph, there are three sinusoidal curves that represent the voltages of each phase (Va, Vb, and Vc). The three waves have a phase angle difference of 120°, which is a typical characteristic of a three-phase power system. From this waveform, it can be observed that the voltage amplitude remains stable, indicating that the transformer is operating under normal conditions without any significant disturbances. If there is a change in the load or an imbalance in the system, the voltage waveform may experience distortion or amplitude shift. The MATLAB simulation allows for accurate monitoring of these changes, which is useful in transformer performance analysis, and Figure 2 shows the three-phase current waveforms generated from the MATLAB simulation. Just like the three-phase voltages, the three-phase currents (Ia, Ib, and Ic) have a phase angle difference of 120° between each other, indicating that the system is operating under balanced load conditions.

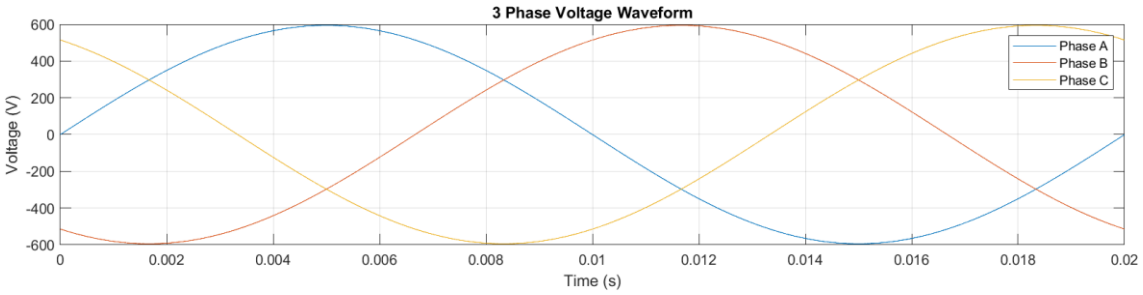

Figure 1. 3-phase voltage waveform

JURNAL ECOTIPE
Electronic, Control, Telecommunication, Information, and Power Engineering
Volume 12, Issue 1, April 2025, pp. 95-102
ISSN 2355-5068 ; e-ISSN 2622-4852
DOI: 10.33019/jurnalecotipe.v12i1.4534

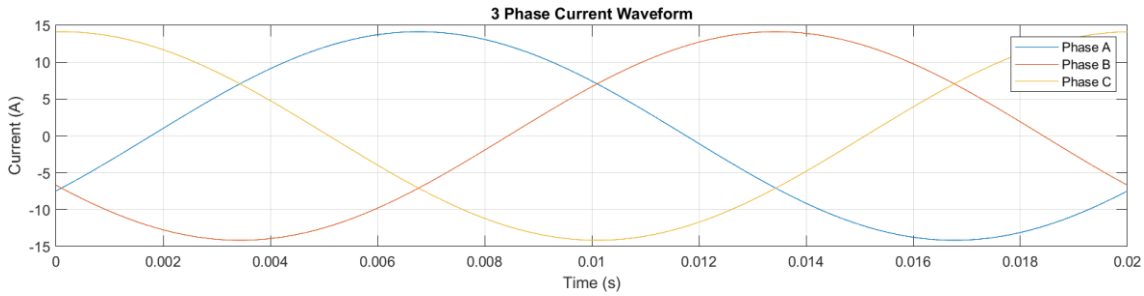

Figure 2. 3-phase current waveform

In a three-phase transformer, there are three main channels for voltage and current, each of which has a different value and phase. The three-phase system can be described by the interconnected voltage and current vectors shown in Figure 3 where the three voltage vectors (A, B, and C) will be distributed at an angle of 120 degrees, forming a triangle on the phasor diagram, and the currents on the primary and secondary sides will describe a similar relationship, but with the influence of the turns ratio. Phase differences between voltage and current can occur, depending on the load impedance.

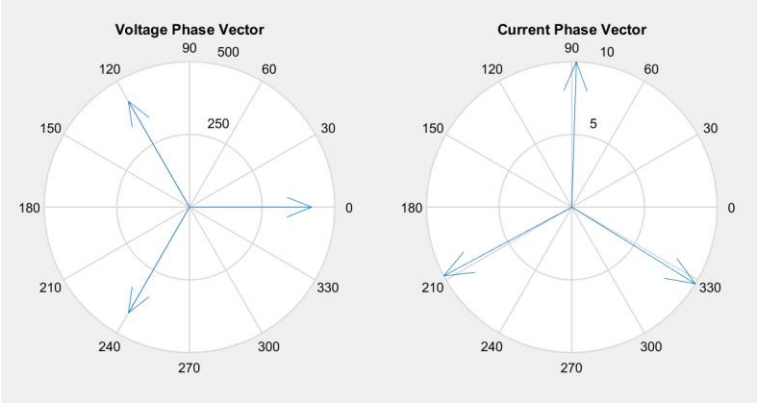

Figure 3. Vector on a 3-phase transformer (voltage and current)

From Figure 1 to Figure 3 above, it can be seen that the research of the characteristics of the 3-phase transformer produces an active power (P) of 6183.42 W, a reactive power (Q) of 3832.14 VAR, an apparent power (S) of 7274.61 VA and a transformer efficiency of 97.75% with a time of 0.02 s and produces losses in copper of 81.65 W can be seen in Figure 4 shows the simulation results of the power generated by a three-phase transformer under various operating conditions. In a three-phase power system, the power transferred can be calculated in several main forms, namely active power (P), reactive power (Q), and apparent power (S). This shows that the 3-phase transformer has met the applicable international standards.

In a 3-phase transformer, it produces an electric field (E-field) and magnetic field (H-field) radiation pattern in the form of a polar graph. The electric field pattern (E-field) shows a cosine-based distribution, with maximum intensity on a certain axis and minimum intensity in other directions. The magnetic field pattern (H-field) shows a sine-based distribution, with maximum intensity in different directions from the electric field, indicating an orthogonal relationship between the E-field and H-field. The operating frequency (50 Hz) produces a radiation pattern with low frequency properties, where the effects of electromagnetic waves are still dominant at close range around the transformer. The field distribution shows a relationship between the intensity of the electric and magnetic fields with the angular position to the transformer core as shown in Figure 5 shows the electromagnetic field distribution generated by a three-phase transformer during operation. This electromagnetic (EM) field radiation occurs due to the electric current in the transformer windings, which produces a magnetic field around the core and windings. Electromagnetic field radiation can be analyzed to understand its impact on transformer efficiency, power losses, and potential electromagnetic interference (EMI) that can affect other electrical equipment in the vicinity.

JURNAL ECTIPE
Electronic, Control, Telecommunication, Information, and Power Engineering
Volume 12, Issue 1, April 2025, pp. 95-102
ISSN 2355-5068 ; e-ISSN 2622-4852
DOI: 10.33019/jurnalecotipe.v12i1.4534

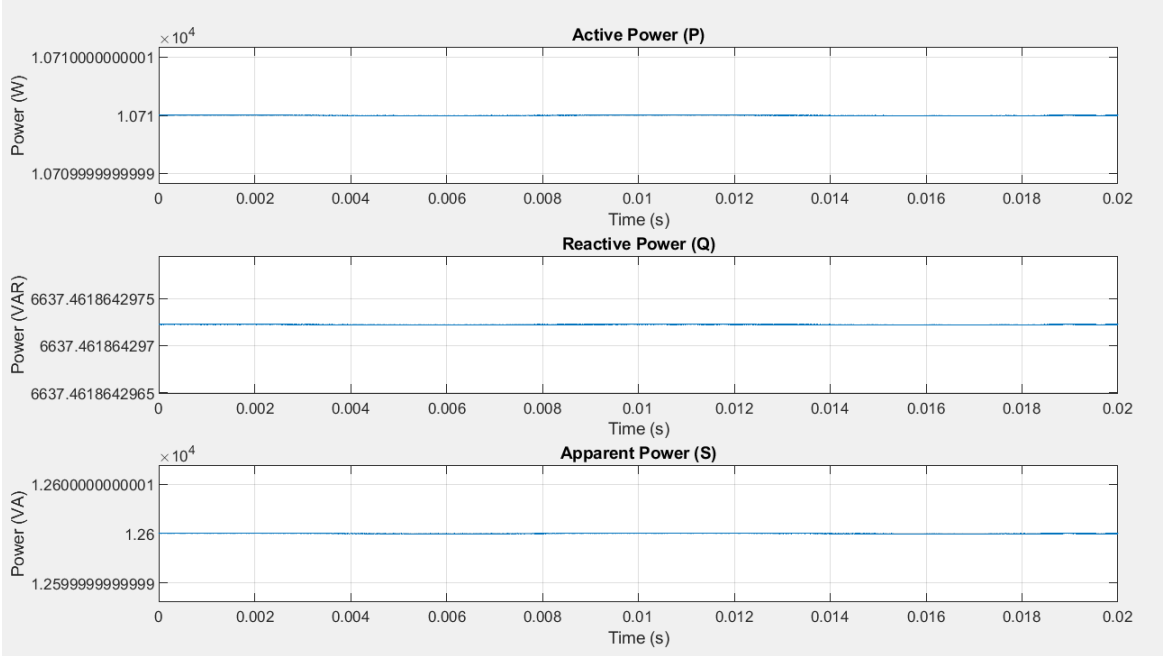

Figure 4. Power generated by a 3-phase transformer

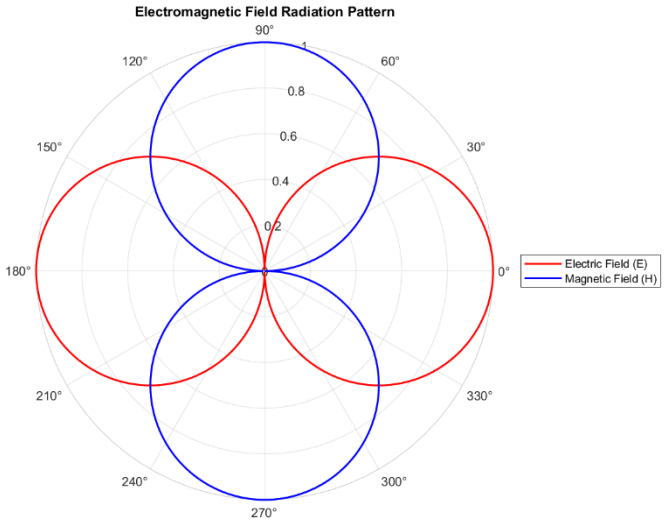

Figure 5. Electromagnetic field radiation in 3 phase transformers

4. CONCLUSION

The MATLAB-based analysis conducted in this study aims to provide a comprehensive understanding of the operating characteristics of a three-phase transformer, especially in relation to the voltage, current, and power generated. With this approach, various key parameters of the transformer can be accurately evaluated, allowing the identification of factors that affect efficiency and power losses. The results of the analysis show that the active power (P) generated by the transformer is 6183.42 W, which is the real power used by the load. The reactive power (Q) generated is 3832.14 VAR, which reflects the energy circulating in the system due to the inductive or capacitive components of the load and the transformer itself. The apparent power (S) generated is 7274.61 VA, which represents the vector combination of active power and reactive power in a three-phase system. With a transformer efficiency reaching 97.75%, it can be concluded that the transformer operates with high performance and only experiences minimal power losses. One important aspect in this analysis is the calculation of copper losses of 81.65 W, which occurs due to resistance in the transformer windings. These losses contribute

Volume 12, Issue 1, April 2025, pp. 95-102
ISSN 2355-5068 ; e-ISSN 2622-4852
DOI: 10.33019/jurnalecotipe.v12i1.4534

to the dissipation of energy in the form of heat and generate electromagnetic field radiation. The study of these radiation patterns shows that the electric field (E field) and the magnetic field (H field) form a polar graph, which describes the distribution of the direction and intensity of the fields in space. The electric field (E) distribution shows a cosine-based pattern, with maximum intensity in certain directions and minimum intensity in other directions. Meanwhile, the magnetic field (H) distribution shows a sine-based pattern, with maximum intensity in different directions from the electric field. This indicates that the electric and magnetic fields have an orthogonal relationship with each other, as expected in the electromagnetic wave theory. With this understanding, it can be concluded that MATLAB-based analysis not only allows the evaluation of the operational parameters of the transformer but also provides deep insight into the interaction of electromagnetic fields generated during operation. These findings emphasize the importance of maintaining an ideal power factor to optimize transformer performance and minimize energy losses, so that the power system can operate more efficiently and stably.

Acknowledgments

We would like to express our deepest thanks to all parties who have helped in preparing the research and writing of this scientific paper, especially the electrical engineering department of Universitas Al-Azhar Medan in collaboration with Universiti Malaysia Perlis (UniMAP) and Universiti Teknikal Malaysia Melaka (UTeM).

REFERENCES

[1] C. Yan, W. Wang, P. Zhang, Z. Liu, J. Shu, and B. Zhang, "Coupled Field–Circuit Modeling and Analysis for Interturn Short-Circuit Faults in an Onboard Traction Transformer," in *2023 IEEE International Magnetic Conference - Short Papers (INTERMAG Short Papers)*, 2023, pp. 1–2. doi: 10.1109/INTERMAGShortPapers58606.2023.10228536.

[2] J. P. Karunadasa, K. G. L. Navarathna, R. Abeyrathna, K. Perera, and K. D. N. Sandaruwan, "Novel Three Phase Transformer Model to Accommodate the Effects of Load Injected DC," in *2018 Moratuwa Engineering Research Conference (MERCon)*, 2018, pp. 138–143. doi: 10.1109/MERCon.2018.8421993.

[3] J. Qin *et al.*, "A Three-phase Combined Transformer with Characteristics of Anti-leakage current and Anti-electromagnetic Interference," in *2021 6th Asia Conference on Power and Electrical Engineering (ACPEE)*, 2021, pp. 1184–1188. doi: 10.1109/ACPEE51499.2021.9437125.

[4] H. S. Oztura and S. Polat, "A Symmetrical-Asymmetrical Fault Characteristics Analysis within Cogeneration Power Plant in Izmir, Turkey: An Experimental Assessment," *Gazi Univ. J. Sci.*, vol. 35, no. 2, pp. 524–540, 2022, doi: 10.35378/gujs.770814.

[5] A. Kokor, S. Smaka, S. Grebović, and V. Helać, "Effects of Neutral Point Grounding Methods on Single-Phase Short Circuit Fault Characteristics," in *2022 21st International Symposium INFOTEH-JAHORINA (INFOTEH)*, 2022, pp. 1–6. doi: 10.1109/INFOTEH53737.2022.9751319.

[6] I. Roza, Y. T. Nugraha, R. Rida, M. Irwanto, and M. A. Othman, "Modeling of Glugur Substation grounding systems using MATLAB graphical user interface," *Int. J. Electr. Comput. Eng.*, vol. 15, no. 1, pp. 15–23, 2025, doi: 10.11591/ijece.v15i1.pp15-23.

[7] M. Irwanto, Y. T. Nugraha, N. Hussin, I. Nisza, D. Perangin-Angin, and H. Alam, "Modelling of Wireless Power Transfer System Using MATLAB SIMULINK," *2022 IEEE 13th Control Syst. Grad. Res. Colloquium, ICSGRC 2022 - Conf. Proc.*, no. July, pp. 21–24, 2022, doi: 10.1109/ICSGRC55096.2022.9845181.

[8] C. Shambare, Y. Sun, and O. Imoru, "A Survey on Recent development of Asymmetrical Three-Phase Short Circuit Faults Computation in Power Systems," in *2019 6th International Conference on Soft Computing & Machine Intelligence (ISCMI)*, 2019, pp. 180–184. doi: 10.1109/ISCMI47871.2019.9004345.

Volume 12, Issue 1, April 2025, pp. 95-102
ISSN 2355-5068 ; e-ISSN 2622-4852
DOI: 10.33019/jurnalecotipe.v12i1.4534

[9] M. Irwanto, Y. T. Nugraha, N. Hussin, and I. Nisja, "Effect of Temperature and Solar Irradiance on the Performance of 50 Hz Photovoltaic Wireless Power Transfer System," *J. Teknol.*, vol. 85, no. 2, pp. 53–67, 2023, doi: 10.11113/jurnalteknologi.v85.18872.

[10] M. Irwanto, M. B. Ali, Y. T. Nugraha, B. Ismail, I. Nisja, and W. Z. Leow, "Analysis on the Effect of DC Current Changes on the Magnetic Field of Wireless Power Transfer," in *2023 IEEE 14th Control and System Graduate Research Colloquium (ICSGRC)*, 2023, pp. 186–191. doi: 10.1109/ICSGRC57744.2023.10215406.

[11] M. Irwanto, H. S. Ibrahim, Y. T. Nugraha, and I. Nisja, "Performance analysis of photovoltaic powered half bridge inverter using sinusoidal pulse width modulation (SPWM) method," *AIP Conf. Proc.*, vol. 2991, no. 1, p. 20018, Jun. 2024, doi: 10.1063/5.0198660.

[12] C. Martineac, P. C. Dărab, H. G. Beleiu, and R. N. Hasanah, "Influence of Soil Resistivity on 110 kV Substation Grounding System," in *2020 International Conference and Exposition on Electrical And Power Engineering (EPE)*, 2020, pp. 715–720. doi: 10.1109/EPE50722.2020.9305645.

[13] H. Alam, M. Irwanto, Y. M. Mashor, and M. Masri, "Design of multiple Pulse Width Modulation (MPWM) Transformerless Photovoltaic Inverter (TPVI) system," *J. Phys. Conf. Ser.*, vol. 1432, no. 1, pp. 0–9, 2020, doi: 10.1088/1742-6596/1432/1/012056.

[14] K. Akom, T. Shongwe, M. K. Joseph, and S. Padmanaban, "Energy Framework and Policy Direction Guidelines: Ghana 2017-2050 Perspectives," *IEEE Access*, vol. 8, pp. 152851–152869, 2020, doi: 10.1109/ACCESS.2020.3018314.

[15] Q. Wu, T. Hong, S. Jazebi, and F. de León, "Experimentally Validated Method to Measure the λ Characteristics of Asymmetric Three-Phase Transformers," *IEEE Trans. Magn.*, vol. 55, no. 4, pp. 1–9, 2019, doi: 10.1109/TMAG.2019.2897962.

[16] T.-H. Han, S.-C. Ko, and S.-H. Lim, "Analysis on Three-Phase Ground Fault Current Limiting Operations of Three-Phase Transformer Type SFCL Using Two Superconducting Modules," *IEEE Trans. Appl. Supercond.*, vol. 32, no. 6, pp. 1–7, 2022, doi: 10.1109/TASC.2022.3181571.

[17] S. Hardi, A. Nasution, F. Fahmi, and F. Purnamasari, "Efficient Design On The Substation Grounding Grid: A Case Study at 2x500MVA Galang," in *2020 4rd International Conference on Electrical, Telecommunication and Computer Engineering (ELTICOM)*, 2020, pp. 180–185. doi: 10.1109/ELTICOM50775.2020.9230492.

[18] A. R. Soman, A. R. Deshmukh, A. D. Kulkarni, A. N. Kulkarni, and P. S. Nagdeote, "Design And Development of Three - Phase Transformer," *IJIREEICE*, vol. 12, no. 4, pp. 264–272, 2024, doi: 10.17148/IJIREEICE.2024.12441.

[19] A. Ge, D. Xie, Z. Shi, G. Yu, and X. Zhang, "Analysis of Grounding Grids Connection Between Photovoltaic Farm and Its Substation," in *2020 IEEE International Conference on High Voltage Engineering and Application (ICHVE)*, 2020, pp. 1–4. doi: 10.1109/ICHVE49031.2020.9280034.

[20] R. Rios, M. Quintana, M. Ramirez, E. Ortigoza, V. Oxilia, and G. Blanco, "Use of electric vehicles to achieve sustainable development goals in countries with surpluses of hydroelectricity: Case of Paraguay," *IEEE Chil. Conf. Electr. Electron. Eng. Inf. Commun. Technol. CHILECON 2019*, pp. 1–6, 2019, doi: 10.1109/CHILECON47746.2019.8988038.

[21] T. Mushiri and C. Mbohwa, "Research on the use of matlab in the modeling of 3-phase power systems," *Lect. Notes Eng. Comput. Sci.*, vol. 2217, pp. 363–369, 2015.

JURNAL ECOTIPE
Electronic, Control, Telecommunication, Information, and Power Engineering

Volume 12, Issue 1, April 2025, pp. 103-112
ISSN 2355-5068 ; e-ISSN 2622-4852
DOI: 10.33019/jurnalecotipe.v12i1.4532

User Capacity Optimization Using the Mobility Load Balancing Algorithm for Downlink Data Long Term Evolution

Miranti[1], Lydia Sari [2], Muhamad Doris [3], Syah Alam [4], Indra Surjati [5]
[1,2,3,4,5] Electrical Engineering Department, Universitas Trisakti, Jl. Kyai Tapa no. 1, Jakarta, Indonesia

ARTICLE INFO

Article historys:

Received : 21/12/2024
Revised : 07/01/2025
Accepted : 18/02/2025

Keywords:

Load Balancing; Long Term Evolution; Mobility; Resource; Throughput

ABSTRACT

The increasing number of users in a Long Term Evolution (LTE) network often decreases network performance. A cell that has high traffic experiences a decline in network performance due to unavailable resources for certain users, while in cells with low traffic, the use of resources in these cells is inefficient. The mobility load balancing (MLB) algorithm balances the intercellular loads in an LTE network and improves the performance by distributing part of the load in a high traffic cell to neighboring cells that have low loads. An activated MLB will detect the network load and calculate the available resource for each cell to determine which cells are overloaded. The MLB will consider the candidate cell where the load could be distributed. MLB simulation results show that the application of MLB has succeeded in reducing the percentage of unsatisfied users by 9.4% and increasing throughput system to 5.617 Mbps.

Corresponding Author:

Lydia Sari
Electrical Engineering Department, Universitas Trisakti, Jl. Kyai Tapa no. 1, Jakarta, Indonesia
lydia_sari@trisakti.ac.id

1. INTRODUCTION

Long Term Evolution (LTE) is a telecommunication technology that offers a data rate of up to 100 Mbps (downlink) and 50 Mbps (uplink), making it suitable to meet the demands of high data rate transfers [1]. However, as the number of users in an LTE network increase, it becomes difficult to achieve stable performance. Overload conditions on cells (congestion) will affect overall user access for both new users and active users and variations in usage time create an unequal load for each cell resulting in a decrease of the system's Quality of Service (QoS)[2,3]. This encourages cellular operators to pay attention to resource blocks in cells to accommodate traffic and maintain a balanced network load. One possible scenario to provide the same user experience to all users is to measure QoS performance by utilizing the Mobility Load Balancing (MLB) algorithm at the cell level [4,5]. The MLB algorithm will detect the load and then calculate the available resources in each cell to determine which cells are overloaded and consider candidate cells that will accept users from overloaded cells [6]. Ideally, optimization will automatically be carried out to balance the load between cells, where the load of cells with excess users will be transferred to cells with fewer users.

In research [2], the decision to move the excess load automatically from the source cell to the neighboring cell is based on the hysteresis value of the MLB simulation analysis on call admission and user throughput. In the proposed work, we analyze the effect of the implementation of the MLB algorithm on network performance on LTE in time division duplex (TDD) access mode. The trigger to activate the MLB algorithm is based on the load and total resources on the cell. The MLB algorithm is

JURNAL ECTIPE
Electronic, Control, Telecommunication, Information, and Power Engineering
Volume 12, Issue 1, April 2025, pp. 103-112
ISSN 2355-5068 ; e-ISSN 2622-4852
DOI: 10.33019/jurnalecotipe.v12i1.4532

expected to increase network capacity and utilization of available resources which in turn will increase the throughput on LTE networks.

The rest of the paper is organized as follows. The second section discusses the LTE network architecture, mobility load balancing scheme and the simulation setup. The simulations results are discussed in the third section, while the conclusion is given in the last section.

2. RESEARCH METHOD

2.1. LTE Network Architecture

LTE consists of three main components, namely User Equipment (UE), Evolved UMTS Terrestial Radio Access Network (E-UTRAN) and Evolved Packet Core (EPC). An LTE network architecture is depicted in Figure 1 [7]. User Equipment (UE) consists of 3 main parts, namely mobile termination (MT) which serves for communication, Terminal Equipment (TE) which serves for disconnection of communication links and Universal Integrated Circuit Card (UICC) which serves to run the Universal Subscriber Identity Module (USIM). USIM is used for identifying and authenticating subscriber devices and as a movable security key to protect radio transmission interfaces. The UE serves as a communication application platform, which can perform various functions required by the end user, such as signal and network regulation and maintenance, as well as communication link disconnection. The radio access interface from the UE to the core network is handled by E-UTRAN on the LTE architecture system. In the previous technology, node B and RNC were separate elements, in LTE architecture the two elements were only one component. The combination of the two elements is called Evolved Node B (eNode B), and functions to monitor and control signals for carrier delivery and authentication. In LTE technology, the EPC serves for end-to-end IP delivery services.

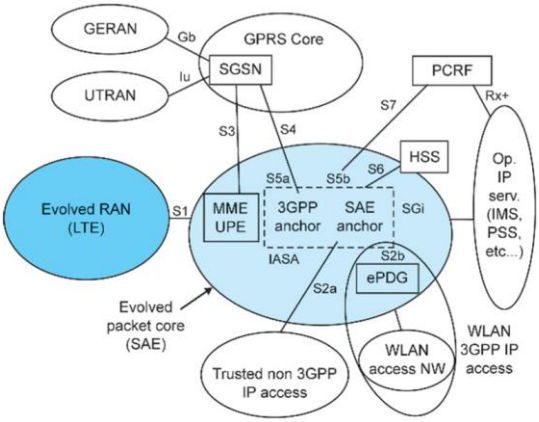

Figure 1. LTE network architecture [7]

The Physical Resource Block (PRB) is illustrated in Figure 2. One resource block consists of 12 subcarriers where the bandwidth of each subcarrier is 15 kHz and there are 7 OFDM symbols or one slot of 0.5 ms. This means in 1 resource block the bandwidth is 15 kHz x 12 subcarriers = 180 kHz. The smallest part of the resource block is the resource element or RE. In one resource block there are 12 subcarriers x 7 OFDM symbols = 84 resource elements. In the LTE system, there are variations in bandwidth, such as 1.4 MHz, 3 MHz, 5 MHz, 10 MHz, and 20 MHz. The choice of bandwidth used by cellular operators will affect the number of resource blocks. The greater the bandwidth used, the greater the number of resource blocks and the maximum throughput generated [8]. Table 1 shows the number of resource block (RB) in accordance to the bandwidth used.

JURNAL ECTIPE
Electronic, Control, Telecommunication, Information, and Power Engineering
Volume 12, Issue 1, April 2025, pp. 103-112
ISSN 2355-5068 ; e-ISSN 2622-4852
DOI: 10.33019/jurnalecotipe.v12i1.4532

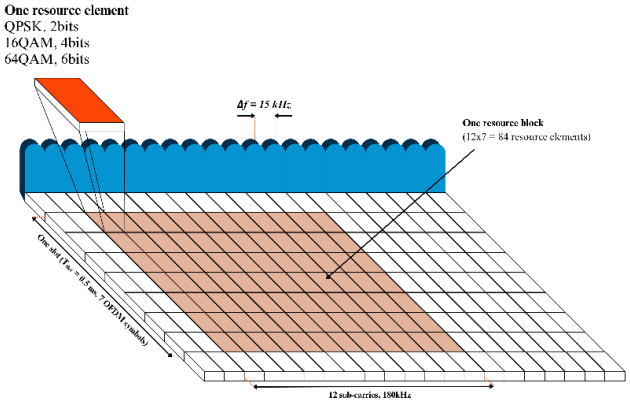

Figure 1. Physical resource block [9]

Table 1. Number of resource block vs channel bandwidth

Number of Resource Blocks	Channel Bandwidth (MHz)
6	1.4
15	3
25	5
50	10
75	15
100	20

In cellular networks, two full duplex techniques are generally used, namely Frequency Division Duplex (FDD) and Time Division Duplex (TDD). FDD allows sending and receiving data simultaneously using different frequencies. This technique requires a guard frequency as a separator between the sending and receiving frequencies and requires an accurate frequency filtering process. TDD uses one frequency for both sender and receiver simultaneously. The multiplexing process for each channel is done on a time basis so that each channel has a different time slot. In the 3GPP Release 8 specifications for TDD and FDD access modes, there is no difference in the basic subframe format and configuration protocol for the OFDMA radio access scheme in the downlink and SC-FDMA in the uplink.

2.2. Mobility Load Balancing (MLB) Algorithm

The MLB algorithm aims to balance the traffic loads between cells to increase system capacity. The algorithm ensures the user equipments (UEs) are distributed optimally across available neighboring cells. By keeping the UEs evenly distributed across the cells, frequent handover process can be avoided and thus drop-calls.

To trigger the start of MLB algorithm, the load of a source cell must exceed a predetermined threshold value, and there must be a neighboring cell which load is low enough to handle the traffic from the source cell. When these two events exist, the source cell will choose several user candidates to be transferred to the neighboring cell [4]. Depending to the types of handover and the handover parameters, MLB can be categorized into three approaches, namely Intra-frequency, Inter-frequency, and Inter-Radio Acces Technologi (Inter-RAT). In Intra-frequency MLB, the handover occurs on systems with the same frequency. On the other hand, in Inter-frequency MLB, the handover process occurs between different frequencies on the LTE network if available. The Inter-RAT MLB is the same as inter-frequency, but the handover occurs between different Radio Access Technologies (RATs).

Load balancing in LTE networks is done in several stages. In the first stage, the eNodeB performs traffic load assessment. If a traffic overload is detected, the source cell and the target cell will exchange information using Resource Status Request, Resource Status Response, and Resource Status Update messages. The next stage is the UE selection stage, where the number of UEs to be offloaded is calculated. If the traffic in a source cell exceeds its maximum threshold, an inter-frequency measurement report is triggered and UEs candidates are selected for handover. Finally the UE offloading is done,

JURNAL ECTIPE
Electronic, Control, Telecommunication, Information, and Power Engineering
Volume 12, Issue 1, April 2025, pp. 103-112
ISSN 2355-5068 ; e-ISSN 2622-4852
DOI: 10.33019/jurnalecotipe.v12i1.4532

prioritizing UEs with non-Guarantee Bit Rate (GBR) to be transferred to the neighboring cell as to maintain the Quality of Service (QoS) of the network.

The LTE systems, TDD attracts growing interests as it is better suited to data traffic, namely data downloading, video conferences and internet browsing. In the TDD-FDD convergence scenarios, load balancing is an important solution to maximize the radio resource utilization efficiency.
The general algorithm mechanism of MLB is illustrated in Figure 3.

A cell is overloaded if the following condition is satisfied [2] :

$$\frac{V_{AR}(0)}{V_{TR}(0)} < Th_{PreMLB} \tag{1}$$

where $V_{AR}(0)$ is the number of resources in each cell 0, $V_{TR}(0)$ is the total resource in cell 0, and Th_{PreMLB} is the trigger to activate the MLB algorithm.

The overloaded cell dynamically configures a new hysteresis threshold for different neighbor cells taking into account the relative amount of resources of the two cells available. The update of the hysteresis threshold is calculated according to the following equations [2]:

$$ThHys(0,i) = \alpha_i . ThHys(0), \quad (0 \le \alpha_i \le 1) \tag{2}$$

$$\alpha_i = \begin{cases} 0 \quad if \ \frac{V_{AR}(i)}{V_{TR}(i)} > Th_{PostMLB} \\ \beta_i \ \ if \ Th_{availMLB} \le \frac{V_{AR}(i)}{V_{TR}(i)} \le Th_{PreMLB} \\ 1 \ \ if \ \frac{V_{AR}(i)}{V_{TR}(i)} \le Th_{AvailMLB} \end{cases} \tag{3}$$

$$\beta_i = 1 - \frac{Th_{AvailMLB} - \frac{V_{AR}(i)}{V_{TR}(i)}}{Th_{AvailMLB} - Th_{PostMLB}} \tag{4}$$

where $V_{AR}(i)$ is the available resources in the i^{th} cell, $V_{TR}(i)$ is the total amount of resources in the i^{th} cell, $V_{AR}(i)/ V_{TR}(i)$ is the relative amount of available resources in cell i, Th_{preMLB} is the predefined threshold for triggering MLB, $Th_{postMLB}$ is the threshold for disabling MLB, and $Th_{availMLB}$ is the threshold to accept MLB.

The variable Th_{Hys} (0) is the cell hysteresis threshold before MLB is run and Th_{Hys} (0, i) is the cell hysteresis threshold (with index 0) to neighbor cells with index i. The variable $Th_{availMLB}$ is the effective threshold when MLB is running and $Th_{postMLB}$ is the threshold for disabling MLB [2]. The cell updates the hysteresis threshold Th_{Hys} (0, i) and sends it to active UEs, namely the UEs residing in the cell. The UEs update the new hysteresis threshold until it returns to the default value. After reaching the MLB condition it will be disabled, namely if the following condition is met [2]:

$$\frac{V_{AR}(0)}{V_{TR}(0)} > Th_{PostMLB} \tag{5}$$

Equation 6 is the effective threshold value when MLB is running [2].

$$\frac{V_{AR}(i)}{V_{TR}(i)} > Th_{AvailMLB} \tag{6}$$

JURNAL ECOTIPE
Electronic, Control, Telecommunication, Information, and Power Engineering
Volume 12, Issue 1, April 2025, pp. 103-112
ISSN 2355-5068 ; e-ISSN 2622-4852
DOI: 10.33019/jurnalecotipe.v12i1.4532

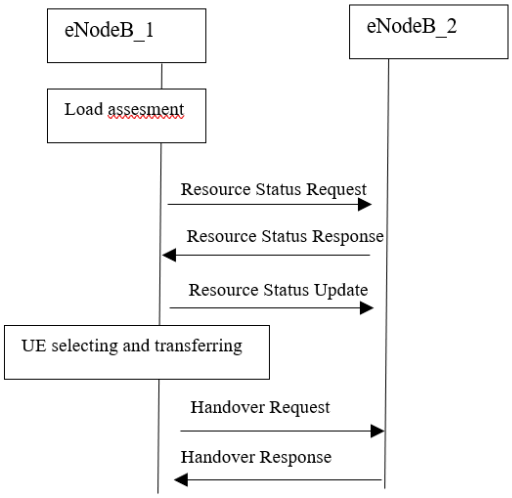

Figure 2. General concept of MLB [10]

The performance of the MLB system is the measurement of the effect of MLB algorithm implementation on the LTE network. The parameters measured as a reference for the performance of the MLB algorithm are the number of unsatisfied user and throughput, which are explained in details in the following:

1. Number of unsatisfied User
   Unsatisfied users are those denied an LTE service. This occurs due to limited cell resources in the LTE network. The number of unsatisfied users on the network is the number of unsatisfied users per cell expressed as [6]:

$$z = \sum_{\forall c} max\ (0, |U|.\left(1 - {}^{1}/_{P_i}\right) \tag{7}$$

   where $|U|$ is the number of users in the cell, and P_i is the load of the 0^{th} cell, and z describes the maximum number of users that will be allocated a resource.
2. Throughput
   Throughput is calculated from the number of symbols per second of data that can be transferred between a UE and eNodeB, which is converted into bits per second depending on the number of bits carried in one symbol. The number of bits per symbol depends on the modulation scheme, namely QPSK, 16-QAM, and 64-QAM. For QPSK, each symbol contains 2 bits per symbol, whereas 16QAM and 64QAM carries 4 and 6 bits per symbol, respectively. User throughput is can be stated as [11]

$$Throughput = \frac{number\ of\ bits}{time\ interval} = \frac{number\ of\ Resource\ Block \times 84 \times modulation\ factor}{0.5\ ms} \tag{8}$$

2.3. Simulation Setup

The system simulates 6 hexagonal cells with uniform radius, as illustrated in Figure 4. The total number of users in the simulated system is 140, where the number of users in each cell has been determined but the distribution of users in each cell is random. Data services are provided in the cell, with 64 Kbps data rate used by 50% of the users, 1280 Kbps used by 30% of the users and 1000 Kbps used by 20% of the users. In the simulated system, one cell is overloaded, namely the total resource blocks used in the cell is more than 60% of the total resource provided. In the simulated system the bandwidth channel is 15 MHz so that the total resource block is 75.

The overloaded cell will be triggered to shift one or more users to other cells. The MLB algorithm is used to determine target cell, namely the appropriate cell where the users from the overloaded cell can be transferred to. Consequently, the user from the overloaded cell will be moved to the target cell. RSRP value is used to determine the position of the user. The user who is located at the edge of cell

Volume 12, Issue 1, April 2025, pp. 103-112
ISSN 2355-5068 ; e-ISSN 2622-4852
DOI: 10.33019/jurnalecotipe.v12i1.4532

will be selected as a candidate user to be moved to the target cell. If none of the users' RSRP values meets the qualification for the move, the MLB cannot be performed.

The flowchart of the MLB algorithm is given in Figure 5. The simulations will be conducted based on the parameters given in Table 2.

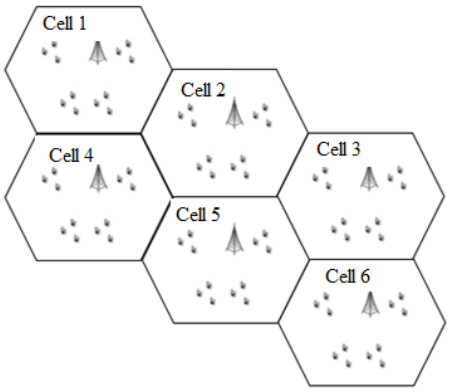

Figure 3. Simulated cells positioning

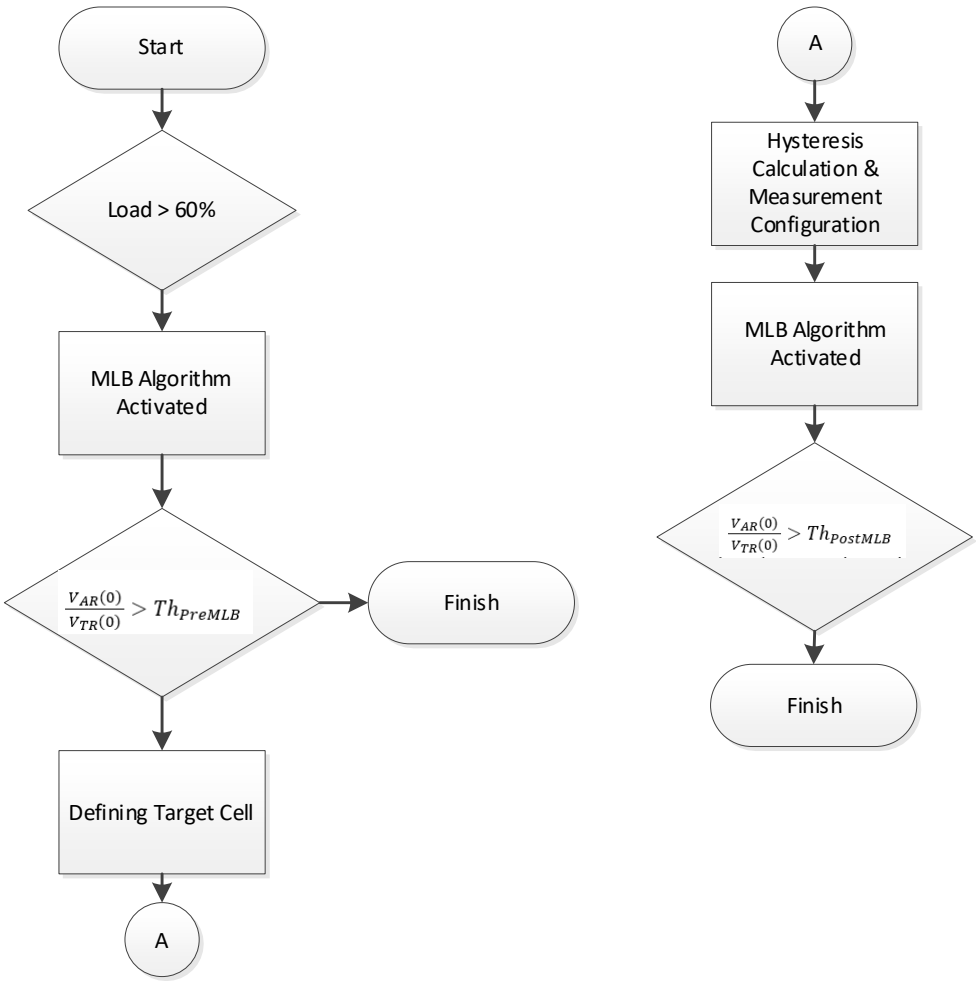

Figure 4. MLB algorithm

Volume 12, Issue 1, April 2025, pp. 103-112
ISSN 2355-5068 ; e-ISSN 2622-4852
DOI: 10.33019/jurnalecotipe.v12i1.4532

Table 2. Simulation Parameters

Parameter	Value
Simulation time	300 s
Number of cell	6
EnodeB distance	500 m
Downlink transmitter power	46 dBm
Downlink bandwidth	15 MHz (72 PRB)
Traffic type	Data
Data Rate	64 Kbps; 1000 Kbps ; 1280 Kbps
SINR	0 ~ 15 dB
RSRP	-120 ~ -75 dBm
Number of user	140
Antenna type	MIMO
Default hysteresis value	3 dB
Default Load	60 % (0.6)
ThPreMLB	40 % (0.4)
ThAvailMLB	30 % (0.3)
ThPost	40 % (0.4)

The simulation steps are as follows:

1. Initialize according to Table 2, where all data are constant except for user position, data rate, RSRP and SINR
2. Generate user positions and distribute the positions randomly within each cells, in accordance with the number of users in each cells
3. Generate data rate
4. Measure SINR and RSRP of each user, considering the user's distance from eNodeB. The farther a user is from eNodeB, the lower its SINR and RSRP value
5. Calculate resource block of each user
6. Calculate the cell load, resource, and number of unsatisfied users
7. Calculate the network throughput before MLB algorithm is implemented
8. Run the MLB algorithm. The simulation time is 300 seconds
9. Measure the SINR until the allocated user resource is transferred to a neighboring cell
10. Calculate the load percentage and the resource of each cell after the MLB algorithm is implemented
11. Calculate the number of unsatisfied users and the network throughput after the MLB algorithm is implemented
12. Create the comparison graph for the conditions before and after the MLB algorithm is implemented

MLB scenarios are applied to analyze network performance with and without the implementation of MLB algorithm. The throughput and number of unsatisfied users are analyzed. In this scenario, the number of cells is 6, and one of the cells is overloaded. The testing scenario is done based on the increase of the number of users in the overloaded cell, with the details as follows:

a. Unsatisfied users
   The number of unsatisfied users is calculated based on (7) only for the overloaded cell
b. Throughput
   The throughput depends on the number of resources allocated for each user, and the type of modulation used. QPSK modulation is used when a user's SINR is between 0-5 dB. If the SINR is between 5-10 dB, the modulation is 16-QAM. The 64-QAM scheme is used for user's which SINR is between 10-15 dB. The throughput is calculated using (8).

The simulation is carried out by increasing the number of users in cell 3 gradually with the scenario as in Table 3. Before the MLB algorithm is run, the number of users, load and available resources is calculated in each cell. Table 4 shows the calculation results for the parameters.

JURNAL ECTIPE
Electronic, Control, Telecommunication, Information, and Power Engineering
Volume 12, Issue 1, April 2025, pp. 103-112
ISSN 2355-5068 ; e-ISSN 2622-4852
DOI: 10.33019/jurnalecotipe.v12i1.4532

Table 1. Simulation scenario

Number of users in observed cell	**Number of users in neighboring cells**				
Cell 3	Cell 1	Cell 2	Cell 4	Cell 5	Cell 6
35	20	10	15	20	15
40	20	10	15	20	15
45	20	10	15	20	15
50	20	10	15	20	15
55	20	10	15	20	15
60	20	10	15	20	15

Table 2. System Parameters

Cell ID	**Number of *users***	**Traffic Load**	**Available Resource**
Cell 1	20	0.426667	0.573333
Cell 2	10	0.226667	0.773333
Cell 3	60	0.986667	0.013333
Cell 4	15	0.32	0.68
Cell 5	20	0.266667	0.733333
Cell 6	15	0.333333	0.666667

3. RESULTS AND DISCUSSION

As shown in Table 4, Cell 3 has a load of 0.9867 which means that the resources in Cell 3 are used up to 99% of the total resources provided. Therefore, the user load in Cell 3 has passed the threshold specified in this simulation, which is 60%.

The selection of target cell is done based on (1), the shortest distance between users in the overloaded cell and the target cell, and whether the target cell has available resources. The cell target candidates are listed from one with the greatest number of available resources, to one with the least number of available resources. As seen in Table 4, the first candidate for cell target is Cell 2. The algorithm will try to find a user in Cell 3 to be moved to Cell 2. If no suitable candidate is found in Cell 3, and the traffic condition in Cell 3 still satisfies (1), the algorithm will choose the next target cell, namely Cell 5. The user which is moved to the target cell will affect the hysteresis calculation for the next user. Hysteresis is calculated repeatedly each time signal quality is measured by the available resource in the target cell.

The simulation is done to analyze the network performance with and without MLB algorithm. During the simulation, the number of users in one of the cells is increased until the cell is overloaded. Some users do not obtain a resource block allocation, and therefore deemed as “unsatisfied users”. Unsatisfied users are only found in an overloaded cell. The percentage of unsatisfied users before and after MLB algorithm is activated is given in Table 5.

Table 3 Percentage of Unsatisfied Users

Number of Users	**Percentage of Unsatisfied Users (%)**	
	Before MLB Activation	**After MLB Activation**
35	0	0
40	0	0
45	0,8	0
50	10	1,3
55	17	6,1
60	24,6	15,2

From Table 5, it is seen that when the number of users are 35 and 40, the percentage of unsatisfied users are 0, both before and after MLB algorithm is activated. This means all users are allocated resource blocks. When the number of users increases, the percentage of unsatisfied users also increases before the MLB is activated. However, the percentage decreases after MLB is activated. For instance, when the number of users is 60, the unsatisfied users before MLB is activated is 24,6%. The percentage lowers to 15,2% when MLB is activated. This means the activation of MLB algorithm will decrease the percentage of unsatisfied users by 9,4%.

JURNAL ECTIPE
Electronic, Control, Telecommunication, Information, and Power Engineering
Volume 12, Issue 1, April 2025, pp. 103-112
ISSN 2355-5068 ; e-ISSN 2622-4852
DOI: 10.33019/jurnalecotipe.v12i1.4532

Figure 6 shows the comparison of unsatisfied users percentage measured before and after the MLB algorithm is activated. The throughput measured in the simulations is the total throughput in the network. Throughput is affected by several factors, namely the number of users, the type of services used and the users' signal quality (SINR).

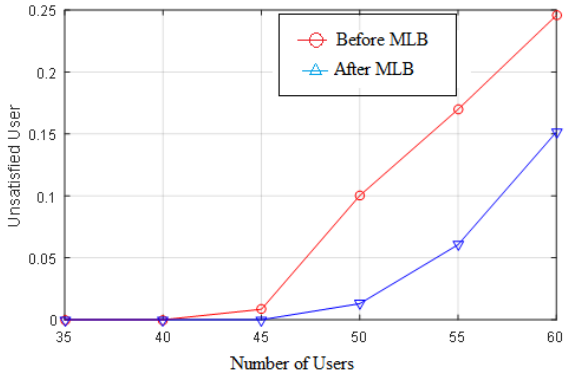

Figure 5. Percentage of Unsatisfied Users Before and After Activation of MLB

The throughput will increase when more of the allocated resource blocks are used in the network, as shown in Table 6. In Table 6, it is seen that when the number of users is 35 and 40, the total throughput decreases as the MLB algorithm is activated. This decrease is because several users are moved to a target cell, which subsequently decreases the signal quality in the target cell. The transfer of users is done to balance the network load. When the number of users is between 45-60, the throughput increases after the MLB algorithm is activated. For instance, when the number of users is 60, the throughput increases from 165.137 Mbps to 170.7552 Mbps. The increase of 5.617 Mbps is because the unsatisfied users in Cell 3 are moved to target cell. This consequently increases the number of users in the target cells and the number of allocated resources being used. The throughput comparison before and after the MLB algorithm is activated is given in Figure 7.

Table 4. Total throughput

Number of Users	**Total Throughput (Mbps)**	
	Before MLB Activation	After MLB Activation
35	150.43392	150.23904
40	158.31648	157.8864
45	163.7664	164.32416
50	163.35104	168.34432
55	164.620	171.4272
60	165.13728	170.7552

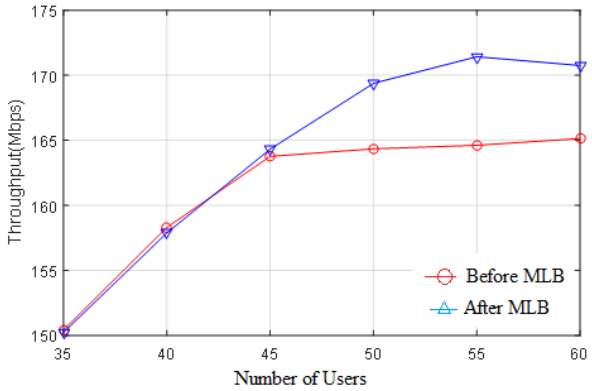

Figure 6. Throughput comparison before and after MLB activation

Volume 12, Issue 1, April 2025, pp. 103-112
ISSN 2355-5068 ; e-ISSN 2622-4852
DOI: 10.33019/jurnalecotipe.v12i1.4532

4. CONCLUSION

Simulations have been done to analyze the impact of MLB algorithm in optimizing the user capacity for downlink data in LTE network. Based on the simulations, it is shown that the use of MLB algorithm can decrease the percentage of unsatisfied users by 9.4%. This means several users which are denied service prior to the activation of MLB algorithm, can obtain resource block after the MLB algorithm is activated. The network throughput increases by 5.617 Mbps after the activation of MLB algorithm, because the resource blocks available in cells with low traffic loads can be utilized by incoming users from the cells with high traffic loads.

The simulations have been done with a limited number of cells and users. Therefore, further researches should be conducted to consider more realistic challenges typically found in real situations. These challenges include dynamic traffic fluctuations, as well radio interferences and channel fading effects. Further research should focus on integrating the LTE network planning and handover mechanism with MLB algorithm, and ideally also consider adaptive MLB based on machine-learning to improve the decision-making process during the MLB algorithm execution.

REFERENCES

[1] S. Chen, S. Sun, Y. Wang, G. Xiao, and R. Tamrakar, "A comprehensive survey of TDD-based mobile communication systems from TD-SCDMA 3G to TD-LTE(A) 4G and 5G directions," 2015. doi: 10.1109/CC.2015.7084401.

[2] M. Escheikh, H. Jouini, and K. Barkaoui, "Modeling, implementation and performance analysis of mobility load balancing for lte downlink data transmission," *International Journal of Computer Networks and Communications*, vol. 8, no. 5, 2016, doi: 10.5121/ijcnc.2016.8505.

[3] E. Gures, I. Shayea, M. Ergen, M. Hadri Azmi, and A. A. El-Saleh, "Machine Learning-Based Load Balancing Algorithms in Future Heterogeneous Networks: A Survey," *IEEE Access* , vol. 10, pp. 37689–37717, 2022.

[4] M. Jaber, Z. Dawy, N. Akl, and E. Yaacoub, "Tutorial on LTE/LTE-A Cellular Network Dimensioning Using Iterative Statistical Analysis," *IEEE Communications Surveys and Tutorials*, vol. 18, no. 2, 2016, doi: 10.1109/COMST.2015.2513440.

[5] G. Ku and J. M. Walsh, "Resource allocation and link adaptation in LTE and LTE advanced: A tutorial," *IEEE Communications Surveys and Tutorials*, vol. 17, no. 3, 2015, doi: 10.1109/COMST.2014.2383691.

[6] A. Lobinger, S. Stefanski, T. Jansen, and I. Balan, "Load balancing in downlink LTE self-optimizing networks," in *IEEE Vehicular Technology Conference*, 2010. doi: 10.1109/VETECS.2010.5493656.

[7] C. Cox, *An Introduction to LTE: LTE, LTE-Advanced, SAE, VoLTE and 4G Mobile Communications: Second Edition*, vol. 9781118818039. 2014. doi: 10.1002/9781118818046.

[8] S. Shukry and Y. Fahmy, "Mobility robustness self-organizing network handover scheme for LTE-Advanced," in *2016 33rd National Radio Science Conference (NRSC)*, Aswan, Egypt: IEEE, Feb. 2016.

[9] S. Rathi, N. Malik, N. Chahal, and S. Malik, "Throughput for TDD and FDD 4 G LTE Systems," *International Journal of Innovative Technology and Exploring Engineering (IJITEE)*, vol. 3, no. 12, pp. 73–77, May 2014.

[10] "TDD/FDD LTE Convergence," Feb. 2015. Accessed: Feb. 15, 2025. [Online]. Available: https://www.gtigroup.org/Uploads/File/2022/03/14/u622f1286b4ac1.pdf

[11] S. Tanwar, H. Khujamatov, B. Turumbetov, E. Reypnazarov, and Z. Allamuratova, "Designing and Calculating Bandwidth of the LTE Network for Rural Areas," *Int J Adv Sci Eng Inf Technol*, vol. 12, no. 2, pp. 437–445, 2022, doi: 10.18517/ijaseit.12.2.14950.

JURNAL ECOTIPE
Electronic, Control, Telecommunication, Information, and Power Engineering

Volume 12, Issue 1, April 2025, pp. 113-119
ISSN 2355-5068 ; e-ISSN 2622-4852
DOI: 10.33019/jurnalecotipe.v12i1.4558

Statistical Analysis of Protection Current Transformer Performance Based on Error Ratio and Knee Voltage on 20 kV Feeder at Bangka Transmission and Substation Service Unit

Maisa Sapitri[1], Asmar[2], Welly Yandi[3], Rudy Kurniawan[4]
[1,2,3,4] Electrical Engineering Department, Bangka Belitung University, Indonesia

ARTICLE INFO

Article historys:

Received : 23/03/2025
Revised : 28/03/2025
Accepted : 24/04/2025

Keywords:

Current Transformer; Knee Voltage; Ratio Error; Statistical Analysis; Protection System

ABSTRACT

Current Transformers (CTs) are essential components in power system protection, ensuring accurate current measurement for relay operations.. This study evaluates the accuracy of protection CTs used in 20kV feeders at the Bangka Transmission and Substation Service Unit. Measurements were conducted on CTs with 5 and 7 years of usage to analyze ratio error and knee voltage compliance with IEC 61869-2 standards. The results indicate that all CTs meet the standard, with ratio errors below 1% and knee voltages exceeding 60V. Normality tests confirmed that the data are normally distributed, allowing statistical analysis using t-tests. The t-test results showed no significant difference in ratio error and knee voltage between CTs used for 5 and 7 years. This study concludes that aging over this period does not significantly affect CT accuracy, ensuring continued reliability in power system protection.

Corresponding Author:

Asmar
Electrical Engineering Department, Bangka Belitung University, Indonesia
Email: asmarubb2@gmail.com

1. INTRODUCTION

Current Transformers (CT) are one of the important components in power systems, especially in protection and measurement applications. CTs function to reduce high currents from the electrical network into lower, safe currents that can be measured or used by protection devices.

Current Transformers operate based on the principle of electromagnetic induction, where a large primary current generates a magnetic field that is induced in the secondary winding. The resulting secondary current is then used for measurement or as an input for protection relays in the power system. One of the most critical parameters in CTs is the current ratio, which is the comparison between the primary current flowing through the CT and the secondary current produced. This parameter is essential in determining the performance of the transformation and the accuracy of the measurement. It ensures that the high current on the primary side is proportionally converted into a smaller, safe current for measurement and protection devices, so that the power system can accurately detect and respond to faults [1, 2, 3].

CTs used in protection must be capable of operating effectively under both normal conditions and during faults in the power system. Several factors must be considered in implementing protection CTs, including accuracy, knee point, safety factor, and burden. CTs must provide accurate current values even during current surges under fault conditions. The more accurate a CT is, the smaller its measurement error will be [4]. There are several common types of errors, namely ratio error, phase error, and composite error. Ratio error measures the difference between the actual secondary current

Volume 12, Issue 1, April 2025, pp. 113-119
ISSN 2355-5068 ; e-ISSN 2622-4852
DOI: 10.33019/jurnalecotipe.v12i1.4558

and the ideal value based on the CT's transformation ratio, while phase error indicates the angular deviation between the primary and secondary currents that can affect the timing and accuracy of the protection system. Composite error is the combination of these two errors, providing an overall picture of the CT's inaccuracy under certain load conditions [5].

Measurement errors in CTs can also be caused by saturation conditions. The saturation condition is influenced by the knee point voltage and the safety factor [6, 7]. The knee point voltage is the voltage at which the CT core begins to saturate, so that the relationship between the primary and secondary currents is no longer linear; a higher knee point indicates that the CT can withstand current surges during fault conditions for a longer period without distorting its measurements [8]. On the other hand, the safety factor (or accuracy limit factor) is a multiplier that describes how far the CT can operate beyond its nominal current before its accuracy starts to significantly deteriorate, essentially providing a safety margin so that the CT can continue to deliver reliable signals to the protection system [9, 10].

CT measurement errors are also influenced by the burden connected to the CT. The burden on a protection CT refers to the total impedance connected on the secondary side, usually measured in VA, and includes measurement equipment, relays, cables, and other connections. This burden is very critical because an excessively high burden can cause an increase in the secondary voltage, resulting in a decrease in measurement accuracy and potential errors, especially under high current fault conditions [11, 12].

The standard governing protection CTs is IEC 61869-2. This standard is designed to ensure accurate current measurements under both normal operating conditions and fault conditions by emphasizing important parameters such as transformation ratio, accuracy class, knee-point voltage, and secondary burden, so that CTs can deliver consistent and reliable signals to the protection system. This standard categorizes protection CTs into several classes, including the 5P and 10P classes. A comparison between these two classes is presented in Table 1 [13].

Table 1. Comparison of protection CT classes 5P and 10P

Parameter	Class 5P	Class 10P
Composite Error	Maximum 5%	Maximum 10%
Ratio Error	Maximum 1%	Maximum 3%
Accuracy Limit Factor (ALF)	5, 10, 20, etc.	5, 10, 20, etc.

Given the crucial role of protection CTs, it is essential to conduct periodic measurements for each unit. These measurements help ensure that the protection CTs in use still comply with standard requirements. Additionally, the collected data can be utilized for estimation and analysis to determine whether the overall use of CTs remains within the specified standard limits.

This study aims to:

a. Assess whether the protection CTs meet the standard limits for ratio error and knee-point voltage.
b. Estimate the allowable range of ratio error and knee-point voltage in protection CTs.
c. Evaluate the significance of differences in ratio error and knee-point voltage between CTs with 5 years of usage and those with 7 years of usage.

2. RESEARCH METHOD

Statistical methods are employed to analyze the data on ratio error and knee voltage in this study. The measured CT ratio errors are compared against established standards. In this research, the ratio error being evaluated is determined for a burden of 15 VA at secondary current levels of 100%, 120%, and 200% of the CT's nominal secondary current.

Meanwhile, the knee voltage measurement results should be compared with the calculated values. The knee voltage (V_k) is determined using the Accuracy Limit Factor (ALF), the nominal secondary current of the CT (I_n), and the burden resistance (R_B), as shown in the following equation [11]:

$$V_k = ALF \times I_n \times R_B \quad (1)$$

JURNAL ECTIPE
Electronic, Control, Telecommunication, Information, and Power Engineering
Volume 12, Issue 1, April 2025, pp. 113-119
ISSN 2355-5068 ; e-ISSN 2622-4852
DOI: 10.33019/jurnalecotipe.v12i1.4558

$$R_B = \frac{Burden\ (VA)}{I_n} \quad (2)$$

All CTs used in this study have a ratio of 400/5 (nominal secondary current of 5 amperes), class 5P, an Accuracy Limit Factor (ALF) of 20, and a nominal burden of 15 VA. Based on the CT data, Equation 1, and Equation 2, the standard knee voltage of the CT is 60 V.

The data analysis process is shown in Figure 1.

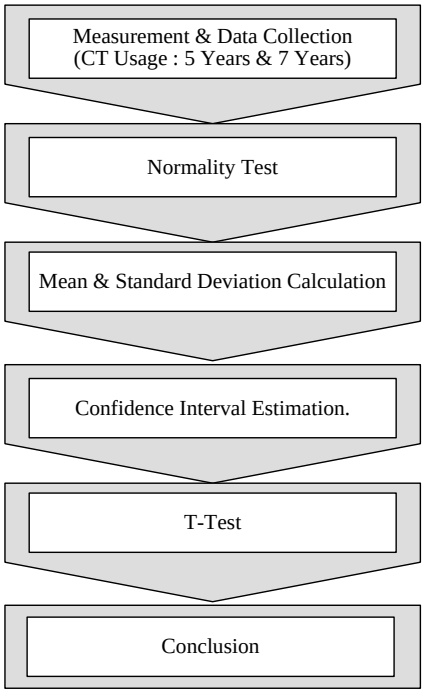

Figure 1. Data Analysis Process

2.1. Measurement and Data Collection

The first step is to collect measurement data on CT ratio error and knee voltage. These data were measured using a CT analyzer in 2024. The number of data points for CTs with a usage duration of 5 years and 7 years is 20 each. The data were obtained from measurements of CTs located in medium voltage feeders (20 kV) at the Bangka transmission and substation service unit, specifically in the Pangkal Pinang, Air Anyir, Toboali, Kelapa, Muntok, Koba, and Sungailiat feeders.

2.2. Normality Test

After the data is collected, the next step is to perform a normality test to ensure that the data distribution approximates a normal distribution. The Kolmogorov-Smirnov test is applied to each group, and if the resulting significance value (typically > 0.05) indicates that the data meets the normality assumption, it qualifies for further parametric statistical analysis [14].

2.3. Mean and Standart Deviation Calculation

The calculation of the mean ($\bar{x}$) and standard deviation (s) is performed to describe the central value and data variation [14]. The mean is calculated as follows :

$$\bar{x} = \frac{1}{n}\sum x_i \quad (3)$$

While the standard deviation is obtained from :

$$s = \sqrt{\frac{\sum(x_i - \bar{x})^2}{n-1}} \quad (4)$$

where x_i represents each measurement value and n is the sample size. This calculation provides a comprehensive overview of the CT performance in both usage duration groups.

JURNAL ECTIPE
Electronic, Control, Telecommunication, Information, and Power Engineering
Volume 12, Issue 1, April 2025, pp. 113-119
ISSN 2355-5068 ; e-ISSN 2622-4852
DOI: 10.33019/jurnalecotipe.v12i1.4558

2.4. Confidence Interval Estimation

Next, parameter estimation is performed by constructing a confidence interval for each variable. This estimation uses the following formula [14]:

$$\bar{x} \pm t \frac{s}{\sqrt{n}} \tag{5}$$

where t is the critical value of the t-distribution at a specific confidence level (e.g., 95%). This confidence interval range indicates the lower and upper bounds where the true population parameter is expected to lie, providing an estimate of the measurement error margin.

2.5. T-test

To determine whether there is a significant difference between CTs used for 5 years and 7 years, an independent t-test is conducted [14]. If the variances of both groups are equal, the t-value is obtained using the formula:

$$t = \frac{\overline{x_1} - \overline{x_2}}{s_p \sqrt{\frac{1}{n_1} + \frac{1}{n_2}}} \tag{5}$$

with s_p as the pooled standard deviation, calculated using:

$$s_p = \sqrt{\frac{(n_1 - 1)s_1^2 + (n_2 - 1)s_2^2}{n_1 + n_2 - 2}} \tag{6}$$

and the degrees of freedom are :

$$df = n_1 + n_2 - 2 \tag{7}$$

The t-value obtained from the equation above is compared with the critical value (from the t-table) at a specified significance level (e.g., $\alpha = 0.05$) to assess whether there is a significant difference between the CT groups with usage durations of 5 years and 7 years. If the t-value falls between -t table and t table, the conclusion is that there is no significant difference between CTs with 5-year and 7-year usage durations.

In addition to comparing the calculated t-value with the t-table, conclusions can also be drawn based on the significance level. If the calculated significance is greater than 5%, then the conclusion is that there is no significant difference between CTs with 5-year and 7-year usage durations. To facilitate the analysis process, the statistical parameters in the equations above will be calculated using statistical software.

3. RESULTS AND DISCUSSION

Figure 2 shows the measurement of protection CTs using a CT analyzer. The measurement results for CTs with a usage duration of 5 years are presented in Table 2, while those for CTs with a usage duration of 7 years are presented in Table 3.

Figure 2. Measurement of ratio error and knee voltage of protection CTs

JURNAL ECOTIPE
Electronic, Control, Telecommunication, Information, and Power Engineering
Volume 12, Issue 1, April 2025, pp. 113-119
ISSN 2355-5068 ; e-ISSN 2622-4852
DOI: 10.33019/jurnalecotipe.v12i1.4558

Table 2. The measurement results of ratio error and knee point voltage on CTs with a usage duration of 5 years

No	Substation	Feeder	Current Ratio Error in % at % of Rated Current			Knee Voltage (Volt)
			100%	120%	200%	
1	GI 150kV KLP	Bakik	0.177	0.18	0.189	71.58
2	GI 150kV KLP	Dalil	0.446	0.448	0.457	71.35
3	GI 150kV KLP	Mayang	0.415	0.421	0.437	71.83
4	GI 150kV KLP	Parit 3	0.451	0.454	0.456	72.40
5	GI 150kV KLP	Pelangas	0.425	0.431	0.446	72.22
6	GI 150kV KLP	Simpang Yul	0.438	0.444	0.449	73.57
7	GI 150kV KLP	Beriga	0.436	0.44	0.443	73.48
8	GI 150kV MTK	Kemang Masam	0.260	0.271	0.262	72.07
9	GI 150kV MTK	Menjelang	0.159	0.163	0.165	73.35
10	GI 150kV SLT	Gunung Muda	0.111	0.113	0.119	75.32
11	GI 150kV SLT	Parai	0.106	0.118	0.124	70.22
12	GI 150kV SLT	Air Ruay	0.334	0.341	0.343	73.05
13	GI 150kV TLB	Air Banten	0.338	0.35	0.355	74.82
14	GI 150kV TLB	Kaposang	0.227	0.234	0.237	73.17
15	GI150kV KOBA	Padang Mulia	0.432	0.437	0.442	71.67
16	GI150kV KOBA	Tungkal	0.429	0.434	0.439	75.22
17	GI150kV KOBA	Paku	0.135	0.140	0.146	71.37
18	GI150kV KOBA	Palas	0.234	0.235	0.245	73.36
19	GI150kV KOBA	Terentang	0.344	0.346	0.350	71.90
20	GI150kV KOBA	Tungkal	0.125	0.127	0.129	73.80

Table 3. The measurement results of ratio error and knee point voltage on CTs with a usage duration of 7 years

No	Substation	Feeder	Current Ratio Error in % at % of Rated Current			Knee Voltage (Volt)
			100%	120%	200%	
1	GI 150kV PKP	Batu Rusa	0.462	0.464	0.473	73.66
2	GI 150kV PKP	Pangkal Balam	0.205	0.213	0.214	74.43
3	GI 150kV PKP	Cengkong Abang	0.155	0.157	0.16	72.87
4	GI 150kV PKP	Air Itam	0.434	0.439	0.452	74.68
5	GI 150kV PKP	Eks Mendo Barat	0.439	0.444	0.457	73.42
6	GI 150kV PKP	Eks Sumerejo	0.350	0.354	0.357	72.3
7	GI 150kV PKP	Transmart	0.320	0.334	0.340	72.35
8	GI 150kV PKP	Kampung Jeruk	0.130	0.137	0.141	69.65
9	GI 150kV PKP	Jelitik	0.242	0.246	0.256	74.75
10	GI 150kV PKP	Bukit Intan	0.560	0.562	0.576	70.85
11	GI 150kV PKP	BTC	0.415	0.416	0.417	71.06
12	GI 150kV PKP	Depati Hamzah	0.386	0.393	0.396	72.65
13	GI 150kV PKP	Bukit Baru	0.316	0.319	0.320	72.15
14	GI 150kV PKP	Lampur	0.465	0.466	0.470	71.35
15	GI 150kV PKP	Lontong Pancur	0.416	0.418	0.419	71.41
16	GI 150kV PKP	Rangkui	0.146	0.147	0.150	70.22
17	GI 150kV PKP	Siloam	0.185	0.187	0.190	69.00
18	GI 150kV PKP	Simpang Katis	0.134	0.135	0.137	71.97
19	GI 150kV AA	Provinsi	0.382	0.389	0.392	74.61
20	GI 150kV AA	Soekarno Hatta	0.217	0.226	0.229	72.43

From the results in Table 2 and Table 3, it can be seen that all CTs provide ratio errors that meet the standard, which is below 1% (0.01). Likewise, the knee voltage of all CTs also complies with the standard, being

JURNAL ECTIPE
Electronic, Control, Telecommunication, Information, and Power Engineering
Volume 12, Issue 1, April 2025, pp. 113-119
ISSN 2355-5068 ; e-ISSN 2622-4852
DOI: 10.33019/jurnalecotipe.v12i1.4558

greater than 60 volts. Next, we will discuss whether there is a significant difference between CTs that have been used for 5 years and those used for 7 years.

Table 4. Results of Normality Test, Mean, Standard Deviation, and Estimation

Parameter	Usage duration of 5 years.				Usage duration of 7 years.			
	Current Ratio Error in % at % of Rated Current			Knee Voltage (Volt)	Current Ratio Error in % at % of Rated Current			Knee Voltage (Volt)
	100%	120%	200%		100%	120%	200%	
Asymptotic Significance (Normality test results)	0.355	0.345	0.247	0.965	0.849	0.800	0.854	0.988
Mean	0.301	0.306	0.312	72.788	0.318	0.322	0.327	72.291
Standart Deviatiom	0.131	0.131	0.132	1.367	0.132	0.131	0.134	1.667
Confidence Interval Estimation (sig. 5%)	0.301±0.061	0.306±0.061	0.312±0.062	72.788±0.640	0.318±0.062	0.322±0.061	0.327±0.063	72.291±0.780

The results of the normality test using the Kolmogorov-Smirnov (K-S test), as shown in Table 4, indicate that all data have an Asymptotic Significance value greater than 0.05 (5%). Therefore, all data are normally distributed, and the t-test can be applied to these data. If we observe the mean error value of the CT ratio, it appears at first glance that the average for a usage duration of 7 years is higher than that of 5 years. However, this cannot be concluded as evidence that a CT with a usage duration of 5 years is better than one with 7 years.

Table 5. T-test results for the comparison between CT usage duration of 5 Years and 7 Years

Parameter	t-value	Significance
Ratio Errors at 100% Nominal Current	-0.406	0.687
Ratio Errors at 120% Nominal Current	-0.384	0.703
Ratio Errors at 200% Nominal Current	-0.373	0.712
Knee voltage	1.031	0.309

Since the number of data points for the 5-year and 7-year usage durations is 20, the t-table value is 2.2024. The calculated t-values in the table 5, all fall between -2.2024 and 2.2024. Similarly, the significance values obtained are all greater than 5% (0.05). Based on these results, it can be concluded that there is no significant difference in ratio error and knee voltage between CTs that have been used for 5 years and those used for 7 years.

4. CONCLUSION

The protection CTs used on the 20kV feeder at the Transmission Service Unit and Bangka Substation remain within the standard requirements. The ratio error is below 1%, and the knee voltage exceeds 60 volts. Furthermore, there is no significant difference between CTs that have been in operation for 5 years and those used for 7 years.

REFERENCES

[1] Harlow, J. H. Electric Power Transformer Engineering. New York: Marcel Dekker, 1998.

[2] Gurevich, V. Instrument Transformers: Theory, Applications, and Testing. New York: Wiley, 2003.

[3] Divan, D. M. "Transient Performance of Current Transformers." IEEE Transactions on Power Delivery, Vol. 12, No. 3, pp. 1103–1111, July 1997.

Volume 12, Issue 1, April 2025, pp. 113-119
ISSN 2355-5068 ; e-ISSN 2622-4852
DOI: 10.33019/jurnalecotipe.v12i1.4558

[4] Gurevich, V., Instrument Transformers: Theory, Applications, and Testing., New York : Wiley, 2003.

[5] Slemon, G. R. "Evaluation of the Accuracy of Protection CTs Under Fault Conditions." IEEE Transactions on Power Delivery, Vol. 14, No. 4, pp. 1234–1242, October 1999

[6] Smith, J., Brown, L., & Patel, R. "Analysis of Current Transformer Saturation and Its Impact on Protective Relay Performance." IEEE Transactions on Power Delivery, vol. 33, no. 3, pp. 1234–1243, 2018.

[7] Kumar, A., Zhang, Y., & Lee, S. "Modeling and Simulation of CT Saturation Effects in Digital Relaying." IEEE Transactions on Power Delivery, vol. 34, no. 4, pp. 5678–5686, 2019.

[8] Wang, X., Li, Y., & Chen, F. "A Study on Knee-Point Voltage and Its Impact on Current Transformer Performance During Fault Conditions." IEEE Transactions on Power Delivery, vol. 37, no. 4, pp. 1895–1904, 2022.

[9] Chen, Z., Li, Y., & Smith, M. "Impact of Accuracy Limit Factor on Protection CT Performance in High Fault Currents." IEEE Transactions on Power Delivery, vol. 36, no. 2, pp. 700–708, April 2021.

[10] Kumar, H., Patel, A., & Zhang, J. "Evaluation of Safety Factor in Current Transformers for Reliable Protection Systems." IEEE Transactions on Instrumentation and Measurement, vol. 70, no. 5, pp. 1–8, May 2022.

[11] Wang, L., Zhang, H., and Lee, S. “Assessment of Burden Effects on Current Transformer Accuracy Under High Fault Conditions.” IEEE Transactions on Power Delivery, vol. 37, no. 3, pp. 1120–1127, July 2022.

[12] Gurevich, V., Instrument Transformers: Theory, Applications, and Testing, New York : Wiley, 2003.

[13] International Electrotechnical Commission. IEC 61869-2: Instrument Transformers – Part 2: Current Transformers. Geneva: International Electrotechnical Commission, 2010.

[14] Montgomery, D. C., Design and Analysis of Experiments (9th ed.), New York : Wiley, 2017.

Volume 12, Issue 1, April 2025
ISSN 2355-5068
e-ISSN 2622-4852

Publisher Address :

Electrical Engineering Department
Faculty of Science and Engineering - Bangka Belitung University
Balunijuk, Kab. Bangka, Prov. Kep. Bangka Belitung
University Phone : (0717) 422145, 422965 Fax. (0717) 421303
Faculty Phone : (0717) 4260033 ext. 2122, 2124
Website : https://ecotipe.ubb.ac.id/index.php/ecotipe
E-mail : jurnalecotipe@ubb.ac.id / jurnal.ecotipe@yahoo.com